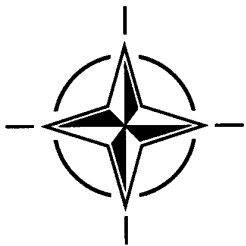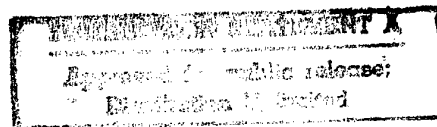AGARD-AG-333

AGARD

ADVISORY GROUP FOR AEROSPACE RESEARCH & DEVELOPMENT

7 RUE ANCELLE, 92200 NEUILLY-SUR-SEINE, FRANCE

AGARDograph 333

Enhancement of Aircraft Ground Handling Simulation Capability

(l'Amélioration des moyens de simulation des manœuvres
au sol des aéronefs)

This AGARDograph has been sponsored by the Flight Vehicle Integration Panel.

19980924 128

NORTH ATLANTIC TREATY ORGANIZATION

Published August 1998

Distribution and Availability on Back Cover

AQF98-12-2560

AGARD

ADVISORY GROUP FOR AEROSPACE RESEARCH & DEVELOPMENT

7 RUE ANCELLE, 92200 NEUILLY-SUR-SEINE, FRANCE

AGARDograph 333

Enhancement of Aircraft Ground Handling Simulation Capability

(l'Amélioration des moyens de simulation des manœuvres au sol des aéronefs)

by

A.G. Barnes
Retired Simulation Engineer
17 North Houses Lane
Lytham St Annes
Lancs. FY8 4NT
UK

and

T.J. Yager
Senior Research Engineer
Structural Dynamics Branch MS 497
NASA Langley Research Center
Hampton VA 23681-0001
USA

North Atlantic Treaty Organization
Organisation du Traité de l'Atlantique Nord

The Mission of AGARD*

According to its Charter, the mission of AGARD is to bring together the leading personalities of the NATO nations in the fields of science and technology relating to aerospace for the following purposes:

— Recommending effective ways for the member nations to use their research and development capabilities for the common benefit of the NATO community;

— Providing scientific and technical advice and assistance to the Military Committee in the field of aerospace research and development (with particular regard to its military application);

— Continuously stimulating advances in the aerospace sciences relevant to strengthening the common defence posture;

— Improving the co-operation among member nations in aerospace research and development;

— Exchange of scientific and technical information;

— Providing assistance to member nations for the purpose of increasing their scientific and technical potential;

— Rendering scientific and technical assistance, as requested, to other NATO bodies and to member nations in connection with research and development problems in the aerospace field.

The highest authority within AGARD is the National Delegates Board consisting of officially appointed senior representatives from each member nation. The mission of AGARD is carried out through the Panels which are composed of experts appointed by the National Delegates, the Consultant and Exchange Programme and the Aerospace Applications Studies Programme. The results of AGARD work are reported to the member nations and the NATO Authorities through the AGARD series of publications of which this is one.

Participation in AGARD activities is by invitation only and is normally limited to citizens of the NATO nations.

* AGARD merged with the Defence Research Group of NATO (DRG) on 1 January 1998 to form the Research and Technology Organization (RTO) of NATO. However, both AGARD and DRG will continue to issue publications under their own names in respect of work performed in 1997.

Enhancement of Aircraft Ground Handling Simulation Capability
(AGARD AG-333)

Executive Summary

This AGARDograph documents the advances made in this field, and provides guidance to simulator engineers on using these improvements to best meet their individual requirements.

The overall capability of simulating aircraft performance both in flight and in ground operations has improved dramatically in recent years. These improvements are a result of advances in computer hardware and software, motion-based systems, visual displays, and modeling data fidelity.

This AGARDograph should be of interest to engineers involved in the design and testing of simulation for aircraft systems. Simulation will play a major role in the production of cost-effective and combat-effective air forces of the future. By providing this report, AGARD hopes to enhance the overall knowledge in the simulation of aircraft ground handling, and thus enhance the capability of design engineers to employ these tools to the benefit of the Alliance.

L'amélioration des moyens de simulation des manœuvres au sol des aéronefs

(AGARD AG-333)

Synthèse

Cette AGARDographie documente les avancées réalisées dans ce domaine et fournit des directives aux ingénieurs responsables des simulateurs, leur permettant de profiter au maximum de ces améliorations pour répondre à leurs besoins.

La simulation des performances des aéronefs en vol et celle des opérations de manutention au sol s'est améliorée de façon spectaculaire au cours des dernières années. Ces améliorations résultent des progrès réalisés dans le domaine informatique, dans les systèmes à base de mouvements, dans les affichages visuels et dans la fidélité de la modélisation des données.

Cette AGARDographie intéressera les ingénieurs impliqués dans la conception et les essais des simulateurs de systèmes aéronautiques. La simulation jouera à l'avenir un rôle déterminant dans la création de forces aériennes de combat rentables et efficaces. En publiant ce rapport, l'AGARD espère apporter sa contribution à l'avancée des connaissances globales en matière de simulation des opérations de manutention au sol des aéronefs et espère aussi promouvoir l'utilisation de ces outils pour les concepteurs au bénéfice global de l'Alliance.

Contents

Preface

In 1985, the Flight Mechanics Panel of AGARD published AGARDograph 285, "Simulation of Aircraft Behaviour on and close to the Ground". The report discusses the benefits derived from using ground-based simulation to represent aircraft on the ground. It presents the then-current standards of modeling and visual/motion hardware technology, and gives examples of experience from specific simulators devoted to research, development, and pilot training.

Since that time, several factors have appeared, to allow higher standards of ground roll simulation to be achieved.

— models of the relevant elements – runway surface, tires, brakes, landing gear, aerodynamics – can be made more accurate, because of increased computer speed and capacity;

— more experimental data is available, relating to runway surface conditions, and surface contamination (rain, snow, ice);

— the technology to provide visual and motion cues to the pilot has improved;

— the need for ground-based simulation of aircraft (and other vehicles) has increased. New ideas, such as active suspension, can be addressed.

The Flight Mechanics Panel invited the authors of AGARDograph 285 to produce a second report on the subject, incorporating the new knowledge, and presenting techniques to enable simulators to improve their representation of aircraft on the ground. In particular, the report deals with dynamic response of an aircraft on the ground, the parameters which influence runway friction forces, and real-time modeling of tire side forces. Bandwidth is identified as the most critical factor in constructing a real-time simulation model. Areas where current simulators could be improved are identified, and topics for research are suggested.

1.   Introduction

The overall capability of simulating aircraft performance both in flight as well as in ground operations has improved dramatically in recent years, due to significant advances in computer hardware/software, motion-based systems, visual displays, and modeling data fidelity. The primary purpose of this AGARDograph to document these advances in regards to aircraft ground handling simulation capability, and to provide helpful guidance to simulator engineers on using these improvements to best meet their individual requirements. It is a continuation of earlier work on this topic, completed 12 years ago, and reported in Reference 1. Before this report was prepared, a study was made of current standards of ground roll simulation for both civil and military aircraft, in training and research simulators.

In general, existing simulators are deficient in one or all of the following areas:

i)   The presentation in the model of the forces generated between the wheels and the ground are over-simplified, and are invalid for extreme conditions, such as large tire slip angles,

ii)   the model does not allow for variation in operating conditions, such as runway contamination or tire pressure, specific to each wheel,

iii)   round undulations and roughness, and runway camber are not simulated,

iv)   the standard of documentation, and model validation, is inadequate.

In this report, a detailed explanation of both the essential requirements and the basic assumptions for aircraft modeling is given, together with a description of the various elements needed in the model structure. The modeling requirements related to bandwidth, accuracy, realism, and validation are discussed. In regards to some of the basic assumptions used in aircraft ground handling simulation, combined and/or simplified components, reference axes, wheel and brake modeling, and wheel torsional forces are explained. A general description of runway surface conditions influencing tire/pavement friction performance is provided, and the approach taken in modeling tire/strut (the key interface component between the aircraft and the runway pavement) performance is given.

Several block diagrams are used to describe various components of the aircraft ground handling simulation and provide the reader a better understanding of how the overall simulation capability is developed. Some existing models are discussed, together with pilot cueing requirements to enhance realism of simulation. Several appendices are included to document mathematical models used for determining ground lateral forces, tire/runway friction, lateral tire force, and ground vertical forces. The paper concludes that the fidelity of simulation capability to replicate aircraft ground handling performance has improved significantly to the extent that pilot training, air traffic control, problem solving (i.e. landing over-run/veer-off, and aborted take-off accidents), and aircraft design evaluations can be conducted using simulation with a high degree of confidence and realism.

2. Modeling Requirements

2.1 General

The last thirty years have seen enormous strides made in computing capability, and it is often assumed today that computer size no longer determines the extent to which a model of a physical system can be constructed. The wide availability of personal computers with pentium processors and memory measured in gigabytes suggest that cost, speed and capacity should not impose constraints. Models for flight simulation, however, are subject to two factors which rarely apply to other sciences which make extensive use of models. The first constraint is associated with the complex coupling existing between the elements which form the model - the aircraft, the aircraft's systems, the atmosphere, the airborne environment, and the ground environment (Figure 2.1).

It has been essential in the past to simplify these elements, and to minimize the interactions between them, because of limitations imposed by computer hardware performance. Even with today's computers, compromises are needed because of the extensive coupling between the elements of the physical world. As flight simulation increases its contribution to training and research, and as the computing hardware improves, it is desirable to use more realistic models of the elements, and to include some of the cross-coupling between them - for example, the relationships between time of day, humidity, temperature, radiation, visibility, and the visual appearance of objects. The issue of coupling between elements is discussed more fully in Reference 2.

The second constraint lies in the range of frequencies which must be modeled to represent the behavior of an aircraft in motion - at the top end, structural vibrations, sensors, actuators - and at the lower end, the permissible deviations in the calculation of geographical position implied by the requirement to simulate inertial navigation. The word length and repeatability of digital computing easily deals with the low frequency end of the bandwidth problem, but the need for real time operation denies the usual techniques for solving the mathematical expressions which have been developed to try to represent the laws of nature. In non-real time, not only may the computer take several hours to determine an accurate picture of events lasting a few seconds, but also, the model elements may be calculated separately, in different time frames, and recombined for the final solution.

A further factor intrudes into the requirements for modeling the behavior of an aircraft on the ground. The natural environment of an aircraft is in flight, where it is sustained by aerodynamic forces, it is subject to external and control excitation, and it is made to perform exacting tasks and maneuvers. Efforts to improve models should be directed at the airborne phase of operation, rather than at the shorter time period during maneuvers on the ground. The case for better models on the ground is stated in Section 1, but it is also true that improvements stemming from computing technology have to be shared with the need for better fidelity when simulating the in-flight phases.

Computer modeling has long been used in aircraft design and development, and the extent of its use continues to grow. Many of the models are highly specialized, and relate to particular components or systems within the aircraft. A model to be used in flight simulation is equally specialized. The nature of the model is influenced by three inter-related factors: bandwidth, accuracy, and realism. The link between accuracy and bandwidth is self-evident - if it can be shown that use of the model will not be compromised if frequencies above a cut-off value are

omitted, the equations of motion can be simplified. Accuracy is then applied to solving equations which describe the aircraft over the chosen bandwidth.

The relationship between accuracy and realism is less intuitive. The requirements for accuracy and realism in flight simulation are often in conflict. A flight simulator has to create, to a greater or lesser extent, the illusion of flight, which must be maintained, even though accuracy (such as correct motion cueing) is sacrificed. This topic is developed in Reference 3.

The modeling requirements relating to bandwidth, accuracy, and realism, are discussed below.

2.2   Bandwidth

The primary application of a model to represent aircraft handling on the ground is in a piloted flight simulator, so that the pilot's performance and comments may be correlated with those observed in the real aircraft. The model must run in real time, and this requirement, more than others, determines the form of the model. Even with today's processing power, imposing an unduly high bandwidth requirement on the model may result in a model which introduces time delays in the control loops which the pilot closes.

An aircraft on the ground is subject to excitation over a large range of frequencies. The variation of the height of the ground surface includes low frequency undulations, bumps, grooves, and textural roughness, and affects the aircraft's progress as a function of speed. The aircraft has structural modes of excitation extending to several hundred Hz, the flight control system has components which respond up to 100 Hz, and the landing gear must respond to the full range of ground excitation.

Landing gear design and development makes extensive use of models to optimize the performance of all components. Energy must be absorbed by the struts and the brakes, and the loads in components must not result in structural or component failures. Models serving this purpose require a bandwidth up to at least 50 Hz. Accurate representation of local phenomena such as wheel spin-up or oil flow inside an oleo may increase this requirement. From the pilot's point of view, however, such levels of detail are irrelevant.

In some respects, pilots are sensitive and demanding. Testimony can be seen in the specifications imposed on visual, motion, audio, and tactile cueing systems. In other ways, the pilot has strictly limited ability. In an aircraft control loop, he is unable to exert stabilizing inputs at frequencies higher than 2 Hz, in spite of his high bandwidth sensors, because of inherent lags in mental processing and limb manipulation. Consequently, does a model used primarily for real-time simulation need to maintain accurate gain and phase relationships above the bandwidth in which the pilot can respond?

The pilot is, of course, aware of, and reacts to, high frequency phenomena such as noise and vibration. He also expects certain correlation - for example, if he sees tar strips on the runway, he needs to feel the forces transmitted through the suspension system to his seat by wheel contact, and to hear the associated noises. This requirement may be met by the use of two modeling techniques which have been implicit in real-time modeling for many years.

The first technique is the use of "equivalent" models, in which the behavior of a simplified model is tuned to reproduce the behavior of a more comprehensive model over a restricted range of frequencies (Reference 2). Equivalent models have always been used implicitly in flight simulators. As mathematical description and implementation have improved, the opportunity to select the most appropriate model for a particular application has followed. In making the selection, the frequency range of interest must be defined. The use of an equivalent model allows the description of a model component (such as the strut) to be simplified, without sacrificing its essential behavior with respect to input and output. In the process, information on some parameters is lost.

In the second technique, the apparent bandwidth of the model is increased by 'dressing' the model. A subsidiary component is added to the equivalent model to emulate behavior at higher frequencies. It is excited by the equivalent model, but its outputs are not fed back, thus avoiding model instability due to computing cycle delays. The loss of phase accuracy at these frequencies is of no consequence, in view of the pilot's own bandwidth limitations. Dressing is also used to give the appearance to the pilot that a system is more fully represented than it is (for example, the failing of a system may be simulated by nothing more than the illumination of a warning light) - simply because the pilot has no indications in the cockpit of the internal workings of that system.

2.3 Accuracy

Accuracy requirements are determined by the application of the model. Each element of the model must be examined, and an assessment made of role played by that element in the total simulation. It is pointless to calculate in the model accurate values of parameters not used either during run-time of the simulator, or in subsequent analysis. Many existing real-time models are based on elements from simulations used for other purposes - a strut compression model, an ABS model, or a wheel spin-up model, used for the detail design of these components. Invariably, they could be simplified and made more tractable for use in a piloted simulator.

Extensive use is now made of modeling to determine dynamic loading conditions during take-off, ground-roll, and landing. The mechanisms by which the loads are generated, and the load paths from tire to c.g., are complicated, resulting in models of considerable size. These models do not run in real time (1/100th of real time is typical). The requirement for accurate loads, and the ability to determine cause and effect, dictates the form of the model (Section 7.4 refers to such a model). In a flight simulator, there is no need to furnish the pilot with information about loads, other than the loads which determine the flight path of the aircraft, or which he feels at the cockpit. Nor is he aware of the number of wheels which support the aircraft, or the paths taken by the loads.

Although local loads within components are not needed for real-time simulation, ground contact loads and aerodynamic loads must be accurate, together with the resulting aircraft trajectory and orientation. Conditions at particular stations - the cockpit, and extremities of the aircraft which might contact the ground, must be calculated. Unlike the loading models, which reproduce events over a brief period of time, accurate position information, correlated with geographical position, must be maintained over long periods, for example, from brake release to climb-out.

The forces generated by the tires are of particular importance. Modeling them accurately is not a trivial matter, but their representation determines the validity of the simulation. The contact conditions (surface type, contamination) at each wheel location must be calculated individually, over large ranges of the parameters involved, so that extreme conditions, such as loss of control in a cross-wind on a flooded runway, can be reproduced with confidence. The modeling of lateral forces generated by the tire must be accurate over large angles, and over the full speed range, to allow the aircraft's steering behavior during take-off/landing, and when maneuvering in the dispersal area to be represented. At very low speeds, the effects of tire scrubbing are important, particularly when simulating large aircraft with multi-bogie gear assemblies.

A further consideration is the extent to which coupling between components of the model are included. The classical approach in flight mechanics separates the lateral-directional modes from the longitudinal short period and phugoid modes, to simplify analysis, and then introduces coupling terms to deal with large perturbations. The aerodynamic data sets are often stored in the form of multi-dimensional arrays (hyper-cubes). Parallels may be drawn with the non-linear multi-parametric nature of the forces and moments generated by ground contact, and how they depend on the dynamic response of the aircraft, and on changing contact conditions. Additionally, the pilot is sensitive to other manifestations of coupling. The visual appearance of the ground (undulations, water or ice on the runway) will lead him to expect control difficulties when braking or steering during ground roll.

2.4   Realism

A simulation model must be accurate within laid-down tolerances. Verification of the model is based both on static measurements, and on dynamic response, open and closed loop. For a piloted simulator, control forces and travels are also checked, together with cockpit geometry, and the disposition of displays and switches. Additionally, the simulator must satisfy subjective assessments by pilots. Within its operating range, the simulator must behave like the aircraft it is meant to represent. In flight, the pilot experiences sensations which are difficult to reproduce on the ground - visual cues, motion cues, noise, and vibration. The creation of the illusion of flight uses similar means of fooling the senses to those used in entertainment and art.

The representation of motion cues illustrates the conflict between accuracy and realism. The travel limits of the motion system necessitate the use of wash-out filters on the drive signals, and a trade-off between wash-out time constants and gain. The illusion of motion is strongly reinforced by the outside world visual cueing, to establish a state of vection in the pilot's mind. Time delays, or disparities between information sources, due to inadequate modeling, can detract from the quality of the simulation.

The representation of higher frequencies, by dressing the model as described above, is important in achieving realism. The high frequency components of the model do not need to be accurate with respect to gain and phase, because the pilot cannot exert control at these frequencies, but they modify his behavior, and contribute greatly to his acceptance of the simulator as a replica of flight.

2.5   Validation

The vital role of simulators, both in pilot training and in research, makes validation an important issue in the qualification of simulators (References 4 and 5). Advances have been made in the past ten years in formalizing the simulation validation process. For example, Certification Authorities have agreed on standard procedures in the acceptance of training simulators. Data sources must be documented. With respect to the model, several factors contribute to efficient validation. It is convenient to recommend standardization, in notation, units, sign convention, and system of axes, but the reality is that standardization has a long way to go, and incentives to standardize are lacking, in spite of the efforts of multi-disciplinary committees, and other international bodies.

Further difficulties arise, peculiar to modeling the behavior of an aircraft on the ground. Compromises must be reached between aircraft design practice and ground vehicle design practice, in which the same Arabic and Greek letters are traditionally used for different parameters. The sheer number of parameters requires extensive use of sub- and super-scripts.

The first step in validation is to confirm the accuracy of input data, by reference either to source or to derivation. Static and quasi-static checks are followed by dynamic response measurements, using both linear analysis of expected modal parameters, and time histories of small and large perturbations, which are then compared to independently derived solutions. The process is greatly aided by having the model structured in a form which allows blocks to be isolated or simplified during the validation testing. A model structure of this type is discussed in Section 6.

3   Modeling Assumptions

There is a need to keep the bandwidth of the model low, because of real-time operation, and the consequent demands on computer power. There is justification to do so, because of the inability of the pilot to apply helpful control inputs at high frequencies. The device of dressing the model has been suggested, to give an appearance of higher bandwidth. A second method of simplifying the load on the computer, the equivalent model, has also been raised. The application of these methods to specific components of the ground roll model will now be discussed. Both methods rely on off-line data reduction. It is important that the methods used in the reduction process are formalized, and that the resulting simplified models have a high standard of documentation. They will then be available for comparison with other source data, such as the outputs of non-real-time models.

3.1   Combined Components

In designing the layout of large aircraft, it is usual to use multi-wheel bogies to support it on the ground, since a lighter, more compact and more efficient assembly can be achieved. On very large aircraft, like the Boeing 747 (Figure 3.1), additional main wheel bogies are used, to further distribute the loads. An equivalent gear, with three bogies, each carrying a wheel, is sufficient for most piloted aircraft simulators. A mean point of contact of the equivalent wheel must be found, and the forces and moments generated by the equivalent tire becomes the sum of the number of wheels in the equivalent model. The effect of a failure, such as a burst tire, may be represented by scaling the forces and moments by the number of wheels combined in the model.

In a similar manner, a simplified model of the strut and its mechanization is required for simulation purposes. The models used by strut manufacturers are highly detailed, and there is no need to reproduce the complex porting and oil flows which occur in the actual devices. Nor is the pilot aware of the mechanical configuration, which ensures that high loads are transmitted, and high energy is absorbed, without structural damage, and no useful purpose is served in attempting to model it. A collaboration with the manufacturer in developing a model for real-time use has much to recommend it.

3.2   Reference Axes

A more universal application of the principle of off-line reduction in model complexity relates to the many systems of axes which are needed for a universal model. In such a model, the location of all active elements, and specific geometrical positions in the airframe need to be known. To do so, many axis transformations, of acceleration, rate, and position, angular and linear, are made. In a real-time model of limited bandwidth, most of this local knowledge is superfluous. For example, the loads generated by the tires are transmitted to the aircraft c.g. by a tortuous route, but the aircraft response, and the loads felt by the pilot, depend only on accurate knowledge of the forces and moments at the c.g.

It is feasible, therefore, to reduce the number of transformations needed in the real-time model by re-defining model components off-line. Figure 3.2 shows the geometry of a simple landing gear. It is characterized by the non-vertical configuration of the gear legs - splay in the y-z plane, and rake in the x-z plane. These angles are chosen either to alleviate loads, or to solve geometric problems, sometimes related to gear retraction.

An equivalent model general arrangement drawing of the aircraft could be constructed, to assist in defining the equivalent model components which relate to the reduced axis set. The objective in designing the equivalent model is to reduce as far as practical the intermediate axis systems between the ground reference axis system (earth axes) and the aircraft reference axes (inertial body axes). Wheel hubs are horizontal, wheel planes of rotation are vertical, forces in the equivalent struts are vertical (all relative to aircraft reference axes), and the point of application of the forces is no longer at the point of attachment of the real gear. The forces, rates, and displacements of the equivalent gear no longer have a physical significance. If needed, an inverse equivalent model could also be constructed, to calculate off-line the approximate loads seen by the real gear, from equivalent model parameters recorded in real-time operation.

3.3   Combined Strut/Tire Model

As well as serving other purposes, pneumatic tires insulate the vehicle from high frequency vibrations. The wheel/tire combination has a high natural frequency, and low damping. During a heavy landing, it absorbs little of the energy which must be dissipated to reduce the high sink rate to zero. This function is performed by the oleo in the strut, which has a much lower natural frequency, and high inherent damping. Also, the damping during compression of the strut is higher than during extension.

The combination of wheel/tire and strut may be compared in simple terms to a double spring, with at least an order of magnitude between the natural frequencies of each component. A high bandwidth model is needed to reproduce correctly the response to excitation near the natural

frequency of the wheel/tire, but a simple analysis shows that virtually no energy is transmitted to the aircraft c.g. Hence an equivalent model of lower bandwidth may be used for real-time simulation without compromising accuracy. The model is based on a single spring-mass, with stiffness and damping coefficients which take account of the strut and the wheel/tire. The derivation of these terms is given in Appendix 1. It is important that the equivalent model takes account of the stiffness of the tire; otherwise the static deflection errors become significant.

3.4   Wheel and Brake Modeling

Tire contact conditions, and the accurate representation of the resulting forces, is of paramount importance in a ground-roll model, and is discussed in Section 4. The need to calculate the rotational behavior of the wheels, including spin-up, is questionable. Wheel spin-up, from zero to the no slip rolling condition, takes a fraction of a second, and although tire wear and high loads occur, it is an event of little significance to the pilot. In real-time, a computer time frame of perhaps 1 ms is required. Because the time frame is so short, the forces generated during spin-up do not greatly affect the aircraft's trajectory or deceleration. Intuitively, main wheel spin-up causes a nose down pitching moment which could modify the landing control task. An off-line calculation can determine the magnitude of the pitching moment, and an open-loop input can be introduced at the moment of touchdown, as part of dressing the model (see Section 7.6).

The wheel braking mechanisms are also an area for compromise in the model. Large amounts of energy must be dissipated, high temperatures are generated, and the properties of the braking materials change. Rather than model the thermodynamic cycle, the effect of brake fade can be represented by dressing the model - reducing the braking friction coefficient as a function of operating conditions and the time intervals between braking application.

Consideration should also be given to the need for representation of the fully developed skid. Most aircraft (and many cars) are fitted with ABS, which prevents wheel lock due to excessive brake application. Most of the measured data on braking friction are from aircraft fitted with ABS, and factors to allow for ABS efficiency are available. Unless one of the purposes of the simulation is to develop an ABS system, the advantage of reduced model bandwidth makes it attractive to omit the simulation of locked wheel conditions.

3.5   Wheel Torsion Forces

The tire on a rolling wheel in contact with the ground produces a drag force, due to rolling braking friction, horizontally, in the plane of rotation. Lateral translation of the wheel produces both a side force, horizontally, at right angles to the plane of rotation, and a torsional force, about a vertical axis through the center of the wheel (Figure 3.3). The mechanisms producing these forces are complex, and accurate modeling is not a trivial task, as will be seen in the next two sections, which deal with translational forces. The behavior of the aircraft on the ground is entirely dependent on how well these forces are represented.

The torsional forces result from small offsets of the translational forces due to tire distortion. For a non-castoring wheel, they do not alter the trajectory of the aircraft, because they are balanced by torsional forces in the strut, and strut attachment to the aircraft. The torsional forces associated with a castored wheel are insignificant, leaving only the steering case to consider. Steering an aircraft on the ground is a low bandwidth task, compared to steering a car.

The driver of a car has a more intimate knowledge of the response to control, and is dealing with a more dynamic situation. Suspension, steering linkage, and force feedback all contribute to the feel of the car. In these circumstances, tire torsional forces cannot be neglected. It is highly unlikely that they influence the pilot's impression of aircraft steering, and if lack of computing capacity (or other considerations) make their representation difficult, their omission can probably be justified.

It is also worth noting that as the load on the wheel decreases, the magnitude of the torsional forces generated by the tire due to yaw decrease more rapidly than the translational forces (which decrease almost linearly) - Figure 3.4. The wheel tire design load is based on the fully loaded condition. Landing weights are much lighter, and aerodynamic forces reduce wheel loads during ground roll. In these circumstances, the case for ignoring tire torsional forces is even stronger.

4. Tire/Runway Surface Interface

4.1 General

Extensive research (References 8 -17) has been performed since the introduction of jet transport aircraft in the late 1950's on the factors influencing tire/runway surface friction capability, to develop the steering and stopping forces required for safe aircraft ground operations. The contact conditions between an aircraft tire and runway surface are critical in determining the cornering and retarding forces that act on the aircraft. These forces are the product of the vertical load (weight) on the tire, F_z, and a coefficient of friction, μ. The value of the coefficient of friction is dependent upon many factors, including: type, texture and roughness of the runway surface; type and amount of pavement contaminant, e.g. snow, ice, water; tire construction, tread design and inflation pressure; type and efficiency of Automatic Brake System (ABS); and aircraft ground speed.

4.2 Braking

Braking is the primary means of stopping the aircraft. When brakes are applied, the tire is constrained to rotate slower than the forward speed of the aircraft. The result is referred to as braking slip, and is usually expressed as a percentage, with zero percent representing free rolling (no braking) and 100 percent indicating locked wheel (full skid). The ABS is designed to modulate the brake pressure so that the tire operates approximately between 15 and 20 percent slip, which is close to the maximum braking friction. The chart in Figure 4.1 shows that when larger tire braking slip values occur, the braking force is reduced.

These longitudinal braking forces generated between the tire and the runway surface are usually classified by the following friction coefficients:

$\mu_{b\,max}$ - maximum braking friction coefficient

μ_{skid} - locked wheel friction coefficient

$\mu_{eff.}$ - effective braking friction coefficient as determined by ABS

4.3   Cornering

The other important force generated between the tire and runway surface is side or cornering force. Side forces are developed as the plane of a rolling tire is yawed relative to the aircraft's direction of motion, and act perpendicular to the wheel plane. As the yaw angle increases, so does the cornering force. Once the peak cornering force is reached, additional increase in yaw angle will reduce the cornering force. The side force variation with yaw angle shown in Figure 4.2 shows this effect.

These lateral tire side forces are usually classified by the following friction coefficients:

$\mu_{\psi\,max}$ - maximum lateral friction coefficient during unbraked yawed rolling

$\mu_{\psi\,lim}$ - maximum braking friction coefficient developed during combined braking and cornering

4.4   Combined Braking and Cornering

Aircraft tires must often generate both braking and cornering forces simultaneously, such as when making crosswind landings. High tire-to-surface loading will help maintain good braking and cornering. The degree to which cornering is lost due to combined braking and cornering depends on how much tire slip is developed. As the slip increases, the cornering force reduces, and at 100 percent slip (locked wheel) the tire cannot generate any sideforce, as indicated in Figure 4.1. During antiskid controlled braking, the degradation in tire side force depends upon the amount of tire slip the antiskid system allows.

4.5   Simulation Requirements

A complete simulation of the ground roll must include these variations in longitudinal and lateral forces generated between the tire and runway surface. Because of computing limitations, some simulators in the past have either had restricted application, or used memory-intensive look-up tables, to store data relating to friction coefficients. An alternative method is to use analytical functions for on-line computation of friction coefficients. Appendix 2 describes such a model, for one type of runway (Type C). Similar models could be formulated for other surfaces. Alternative functions, either for better accuracy or ease of implementation, could also be derived.

5.   Struts/Tires

The struts, wheels and tires attenuate and transfer loads from the ground to the airframe. Near instantaneous, high loads can occur, particularly at touch-down, and large amounts of energy must be absorbed by the oleos and brakes. The struts and tires transmit the forces which give control of steering and braking, and determine the ride quality of the aircraft on the ground. Suspension systems, for both road vehicles and aircraft, have evolved and been progressively developed over many years, which has resulted in high performance components of great complexity.

The success of a simulation of the ground roll is critically dependent on how well the struts and tires are modeled. Highly detailed models, such as those used in non-real-time calculations

associated with landing gear design, are not appropriated for real-time pilot in the loop simulation, because of their computing overhead. Nor is it possible to use linearized approximations of either the strut or the tire. Some of the considerations are discussed below.

5.1   Struts

Most high performance aircraft use a two-stage oleo-pneumatic strut on the main gear, to meet the diverse requirements of high stiffness and damping at touchdown, and lower stiffness and damping when taxiing. A simplified diagram of a two-stage strut is seen on Figure 5.1.

As the strut compresses, the piston in the main chamber forces oil through the main orifices, and the compression increases the gas pressure, for additional stiffness. Stiffness and damping of the strut is controlled by chamber and orifice areas, flapper valves, and metering pins. Seal and bearing friction effects may also be significant.

For flight simulation purposes, the internal state of the strut is of little interest. It approximates to a spring, with stiffness and damping which are discontinuous functions of closure, and rate of closure. This information, from the manufacturer's data sheets, allow a strut model to be formulated. For small perturbations about a given deflection, the local slope of the force/deflection curve gives a stiffness coefficient for use in linear analysis, for model validation. The modal parameters which define the dynamic response of the model at different loading conditions are calculated.

Most real-time simulations combine the tire and strut models into an equivalent spring, as discussed in Section 3.3, and Appendix 1. The behavior of the aircraft on the ground may then be analyzed, by combining its geometry and mass information with the nose and main gear equivalent strut models. Both the static and dynamic behavior must be calculated, since they are observed directly by the pilot. The static balance determines the attitude of the aircraft, and the pitch and heave modes are seen and felt by the pilot.

5.2   Tires

The friction coefficients defined in Section 4 describe the behavior of a pneumatic tire in contact with the ground. The vertical, longitudinal, and lateral forces transmitted to the tire by the strut cause deformation of the tire which generates reactionary forces, which are a function of the tire construction and dimensions, its inflation pressure and tread. The longitudinal and lateral forces are also a function of load, speed, surface contamination, tire slip angle, and degree of braking (References 17 and 18). The parameters which determine longitudinal forces are given in Section 4, and Appendix 2

The forces due to lateral slip of the tire, and the factors which affect them, also need to be understood. If a rolling wheel is subjected to a small lateral force, the tire produces an equal and opposite force, and the direction of the wheel changes by an angle ψ, the slip angle of the tire. If the lateral force is increased, a point is reached where the slip angle needed is not proportional to the applied force. Eventually the available friction can no longer balance the applied force (Figure 5.2) and gross sliding of the wheel occurs. This effect is most pronounced when the wheel is lightly loaded, and the runway is wet or slippery. It is important to simulate this non-linear behavior, at each wheel, even though it is complex in nature, and subject to many variables,

because it directly affects the handling qualities on the ground, and is often the cause of pilot control difficulties.

Many piloted simulators in the past have severely restricted the tire model, to economize on computing requirements - for example, by assuming only small tire slip angles, or by simplifying the model of runway contamination. More complete models have used multi-function look-up tables, for on-line retrieval of tire data, placing large demands on computer memory, and making an update into a major task. With the computer improvements now available, analytical functions can replace the look-up table method.

A model using analytical functions is described in Appendix 3. It is valid for large slip angles, and allows the parameters which influence tire side force to be varied continuously. The model correlates with the published data from the referenced sources. These sources also cover the torsional forces generated by the tire (see Section 3.5). A model for torsional forces, similar to the direct side force model, and using analytical functions, could be developed, for use in simulations in which the torsional forces are significant. For example, they would be needed in a model to represent wheel shimmy.

6. Model Structure

6.1 Model Elements

Models of complex systems are constructed from blocks which contain elements of the model. Each block represents a component of the model, such as the forces generated by the ground, or the position of the wheels, and the outputs of each block are used as inputs by other blocks. Careful choice of the elements contained in each block, reduces the links between blocks, and eases the construction and validation of the complete model. It is important that elements can be isolated and tested independently, as the model is built. It is convenient also if individual blocks can be replaced by alternative versions, of differing degrees of complexity, depending on the model application, without the need to re-validate the rest of the model.

An example of such a model structure is included in Reference 1. The five major blocks, A, B, C, D, E and F (Figure 6.1), are respectively normal wheel forces, strut dynamics, aircraft/runway geometry, friction forces, gear forces/moments, and kinematics. The reference also includes expanded diagrams of the blocks, taken directly from the NASA reports which describe the whole program (References 19, 20, 21). This large program was conducted in the 1970's by McDonnell Douglas in St. Louis (a simulation of the F4 on the ground) and by Douglas Aircraft Company in Los Angeles (a simulation of the DC9 on the ground). It represented a major achievement, not only in terms of the standard of modeling achieved, but also in the results obtained from pilot assessments, and the recommendations which emerged. For example, the importance of including runway roughness and the runway crown was identified.

Reference 1 includes the equations of motion used for this work, and an Appendix of the parameters and notation, converted to metric units. They highlight the magnitude of the modeling task. One purpose of this report is to suggest changes to the block structure described in Reference 3, partly to provide a more instinctive and flexible arrangement, and partly to allow the implementation of features proposed earlier in this report.

6.2   Block Diagram

A structural layout which gives good identification of signal flow paths and their relationship to the components of the model is seen on Figure 6.2.

Blocks 1, 2, 3 and 4, in the upper part of the layout, operate both in the airborne and in the ground-borne phases of the simulation. The equations used to mechanize these blocks will not be discussed, because they are well established and well covered in the literature (for example, Reference 22). Block 1 accounts for the forces and moments generated on the airframe by its progression through the air, by proximity to the ground (aerodynamic ground effect) and by the propulsion system. Block 2 contains the simulated flight control system, and the model in Block 3 accounts for atmospheric influences. Block 4 solves the kinematic equations which calculate the many parameters describing the state of the aircraft - rotational and linear accelerations, velocities, position and orientation in space, in convenient systems of axes. Some of these parameters are used as feed-backs in the flight control system; others are needed to drive simulator hardware, such as the visual and motion systems, and the cockpit displays.

Blocks A, B, C, D and E, in the lower half of the diagram, calculate the forces and moments applied to the aircraft by contact with the ground. They differ from Blocks 1, 2, 3 and 4 because they are multiplex - an independent set of blocks is required for the calculation of the forces and moments from each wheel (or equivalent wheel). In a simple aircraft model, three sets would be needed, to represent the nose wheel, port wheel and starboard wheel - but any number of wheels, in any configuration, can be accommodated in this way. It may also be desirable to include in the model other parts of the aircraft (such as a wingtip) which might inadvertently contact the ground, or an obstacle on the ground.

Computer implementation of the model is helped by using this structural layout - the equations solved in Blocks A-E are identical for each wheel. Only the data sets change, easing the programming and validation task. The layout of Figure 6.2 also allows blocks to be removed or replaced, depending on the desired complexity of the model. Blocks could be added - for example, to complement Block D, the horizontal forces produced by the tire, could be added a block to represent the torsional forces produced by the tire (Section 3.5). Using this structural layout, models could be constructed to simulate other problems, such as a road vehicle, or a bouncing ball.

6.2.1   Block A. The Ground Profile

This block receives the geographic x-y location of the tire, determines the height of the ground at that place, and subtracts it from the height of the tire relative to the ground datum, so that tire/strut compression occurs when the local height is less than zero. The height of the ground must be correlated with the data base used for the visual system, which could including the undulations in taxiways and parking areas, as well as buildings. A simpler task, but still omitted from most simulations of ground roll, is the representation of runway camber.

6.2.2   Block B. Vertical Gear Forces

This block provides the vertical force which the wheel and strut transfer from the ground to the aircraft, for use both in calculating the total force on the aircraft, and in calculating the tire

lateral forces (Block D). The model contained by the block simulates the dynamic behavior of the tire and the strut, as deflections are imposed, based on parameters loaded into the model. The trade off between the complexity of the tire/strut model and the accuracy required, in terms of accuracy and bandwidth, is discussed in Section 3.3 and Appendix 1. Block B also contains the transforms between aircraft body axes, strut axes, and earth axes.

6.2.3. Block C. Wheel Location and Translation

Information from Block 2, which solves the kinematic equations of the aircraft, is used in Block C to calculate the position and velocity in earth axes of the point of contact of the wheel. Account is taken of the orientation, rates of rotation, and translational velocities of the aircraft. The block contains the gear geometrical data which determines its location relative to the aircraft c.g. Vertical velocity and aircraft orientation are fed from Block C to Block B. Forward velocity and side velocity of the wheel are calculated in Block C, and are used in Block D to calculate tire slip angle and the lateral tire forces.

6.2.4. Block D. Horizontal Tire Forces

In this block, the braking and lateral forces generated by the tire are calculated from the braking and lateral friction coefficients corresponding to the wheel location, and from the vertical load, forward velocity, and slip angle of the tire. The forces are also dependent on two pilot control inputs - the degree of braking applied to the wheel, and the wheel steering angle. Appendix 3 describes a method of deriving the forces suitable for real-time simulation, as an alternative to look-up tables.

6.2.5 Block E. Wheel/Aircraft Transformations

Three orthogonal forces are transmitted from the ground to the point of attachment of the strut. The calculation of these forces can be simplified by the use of an equivalent wheel-strut model (see Section 3.2), to reduce the number of axes systems in the load path associated with most gear designs. Block E also transforms the forces into forces and moments in aircraft body axes, about the c.g.

6.2.6 Block F. Local conditions at the wheel

The forces calculated in Block D depend on several friction coefficients. They are a function of aircraft speed, runway surface type, surface contamination, and tire pressure. The relationships which relate to a type C runway are given in Appendix 2. With this model structure, the wheel (or equivalent wheel) forces are calculated independently for each wheel, and local conditions can be simulated. In consequence, realistic situations, such as wet patches on the runway, a wheel leaving the taxiway, or a deflated tire, can be accommodated.

6.3   Block Diagram Implementation

To illustrate the use of the model structure described above, consider the specific case of a simulation restricted to the aircraft longitudinal degrees of freedom - forward speed, vertical speed, and pitch. Also assume that no aerodynamic forces act on the aircraft, and that a conventional wheel layout applies (as in Appendix 4). The relevant block diagram is seen on Figure 6.3.

Blocks A-E are each duplicated, to calculate the behavior of the mainwheel and the nosewheel contributions. Without the lateral degrees of freedom, some of the blocks are simplified. Specifically, the Block D elements only receive aircraft ground speed, vertical load on the wheel, braking coefficients of friction, and the percentage of applied braking. Block D supplies to Block E the decelerating forces generated by the wheels. For flat ground, and for uniform runway surface conditions, Blocks A and F are trivial.

This standard of model could be used to compare a fully comprehensive model of the tire, wheel, and strut with the simpler forms of model recommended in Section 3.3. Alternatively, methods of representing the ground profile at each wheel could be tested, using a linearized tire/strut model, and then compared with more complex gear models. The use of a pilot in these comparisons would help to determine his sensitivity to the accuracy and bandwidth of the model.

7.   Existing Models

Prior to writing this paper, advice was sought from a range of simulation users on the quality of their current models. The response was positive and supportive. In general, a need was expressed to improve ground roll models, for a variety of reasons. In many cases, the model in use has not been changed over a period of years, the background and understanding of the basic model has to a large extent been lost, and desirable features are lacking. The documentation available to some users is part hand-written, and/or incomplete. Other users, in describing their models, are restricted by commercial considerations, but support this review. In some cases, the model in the simulator is a direct transfer from a model originally intended for non-real-time use (gear design). Some users reported occasional inexplicable behavior of their simulation. One example was that of the simulated aircraft rolling over during aggressive lateral maneuvers at high taxi speed. In these cases, it is usual to suspect the model - for example, the calculation of tire side forces.

It is instructive to compare some of the better-documented models with the earlier sections of this report. The following examples highlight features of existing models.

7.1   NASA/Boeing 747 Model (References 23, 24)

These references gives a comprehensive description of all aspects of a real-time model of the 747. Although it is more than twenty years old, this model is the basis of the model used in many commercial aircraft training simulators. It illustrates the central theme of this report: the need to compromise between model complexity and computer speed. The model uses an equivalent landing gear, combining the wing mounted and body mounted main gears into equivalent left and right gears at a mean location, and combining the wheel assemblies of each bogie into a single wheel, factored by the number of wheels on the bogie.

A combined strut/tire model is used, and the strut forces are calculated from non-linear stiffness and damping curves. A flat runway is assumed, and the only runway friction coefficient which is a function of contamination is the braking friction coefficient. The determination of wheel drag forces is seen on Figure 7.1.

To reduce the number of axis transformations, small angle approximations are used to calculate the body axis forces and moments due to gear compression. Wheel spin-up effects are neglected. (In a later Boeing model, spin-up is simulated by assuming that, on first mainwheel contact, full wheel braking is applied for 0.2 seconds. In this way, drag and pitching moment increments of roughly the right order are generated, without the need for a full representation of spin-up).

7.2   Space Shuttle

Many Space Shuttle simulation models have been developed to duplicate the Orbiter's flight and ground roll characteristics (Reference 25). The primary requirements of the tire friction math models (Reference 26) are to determine forces (normal, longitudinal, and lateral) on the landing gear, as well as tire wear behavior. Use is made of Euler transforms between the Orbiter body axes frame, the strut frame, the wheel frame, and the ground frame (the effects of the runway crown, surface texture and surface wetness are included). Non-linear curves of strut stiffness and damping coefficients are used with strut deflection to calculate forces in the struts. The current updated models (References 27, 28) include failed tire and vertical tire deflection dynamics, tire wear and hydroplaning effects, dry and wet cornering friction characteristics, braking friction performance and the interaction of braking and cornering. The detailed model of tire lateral forces and wear, which has been validated in flight tests with a specially modified CV-990 aircraft (References 29, 30) includes effects of tire slip angle, vertical load and lateral spring rate, together with vehicle ground speed and runway surface conditions. An example of the variation in Orbiter main gear tire side-force coefficient with yaw angle and load ratio (R) is shown in Figure 7.2. The load ratio is the ratio of the actual tire vertical load to the rated tire load, which is 60,900 pounds.

7.3   McDonnell Douglas C17

The model described in Reference 31 is a comprehensive description of the C17 during ground roll, for use in real-time simulation. In common with other real-time models, the unsprung weight of the wheels is ignored, but the tire deflection due to wheel load is calculated, to obtain the wheel axle height. Strut air loads and oil loads from look-up tables are used to calculate strut rates and deflections.

Each of the five struts (four main, one nose) are modeled, but the tires on each strut (Figure 7.3) are lumped, to act at a centroid. The model of braking friction and lateral friction is comprehensive, and includes the reduction in maximum friction associated with simultaneous braking and cornering. Wheel spin-up is represented. Tire scrub, when maneuvering at low speed, is modeled, and measured data is available for model validation purposes (Figure 7.4).

7.4   Aircraft Landing Gear Generic Model - Stirling Dynamics Ltd.

A non-real time model of the ground roll (Reference 32) has been developed by Stirling Dynamics of Bristol, UK, and used in the development of the landing gear of the Airbus A320. A simplified version, for real-time use, has been developed for the Defence Research Agency at Bedford, UK. The full model represents each component of the gear in great detail, and allows component models to be validated against specific tests, such as drop tests and dynamometer tests. The correct number of gear components (legs, wheels, and tires), with accurate geometry and linkages (Figure 7.5). The model allows comprehensive integrated dynamic analysis of a landing gear system.

The model is intended for gear design and trouble shooting. Finite element modeling is used for the leg structure, and represents the stiffness, loads, and behavior of joints, stays, and torque links. The representation of airframe structural modes may be included later.

7.5   Flight Simulation Model - University of Brighton, UK

For several years, the Control and Dynamics Research Unit at the University of Brighton has worked on modeling the transition from airborne to ground-borne flight (Reference 33). Concern is expressed regarding the approximations in current models, leading to inaccuracies and unrepresentative behavior. Examples of these inaccuracies are neglecting the unsprung mass, combining the tire/strut models, simplifying axis transformations, neglecting strut seal and bearing friction, and neglecting longitudinal and lateral tire deformations. The tire model is seen on Figure 7.6.

The system root equations are in state vector form, and the model requires an iteration rate of 1000 Hz.. It provides a linear solution at each iteration, as eigen values, for validation purposes. Reference 27 suggests that the bandwidth of "the pilot feel regime" is up to 12 Hz.

7.6   Transall C-160 Ground Handling Model (Reference 34)

As part of the development of the Transall C-160 training simulator, the Institute for Flight Mechanics at DLR, Braunschweig, developed the mathematical model, supported by an extensive flight and ground test program, including a new ground handling model. Components of the original model were replaced by equivalent models developed at DLR, which reduced the complexity of the model, with insignificant loss of simulator fidelity. For example, the unsprung mass was assumed to be zero. The reference makes several good points:

i)   aircraft tests showed that, for nominal symmetric braking, there was 5% variation between the associated port and starboard drag forces, with a consequent influence on the pilot's lateral steering task.

ii)   a necessary and adequate model of wheel spin-up is provided by applying a drag impulse for 0.2 seconds at wheel touchdown. A good match between simulator and aircraft was then achieved, in terms of deceleration, pitch attitude, and oleo compression (Figure 7.7).

iii)   a need was established to calculate tire side force as a function of wheel load, speed, and runway contamination.

iv)   to simulate the capability of the C-160 to use reverse thrust to taxi backwards, the equations of motion had to be modified.

The report concludes that to allow full model validation, a clearly arranged structure of the model is essential. The main criterion in determining the complexity of the model is pilot awareness, and the use of equivalent models is recommended.

7.7   CAE Ground Model

In the past decade, CAE, Montreal, Canada, have put a major effort (over 10,000 man-hours) into developing a new model of aircraft ground handling for use in real-time simulation. It eliminates many of the simplifications of previous models, which were imposed by lack of computing capacity. Features of the model are:

i)   struts and tires are not combined into an equivalent single spring, but are represented individually. To do so requires a computer iteration rate of 900 Hz.,

ii)   wheel spin-up, tire skid ratio, and locked wheel skid, are modeled, allowing full modeling of the ABS (with the consequential need for high computer iteration rate),

iii)   the force on each individual tire is calculated, rather than using an equivalent all the wheels on a bogey. In the case of the Boeing 747, 18 tires are simulated,

iv)   the simulation of runway contamination includes dry, wet, flooded, with or without rubber residue, dry and wet snow, slush, frozen and melting ice. The depth of contamination can be varied, and can be in patches,

v)   tire failure simulation includes all contributory factors - wheel lock, excessive taxiing, hard landing, ambient temperature, and brake temperature,

vi)   detailed modeling of runway roughness.

CAE report favorable comments from the pilots on the additional realism that this model provides, including more realistic bounce due to runway roughness, and better directional control on the runway.

These examples of ground models show marked differences in approach. The application largely dictates the complexity of the model, and the features which are incorporated. Many of the ideas for model improvements which have been presented earlier in this report are vindicated - for example, the need to give more attention to the modeling of runway surface conditions, of the forces generated by the tires, and of runway contours. They also highlight the question of the model bandwidth needed for pilot in the loop, real-time simulation. Earlier in this report, it is argued that phase and gain relationships need only be preserved up to 5 Hz.; higher frequencies can be super-imposed by dressing the model. Clearly, the Brighton and CAE models do not accept this technique. A better understanding of the benefits of high bandwidth in real-time

models is needed. The features of the high bandwidth models which result in improved subjective acceptance of the simulation need to be isolated, through time histories of response to various forms of excitation, and by trials with successive simplifications of the model.

8.   Pilot Cueing

The emphasis in this report is on the mathematical model needed to describe the ground roll, particularly with respect to the forces generated by wheel contact with the ground. In Reference 1, attention is given to conditions prior to wheel contact, and the difficulties associated with simulating the flare maneuver. The critical parameters for the visual display are identified as wide field of view (to allow accurate orientation in roll and pitch to be achieved), and high resolution (to assist in the judgment of height and distance). The deterioration in performance, in terms of sink rate on touch-down due to display latency, is quantified. Modern display systems can address each of these areas, and help to achieve a closer representation of the landing flare maneuver, particularly when linked to motion and aural cues.

At touchdown, pilots are quickly aware of ground contact, and change their control strategy. Simulators must also give the appropriate cues, through the motion and noise systems. On some aircraft, pilots claim that changes in noise are useful during the flare. Immediately after touchdown, as well as any audio cues, such as wheel rumble, the pilot is likely to be aware of structural mode excitation, due to runway surface undulations or tar strips (which may also give a speed cue). He also senses the deceleration provided by braking and other means, and relates them to runway surface conditions and available stopping distance.

During ground roll and taxiing, the outside world visual display requirements still call for a wide field of view, both downwards and in azimuth, and good resolution, so that ground traffic, signs, markings, indicators and personnel can be detected. The textural quality of the runway surface is important, since it allows the pilot to differentiate between heading change and drift, during ground roll. The visual system must reflect the weather conditions and the appearance of the runway in precipitation, including patchiness, and must be consistent with the degree of contamination selected in the mathematical model.

Similarly, the data base of the visual system should include the contours of the airfield and taxiways, runway slope and camber. As stated earlier, many current flight simulators only represent flat ground. Slopes on runways and taxiways add to the pilot's workload when maneuvering on the ground, and contribute to the engine handling and braking techniques required for safe operation. Modern simulators can be given the capability to represent stressful situations, such as high weight operation during an aborted take-off, or following brake failure on landing, on a flooded runway with maximum crosswind, and an unhelpful slope.

Pilot workload during take-off and landing roll is high, the energy state of the aircraft is changing rapidly, and the level of noise and vibration is higher than in other flight phases. Successful simulation therefore calls for a high degree of realism, to ensure that pilots behave in the same manner as they do in flight. The requirement for realism is discussed in Section 2.4. The cues needed for realism are spread over a large range of frequencies, using a combination of the audio, motion, vibration, feel, and visual systems. Noise and vibrations contribute to 'atmospheric' cueing, and help the pilot to recognize the aircraft. Aircraft differ greatly with respect to ride quality on the ground. It is obvious that small aircraft give the pilot a bumpier ride over undulating ground than large aircraft. A second factor is the tire/suspension system design -

high tire pressures result in a harsher ride for the pilot. There will also be a difference in ride if the pilot is near a structural node, or close to the nose-wheel attachment point.

Visual and motion cues also help the pilot to recognize the type of aircraft he is flying - its physical size, and where he is, relative to the c.g., the wig-tips and the ground. Some of the physical sensations are entirely due to his location in the airframe. The pilots of most modern jet aircraft are high above, and well forward of, the c.g.. In older fighters - piston-engine tail-sitters - the pilot is aft of the c.g. (with severely restricted forward view of the ground). There are considerable differences between flying such aircraft and their successors, based solely on pilot location. Spitfire pilots speak of 'following the engine around', or 'being strapped to the tail'; jet fighter pilots in comparison 'have a machine strapped on their back'. There is even a difference in feel between flying tandem two-seat trainers from the front or the back seat.

It is vital, therefore, that in simulating an aircraft in ground roll, the reference point for the inputs to the visual and motion systems (accelerations, rates, and displacements) is the pilot's eye point, and not at the c.g.. A common criticism by pilots of ground handling in simulators is that the steering is not as precise as the aircraft. If the mathematical model is not at fault, then the visual or motion cueing should be examined. If the pilot is located ahead of the c.g., in response to a steering command, significantly higher lateral acceleration and lateral displacement occur at the cockpit than at the c.g. (see Appendix 4, Section A 4.3). These feedbacks provide the pilot with lead information, and assist the closed loop control task.

The simulation of handling qualities and ride qualities on the ground have been largely neglected by researchers. Effort in both areas would be of benefit to most users of flight simulators. One such study could be an investigation of the influence of pilot location on steering on the ground, both at high speed on the runway, and at low speed, in tight maneuvers. The contribution of motion cues, including suitable drive laws, could be part of the study.

9.   Conclusions

9.1   Prior to this report, discussions with users of flight simulation showed that many existing simulators are criticized by pilots for the way they represent the aircraft on the ground. The ground roll models are, in some cases, out-dated, and badly documented. It is timely, therefore, to review the requirements for the simulation of this phase of flight, and to examine methods of implementation.

9.2   Hardware and software improvements in the last decade can be used to enhance the capability of flight simulators in ground roll. Increased computer capacity can be used to improve the modeling of ground contact conditions, and the forces generated between the wheels and the runway surface. The effects of ground undulations, slopes, and runway camber can be represented, and coordinated with visual cues from the image generator.

9.3   The report highlights the differences in requirements for non-real-time simulation, intended for component design purposes, and real-time pilot-in-the-loop simulation, for pilot training and handling qualities research. One difference is the lower model bandwidth which can be used in the latter case. Although the pilot is receptive over a large bandwidth (including audio frequencies), his ability and opportunity for closed loop control is not higher than 2 or 3 Hz. Above this frequency, it should be possible to use model modifications, such as equivalent

models, and dressing the model, which do not detract from the realism of the simulation, but which ease the computing task. The choice of bandwidth is still an open issue.

9.4   Depending on the application of the simulation, trade-offs can be made between the complexity of the model, and accuracy. It is suggested that little is lost by combining components into a single model, such as representing a multi-wheel bogie as a single point of contact, or by combining the dynamic response of the strut and tire. It is also economical to reduce the number of real-time axis transformations, by prior reduction of the complex load paths.

9.5   A good representation of wheel braking forces and wheel side forces, in the frequency band of the pilot's control inputs, is essential. The need for high bandwidth may be reduced by avoiding a full simulation of wheel spin-up, and if ABS is assumed. The Appendices contain methods of representing braking and side force friction coefficients by analytical functions, valid over a large range of operating conditions.

9.6   A key element in simulating the ground roll is the structure of the model. The model layout should allow the interaction between model components (the airframe, the struts, the tires and the ground) to be readily understood. It must be possible to replace components by simpler or more complex models, to permit static and dynamic testing, and validation. Respect must be given to the oft-heard cry for standardization, in the choice of notation and methods. Differences in this regard are common between existing ground roll models, but users seem to be open to change.

9.7   To meet past pilot criticisms, more attention must be given to the provision of the essential cues used in this phase of flight. It is important that visual and motion cues are referenced to the pilot's position, and not the c.g., to allow:

  i)   unambiguous detection by the pilot of aircraft heading and track (to determine wheel slip), by good visual cueing, and

  ii)   motion cueing of accelerations at the cockpit (pilots are very aware of location relative to the c.g.).

    It is also important to provide atmospheric cueing - the noises and vibrations, often intense, which characterize different phases of operations on the ground.

9.8   Topics for research which emerge from this report are as follows:

  i)   build a new generic model of the ground roll phase of flight, of general availability, based on either the structure described in this report, or an existing structure incorporating the features recommended in this report. Requirements for the model include good documentation, and a level of standardization to allow an exchange of components between users.

  ii)   develop testing and validation methods for the model (and other models) based both on analysis (static balance calculations and time histories of dynamic response, with and without aerodynamic terms), and on measurements from aircraft. A progressive build-up in degrees of freedom is recommended.

iii)   investigate new methods of component modeling. Models could include additional types of runway and taxiing surface, different levels of strut complexity, and a model of undulating ground to provide in real-time the height at all ground contact points for a moving aircraft.

iv)   practical experiments to isolate the motion and visual cues which contribute to a) pilot control tasks in ground-borne operation, and b) the realism of the simulator.

10.   References

1.   A G Barnes, T J Yager "Simulation of Aircraft Behavior on and close to the Ground".
        AGARDograph AG 285   January 1985

2.   A G Barnes "Modeling Requirements in Flight Simulation", The Aeronautical Journal of the Royal Aeronautical Society.
        Paper No. 2010   December 1994

3.   A G Barnes "The Compromise between Accuracy and Realism in Flight Simulation", Proceedings of AIAA Flight Simulation Technologies Conference, New Orleans, August 12-14, 1991.
        AIAA -91-2920   August 1991

4.   FAA Advisory Circular "Airplane Simulator Qualification".
        AC 120-40B   August 1991

5.   Ed. AA Woodfield "Aircraft and Sub-system Certification by Piloted Simulation", Report from AGARD FMP WG16.
        AGARD Advisory Report AR 278   1994

6.   F O Smetana "Introduction to the Control of Dynamic Systems", AIAA Publication.
        ISBN 1-56347-083-7   1994

7.   J Y Wong "Theory of Ground Vehicles".
        ISBN 0-471-03470-3 John Wiley & Sons   1978

8.   UK Engineering Sciences Data Unit "Friction and Retarding Forces on Aircraft Tires, Part 2. Braking Forces".
        ESDU 71026   1981

9.   UK Engineering Sciences Data Unit "Friction and Retarding Forces on Aircraft Tires. Part 4. Estimation of Effects of Yaw."
        ESDU 86016   1986

10.   T J Yager "A Summary of Recent Aircraft/Ground Vehicle Friction Measurement Tests", SAE Aerospace Technology Conference, Anaheim, Ca.
                                                                    October 1988

11.   T J Yager, W A Vogler, P Baldasare "Summary Report on Aircraft and Ground Vehicle Friction Correlation Test Results obtained under Winter Runway Conditions".
NASA TM 100506   March 1988

12.   H K Brewer "Parameters affecting Tire Control Forces".
AIAA Paper 74-966   1974

13.   T J Yager "Factors influencing Ground Handling Performance".
NASA TM 85652   June 1983

14.   T J Yager, E J White "Recent progress towards predicting Aircraft Ground Handling Performance"
NASA TM 81952   March 1981

15.   T J Yager, W A Vogler, P Baldasare "Evaluation of Two Transport Aircraft and several Ground Test Vehicle Friction Measurements obtained for various Runway Surface Types and Conditions".
NASA Tech Paper 2917   February 1990

16.   UK Engineering Sciences Data Unit "Friction and Retarding Forces on Aircraft Tires. Part 1. Introduction".
ESDU 71025   1971/April 1995

17.   R E Smiley, W B Horne "Mechanical Properties of Pneumatic Tires with special reference to Modern Aircraft Tires".
NASA TR 64   July 1957

18.   John A Tanner, Sandy M Stubbs, John L McCarey "Static and Yawed-Rolling Mechanical Properties of two Type VII Aircraft Tires".
NASA Technical Paper 1863   May 1981

19.   "Expansion of Flight Simulator Capability for Study and Solution of Aircraft Directional Control Problems on Runways", Phase I.
NASA CR 145084   March 1975

20.   "Expansion of Flight Simulator Capability for Study and Solution of Aircraft Directional Control Problems on Runways", Phase II.
NASA CR 145044   August 1975

21.   C W Kibbee "Expansion of Flight Simulator Capability for Study and Solution of Aircraft Directional Control Problems on Runways".
NASA CR 2970   April 1978

22.   B L Stevens, F L Lewis "Aircraft Control and Simulation", Wiley & Sons, N.Y.
ISBN 0-471-61397-5   1992

23.   C Rodney Hanke "The simulation of a large jet transport aircraft - Vol. 1 Mathematical model".
NASA CR 1756   March 1971

24. C Rodney Hanke et al. "The simulation of a jumbo jet transport aircraft - Vol.2 modeling data".
US National Technical Information Service N73-10027   September 1970

25. W M McGuire "6 DOF Gear/Ground Force Equations".
Honeywell   March 1987

26. NASA National Space Transportation System (NSTS) Report 08192, Revision A: "Math Models of Friction Characteristics for Orbiter Main and Nose Gear Tires".
April 1993

27. Robert H Daugherty, Sandy M Stubbs "The Effect of Runway Surface and Braking on Shuttle Orbiter Main Gear Tire Wear", Aerospace Technology Conference and Exposition, Anaheim, Ca.
SAE Paper 922038.   October 1992

28. Robert H Daugherty, Thomas J Yager, Sandy M Stubbs "Shuttle Landing Runway Modification to Improve Tire Spin-Up Wear Performance", Aerospace Technology Conference and Exposition, Anaheim, Ca.
SAE Paper 881402   October 1988

29. John F Carter, Christopher J Nagy "The NASA Landing Gear Test Airplane".
NASA TM 4703   June 1995

30. Robert H Daugherty, Thomas J Yager "Texture Modification of the Shuttle Landing Facility Runway at the NASA Kennedy Space Center".
NASA TM 110269   July 1996

31. J W Bunnell, SYRE, Moffett Field, Ca. Data sent to T J Yager
11 November 1994

32. A Shepherd et al. "The Simulation of Aircraft Landing Gear Dynamics".
Paper given at ICAS 92, Beijing, China.   21-25 September 1992

33. G G Kapadoukas, A Self "Taxonomy of Aircraft Ground Modal Behavior: a Brief Report"
Simulation 65:4 257-266 ISSN0037-5497/95   October 1995

34. D Fischenberg, W Monnich "C-160 Ground Handling Model Update using Taxi Test Data".
Paper 12 AGARD FVP Panel Symposium. Braunschweig   22-25 May 1995

11. Notation

		Units
A_g	Tire footprint area	ft^2
B	aircraft inertia in pitch	$kg\ m^2$
C	aircraft inertia in yaw	$kg\ m^2$
F_R	Rated tire load	lbs

F_x	Retarding force on tire due to braking, in plane of wheel rotation	N
F_y	Cornering force on a yawed tire, perpendicular to plane of wheel rotation	N
F_z	Vertical load on tire	N
N	Tire cornering power	N/rad
V	aircraft forward speed	knots
$X_{n,m}$	nosewheel, mainwheel longitudinal load	N
$Y_{n,m}$	nosewheel, mainwheel lateral load (body axes)	N
$Z_{n,m}$	nosewheel, mainwheel vertical load	N
a	distance of c.g. to nosewheel	m
b	distance of c.g. to mainwheel	m
d	Undeflected tire diameter	ins
d_m	linearized damping coefficient, mainwheel strut	kN/m/s
d_n	linearized damping coefficient, nosewheel strut	kN/m/s
d_s	strut/tire sprung mass damping coefficient	kN/m/s
d_u	strut/tire un-sprung mass damping coefficient	kN/m/s
h	subsidiary function to calculate μ_{lya}	
i	subsidiary function to calculate μ_{lya}	
j	subsidiary function to calculate μ_{lya}	
k_b	proportion of braking applied	
k_m	linearized stiffness coefficient, mainwheel strut	kN/m
k_n	linearized stiffness coefficient, nosewheel strut	kN/m
k_s	strut/tire sprung mass stiffness coefficient	kN/m
k_u	strut/tire un-sprung mass stiffness coefficient	kN/m
m	mass of aircraft	kg
m_s	sprung mass of aircraft	kg
m_u	un-sprung mass of aircraft	kg
p	tire pressure	psi
p_g	tire footprint pressure	psi
p_r	rated tire pressure	psi
r	aircraft yaw rate (body axes)	rad/s
s	braking slip ratio	
v	lateral velocity at c. g. (body axes)	m/s
v_m	lateral velocity at mainwheel (body axes)	m/s
v_n	lateral velocity at nosewheel (body axes)	m/s
v_n'	lateral velocity at nosewheel (nosewheel axes)	m/s
w	undeflected tire width	ins
x	subsidiary function to calculate cornering power	
z	vertical displacement of c.g.	m
z_m	vertical displacement of mainwheel axle	m
z_n	vertical displacement of nosewheel axle	m
δ	nosewheel steering angle	rad
λ	slip angle at c.g. $= v/V$	rad
λ_n	slip angle at nosewheel	rad
λ_m	slip angle at mainwheel	rad
$\mu_{\lambda n}$	lateral friction coefficient of nosewheel	
$\mu_{\lambda m}$	lateral friction coefficient of mainwheel	

$d\mu_{\lambda n}/d\lambda_n$	initial slope of $\mu_{\lambda n}$ v λ_n curve	
$d\mu_{\lambda m}/d\lambda_m$	initial slope of $\mu_{\lambda m}$ v λ_m curve	
δ'	vertical deflection of the tire	· ins
ϕ	subsidiary function to calculate cornering force	
ψ	tire yaw angle, between plane of wheel rotation and direction of motion	rad
μ	coefficient of friction	
$\mu_{b\max}$	maximum braking coefficient of friction	
μ_{eff}	braking effectiveness coefficient (dependent on automatic braking)	
μ_{skid}	friction coefficient of locked wheel (fully developed skid)	
μ_ψ	lateral friction coefficient	
$\mu_{\psi\lim}$	maximum attainable lateral friction coefficient in braked yawed rolling	
$\mu_{\psi\max}$	maximum attainable lateral friction coefficient in unbraked yawed rolling	
μ_{sya}	lateral friction coefficient for small angles of yaw	
μ_{lya}	lateral friction coefficient for large yaw angles	

12   Figures

AIRCRAFT MODEL

- MASS, INERTIAS, DIMENSIONS
- AERODYNAMIC FORCES AND MOMENTS
- STRUCTURAL LOADS AND DEFLECTIONS
- UNDERCARRIAGE FORCES AND MOMENTS: Struts, wheels, tyres, steering, braking
- FLIGHT CONTROL SYSTEM Algorithms, sensors, actuators
- ENGINE FORCES AND MOMENTS Turbine/Propeller Fuel flow Power off-take Thrust reverser
- ENGINE CONTROL SYSTEM Algorithms, sensors, actuators
- UTILITIES Fuel, hydraulics, electrics, pneumatics
- STORES MANAGEMENT SYSTEM Munitions, radar, EW
- FLIGHT MANAGEMENT SYSTEM Navigation, communication, GPWS, Warnings, failures
- AIR DATA SYSTEMS

AIR ENVIRONMENT MODEL

- STANDARD/NON-STANDARD ATMOSPHERE
- WINDS AND TURBULENCE
- CLOUDS, PRECIPITATION, LIGHTNING
- ICING CONDITIONS
- VISIBILITY, LIGHTING
- SEASONAL CHANGES
- STORMS, DOWNBURSTS, ROTOR WINDS
- OTHER AIRBORNE OBJECTS Co-operative, passive and hostile:- aircraft, airships, balloons, rockets, missiles, bullets, birds, dust, debris
- EMISSIONS AND REFLECTIONS Light, heat, smoke, IR, radio, radar

GROUND ENVIRONMENT MODEL

- GEOGRAPHIC LOCATION
- DATA BASE (DMA OR EQUIVALENT)
- MAPS, CHARTS
- LAND MASSES
- WATER
- TERRAIN FEATURES
- CULTURAL FEATURES
- AIRFIELD DETAILS Identification, Layout, Aids, Obstructions
- RUNWAY DETAILS Dimensions, contours, roughness, contamination
- GROUND-BORNE OBJECTS Stationary and moving Co-operative, passive and hostile
- EMISSIONS AND REFLECTIONS Light, heat, smoke, IR, radio, radar

Figure 2.1 Model elements for flight simulation
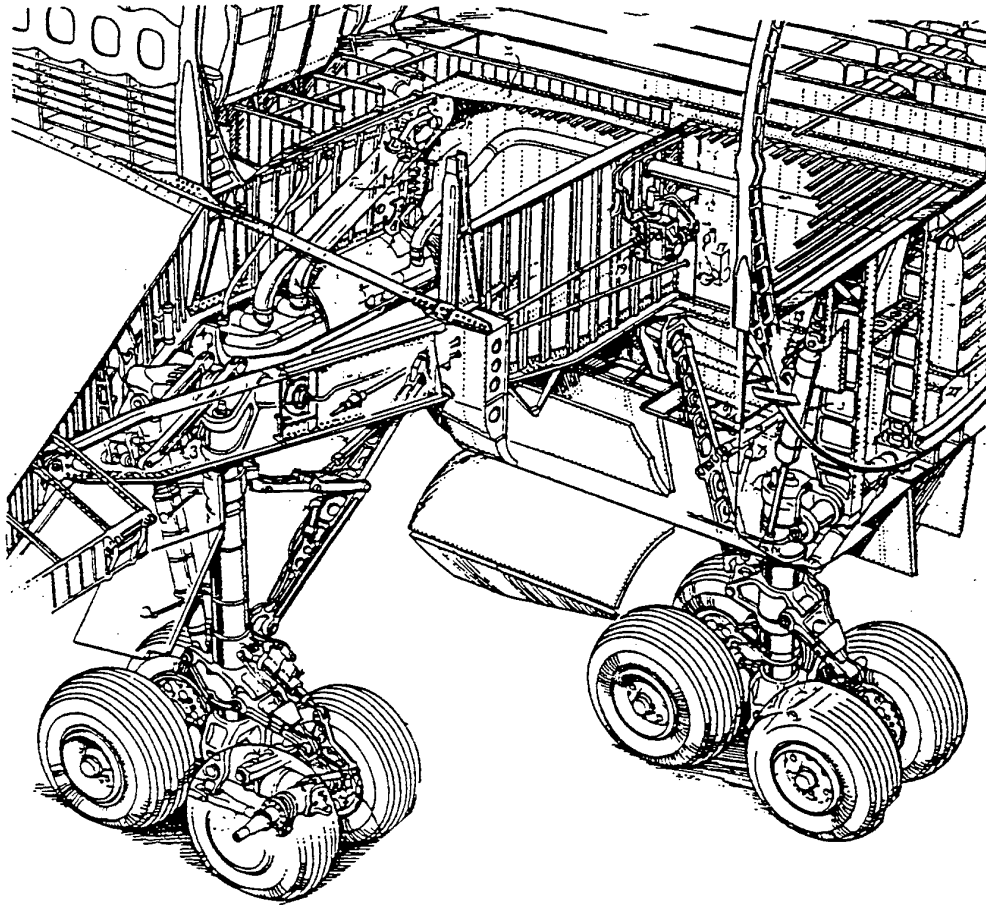
Figure 3.1 Boeing 747 main gear (port)
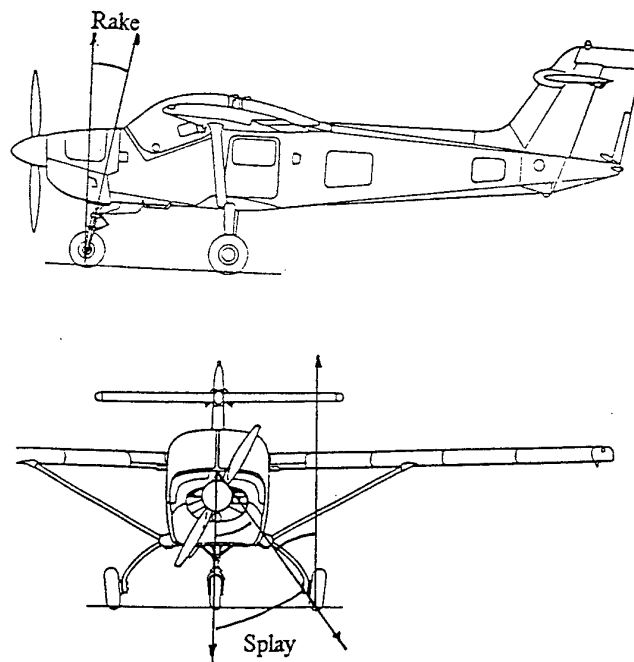
Figure 3.2   Rake and splay
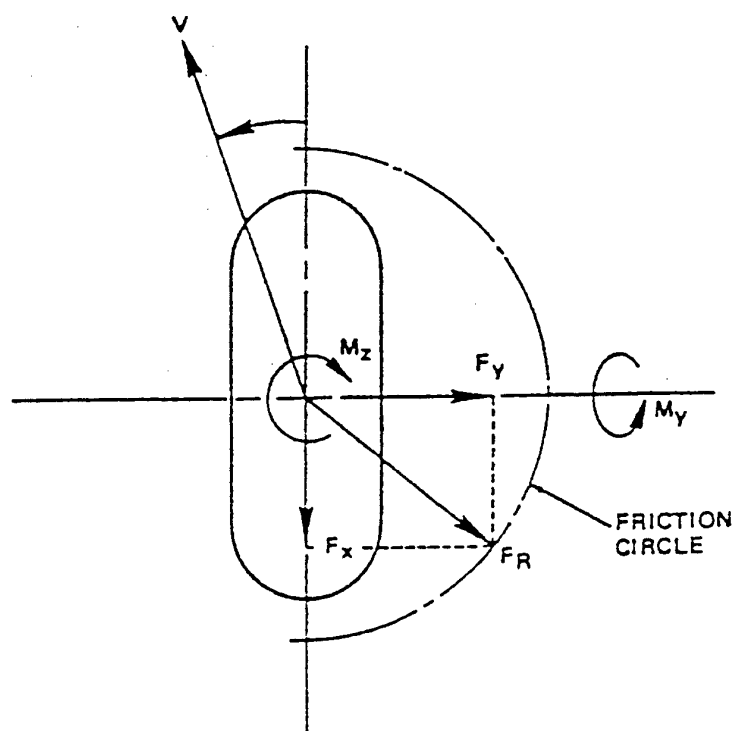
Figure 3.3 Rolling tire with braking and slip

Lateral Force vs. Slip Angle
25.0x9.0-13 Formula 1 Front Tire

Infl. = 21 psi

Lateral force (lb.) vs. Slip angle (deg.)

F_z ——— -1000 ·········· -800 – – – – -600 —··— -400

Aligning Torque vs. Slip Angle

Aligning torque (lb.-ft.) vs. Slip angle (deg.)

F_z ——— -1000 ·········· -800 – – – – -600 —··— -400
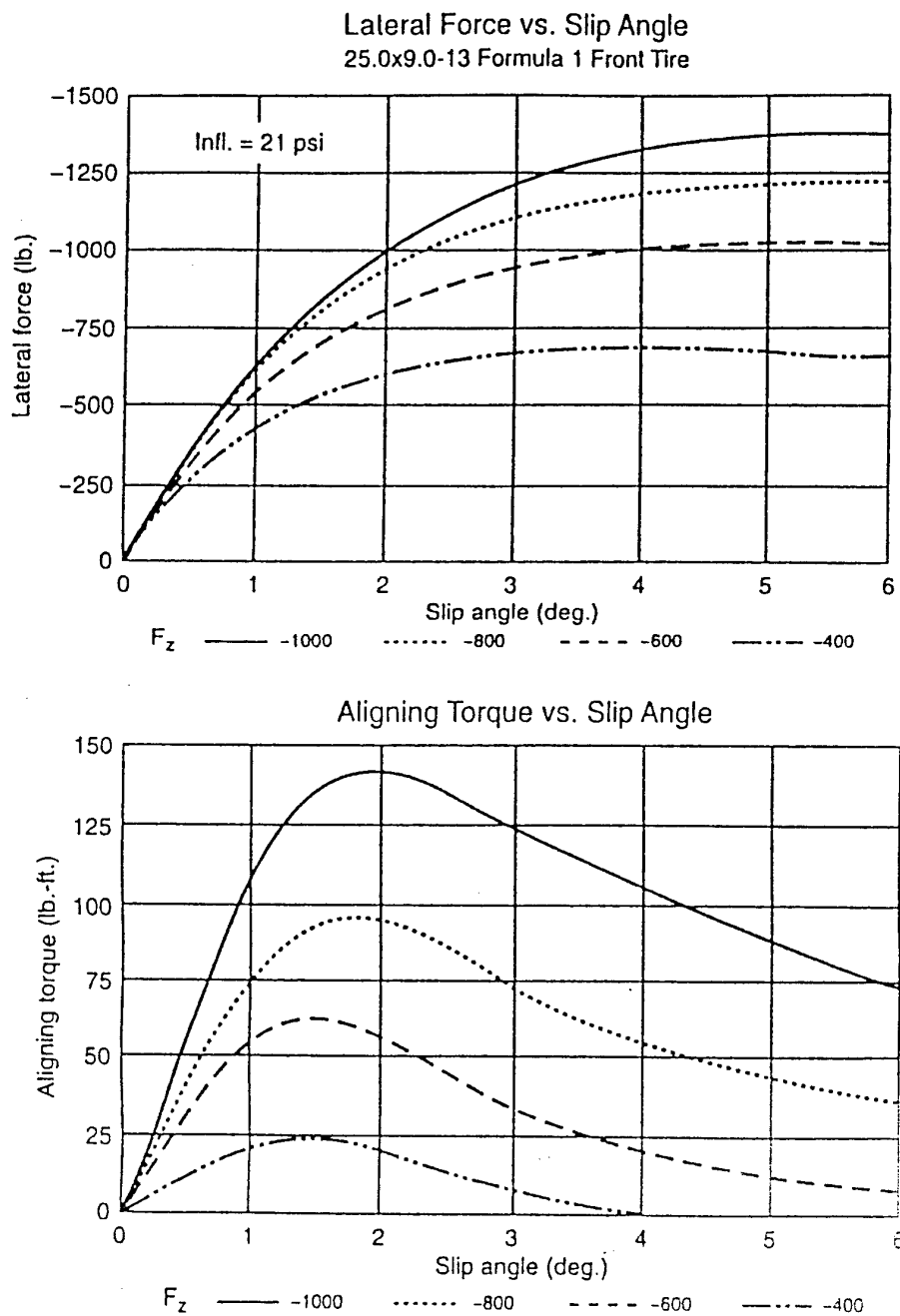
Figure 3.4   Lateral force and aligning torque v slip angle
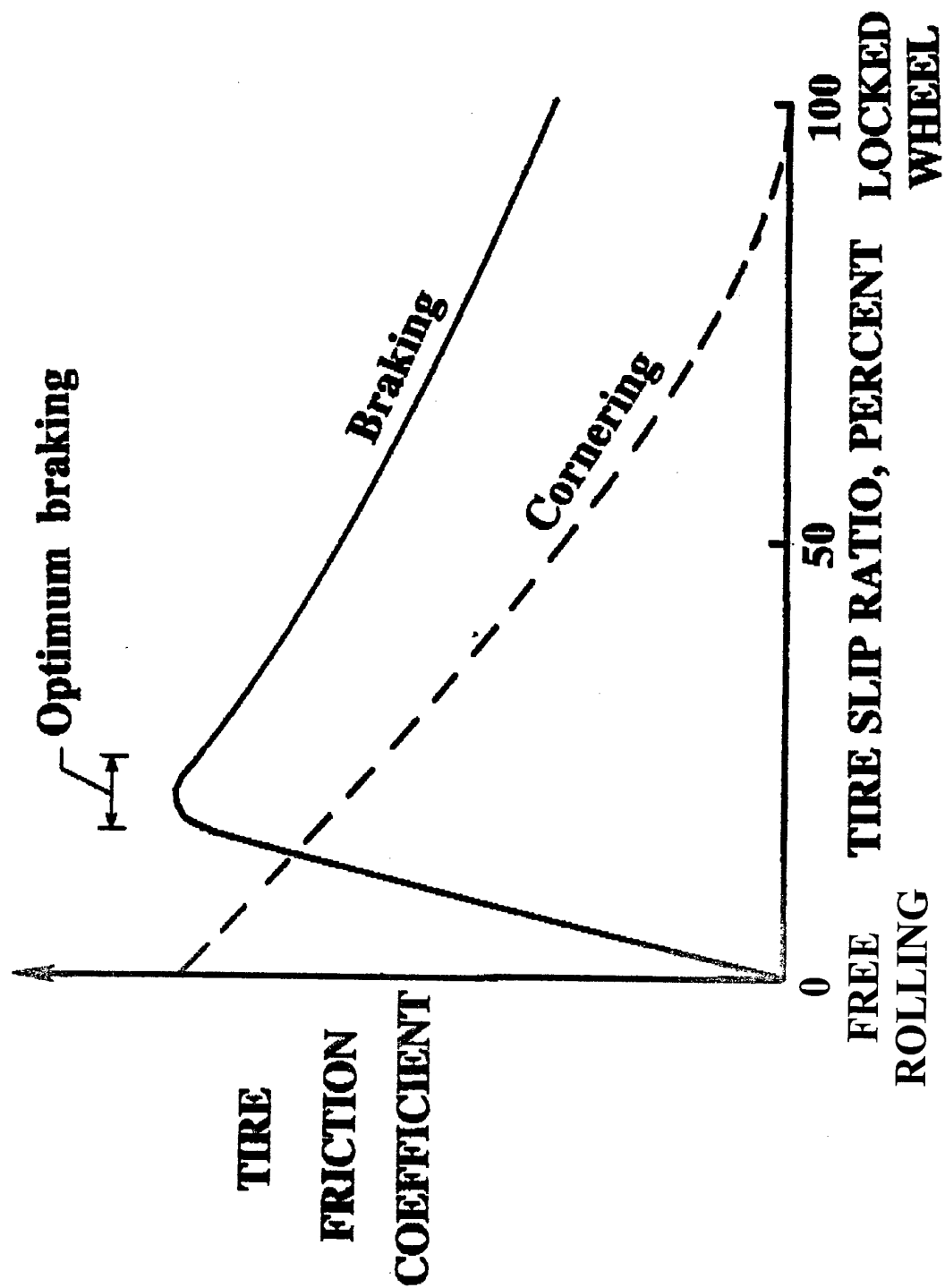
Figure 4.1   Variation in tire friction coefficient with slip ratio.

Figure 4.2 Tire side-force friction coefficient variation with yaw angle, speed and rated load.

49 X 17, Type VII, 26 PR aircraft tire; rated load = 176.1 kN (39.6 kips); dry concrete

COMPRESSION
DAMPING
CHAMBER

RECOIL
DAMPING
CHAMBER

DAMPING
CONTROL
PLATE

SEPARATOR
PISTONS

LOW PRESSURE
GAS CHAMBER

HIGH PRESSURE
GAS CHAMBER
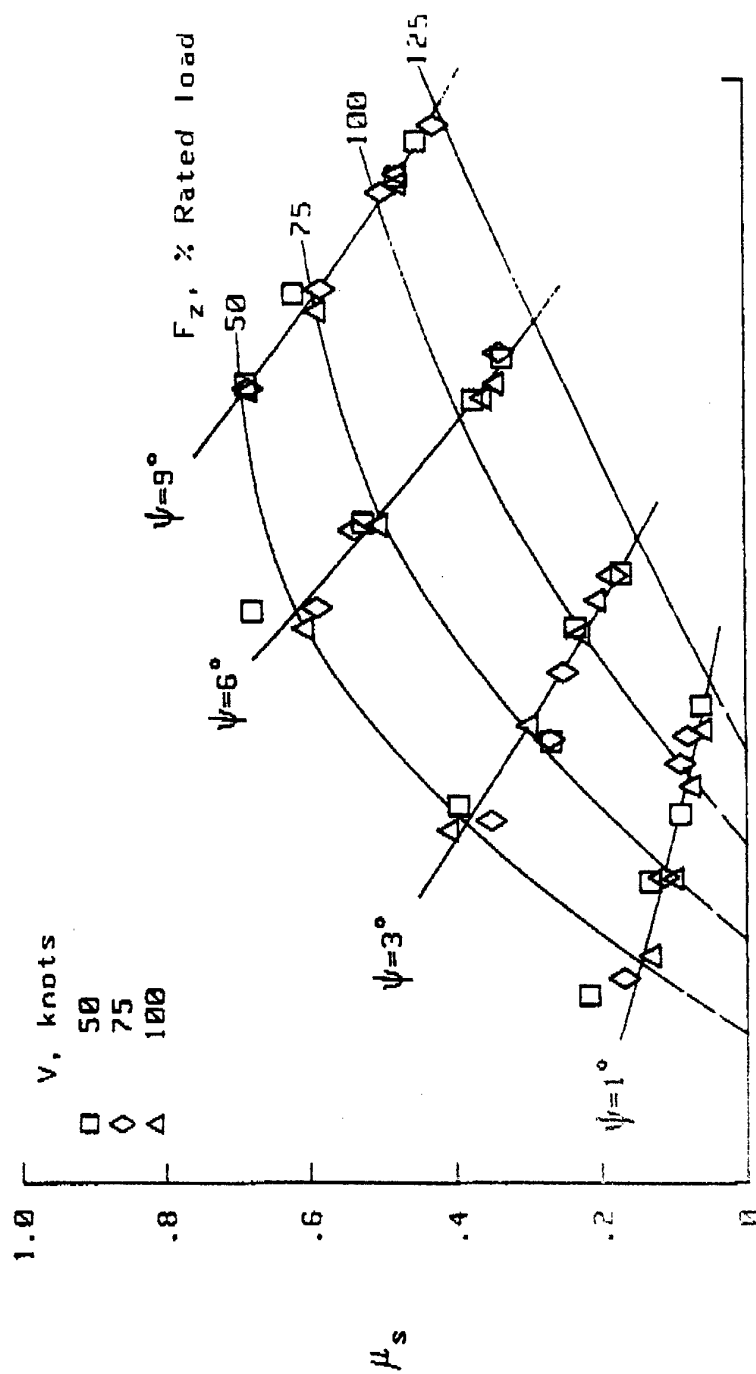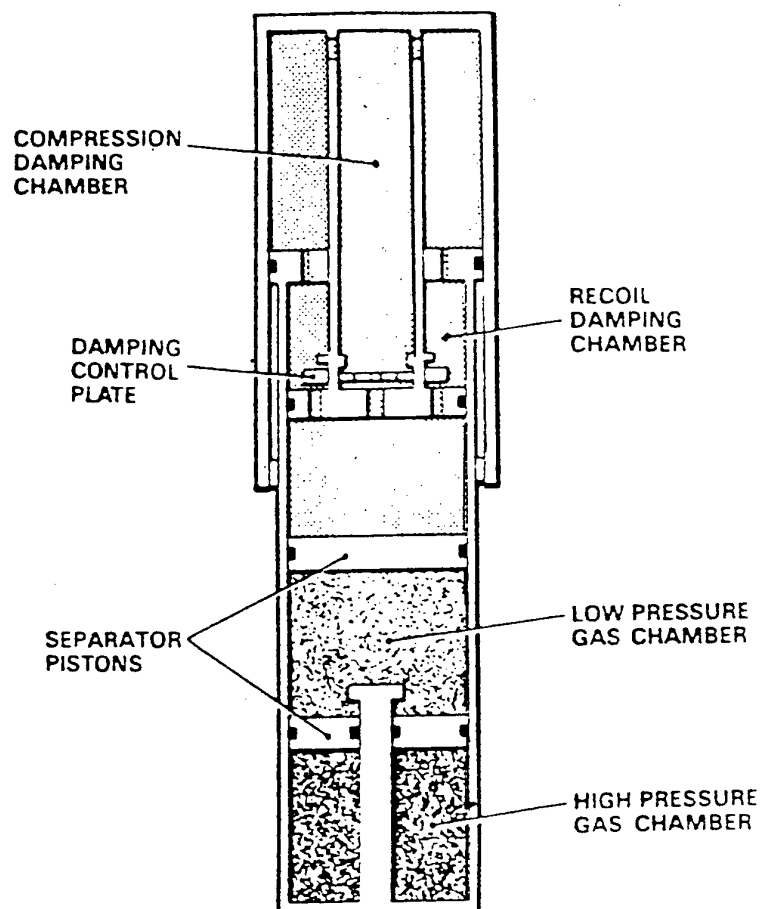
Figure 5.1 Main gear two-stage strut - schematic diagram

Figure 5.2 Tire side force variation with yaw angle, speed and rated load.

49 X 17, Type VII, 26 PR aircraft tire; rated load = 176.1 kN (39.6 kips); dry concrete
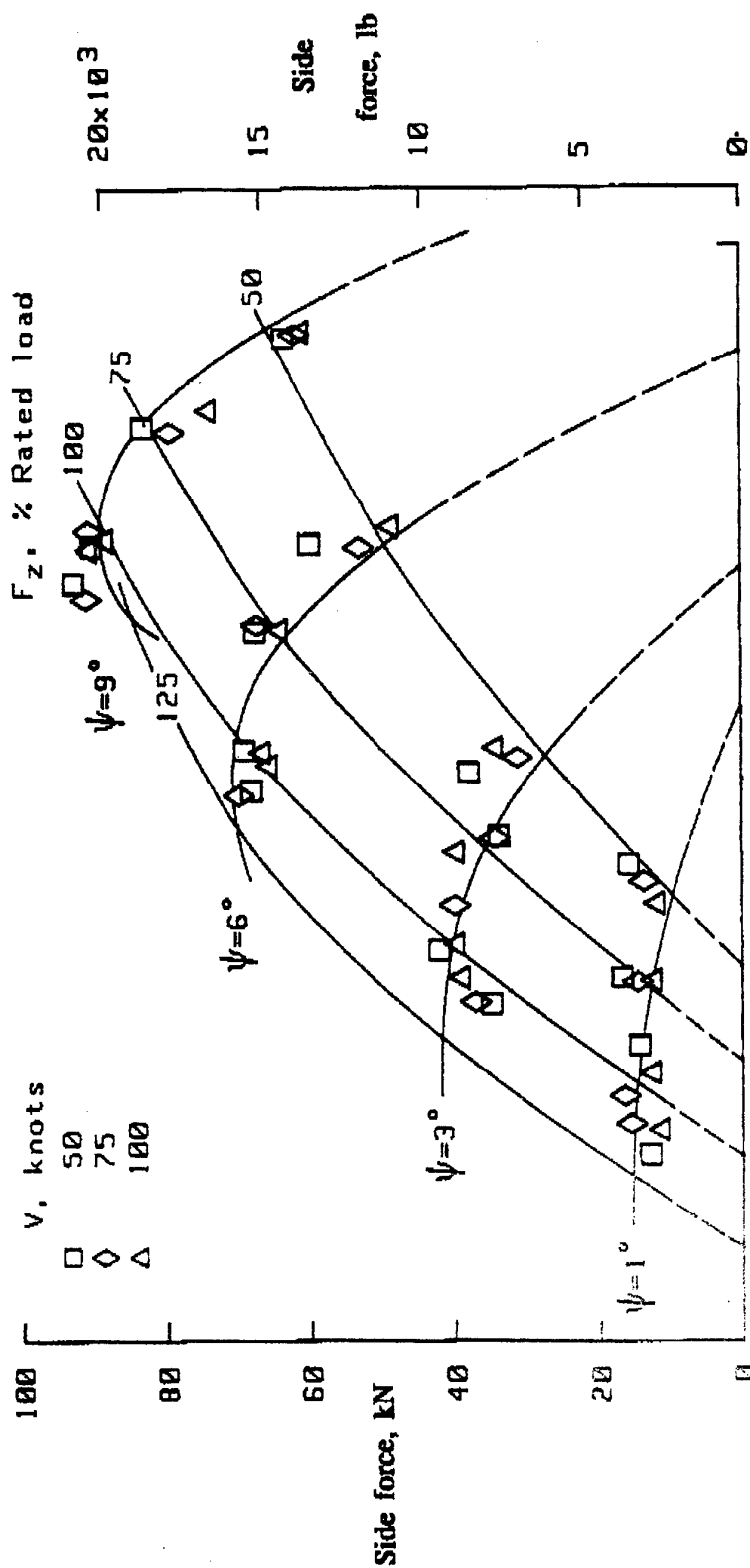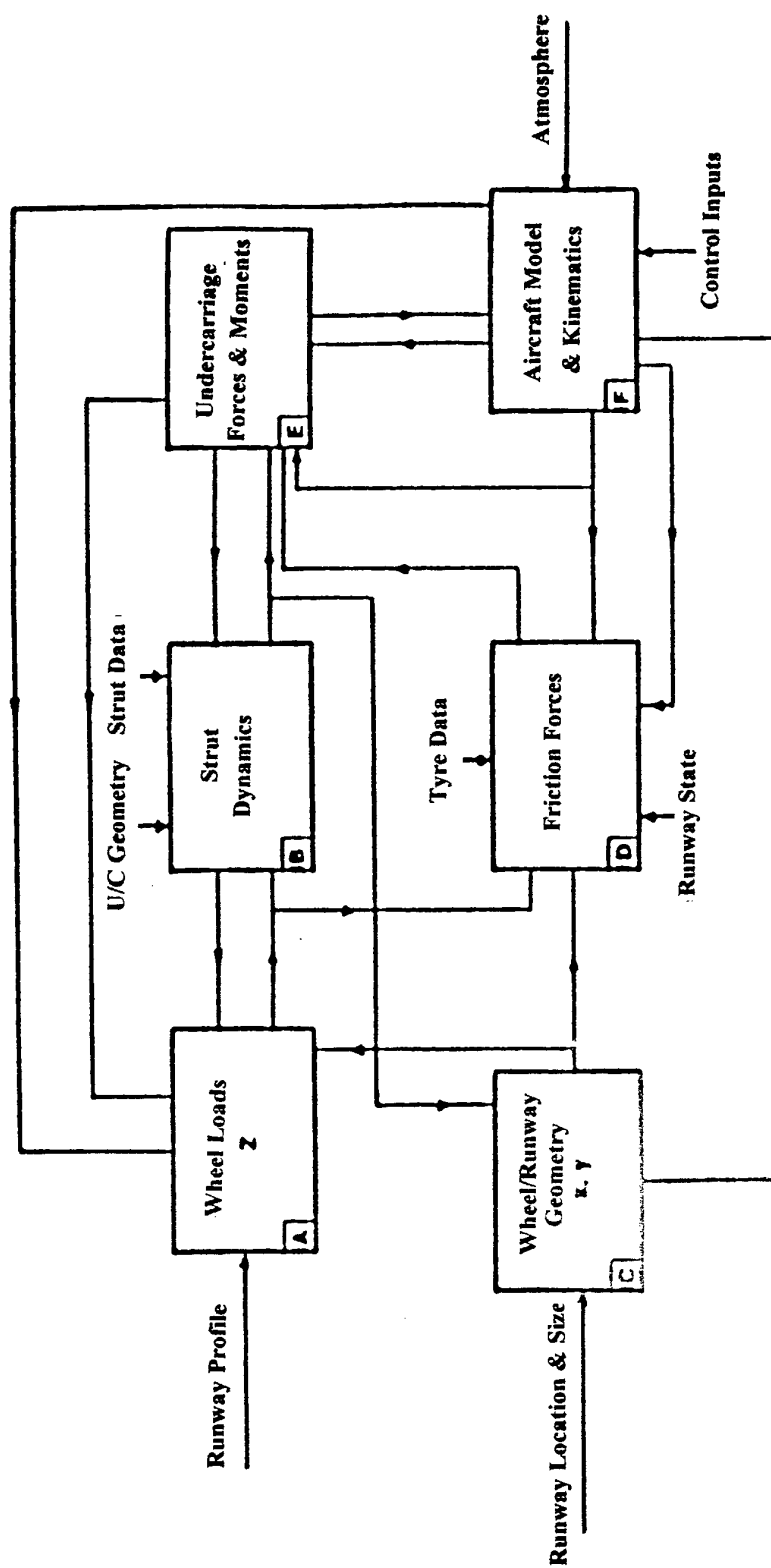
Figure 6.1 Model structure of reference 1
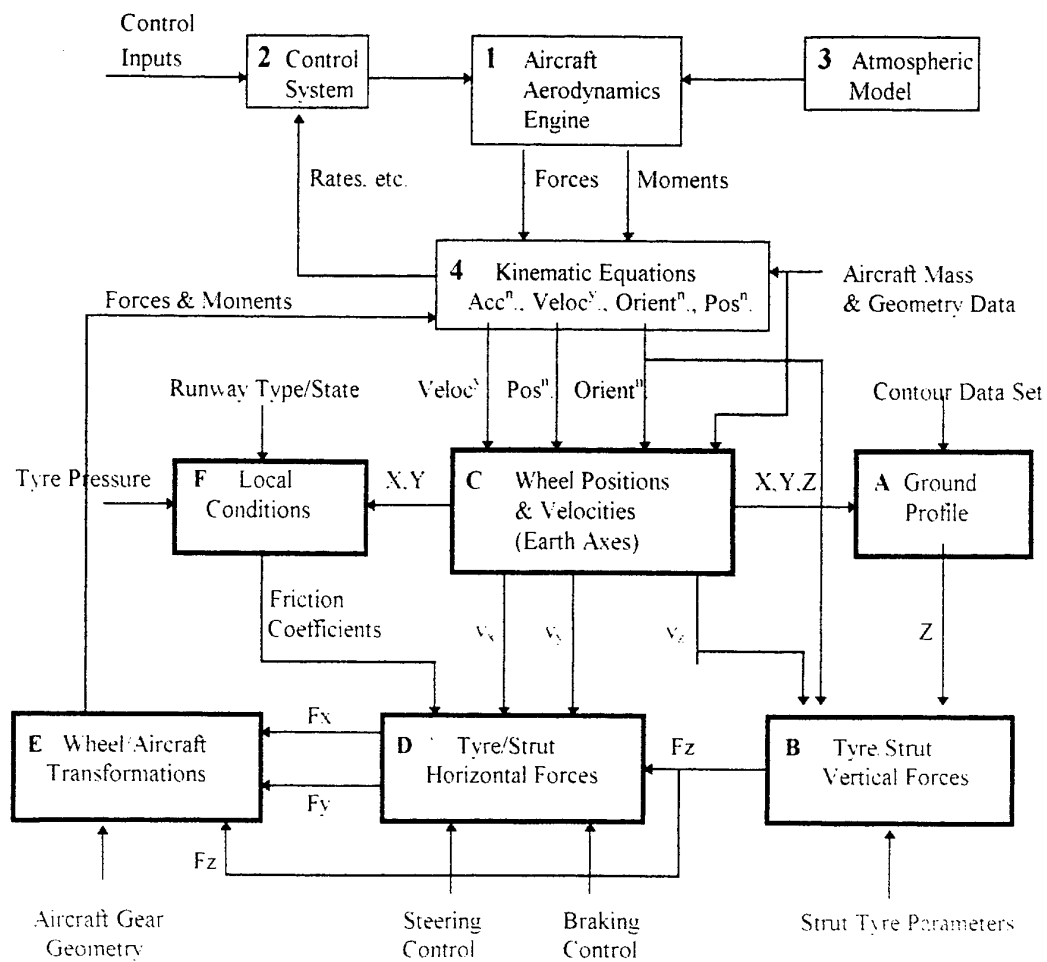
Figure 6.2 Structural model for ground roll simulation
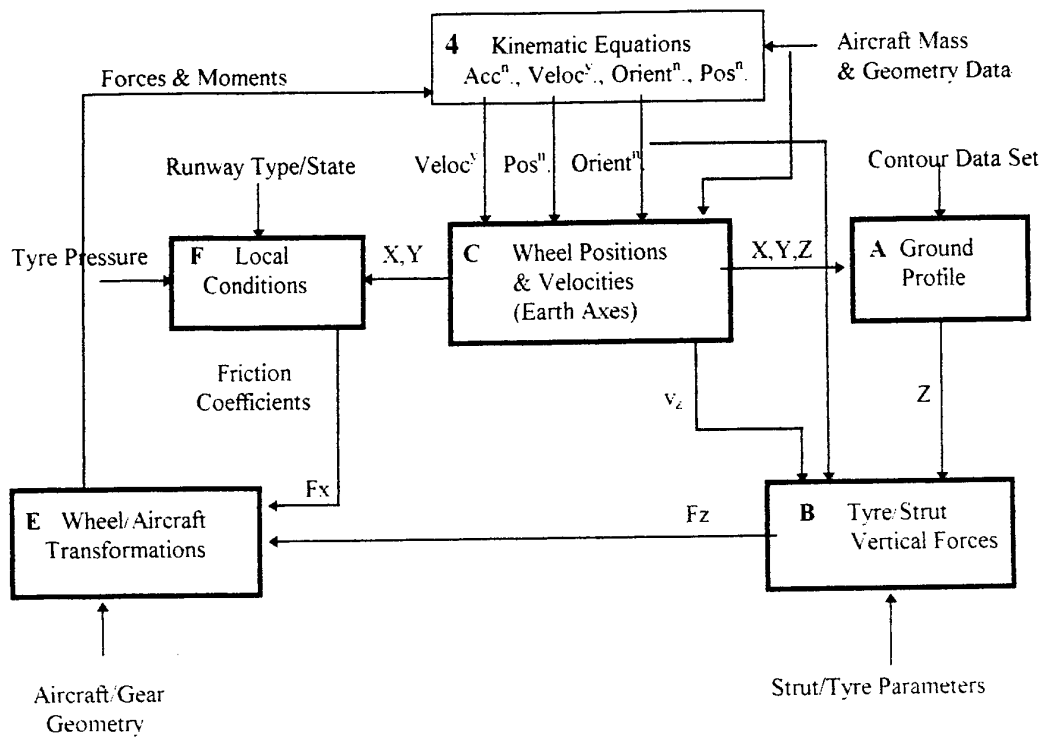
Figure 6.3   Structural model - longitudinal, without aerodynamic terms
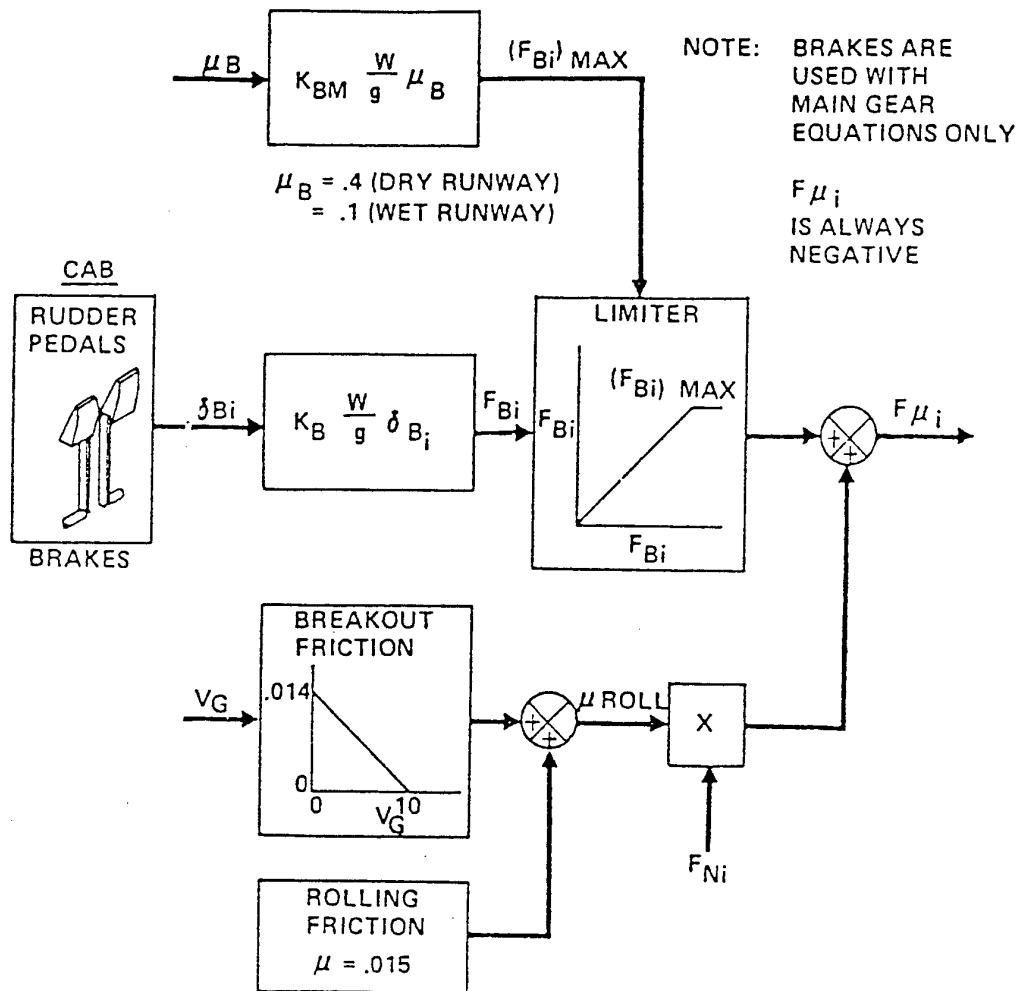
Figure 7.1 Wheel drag forces -Boeing /Nasa model
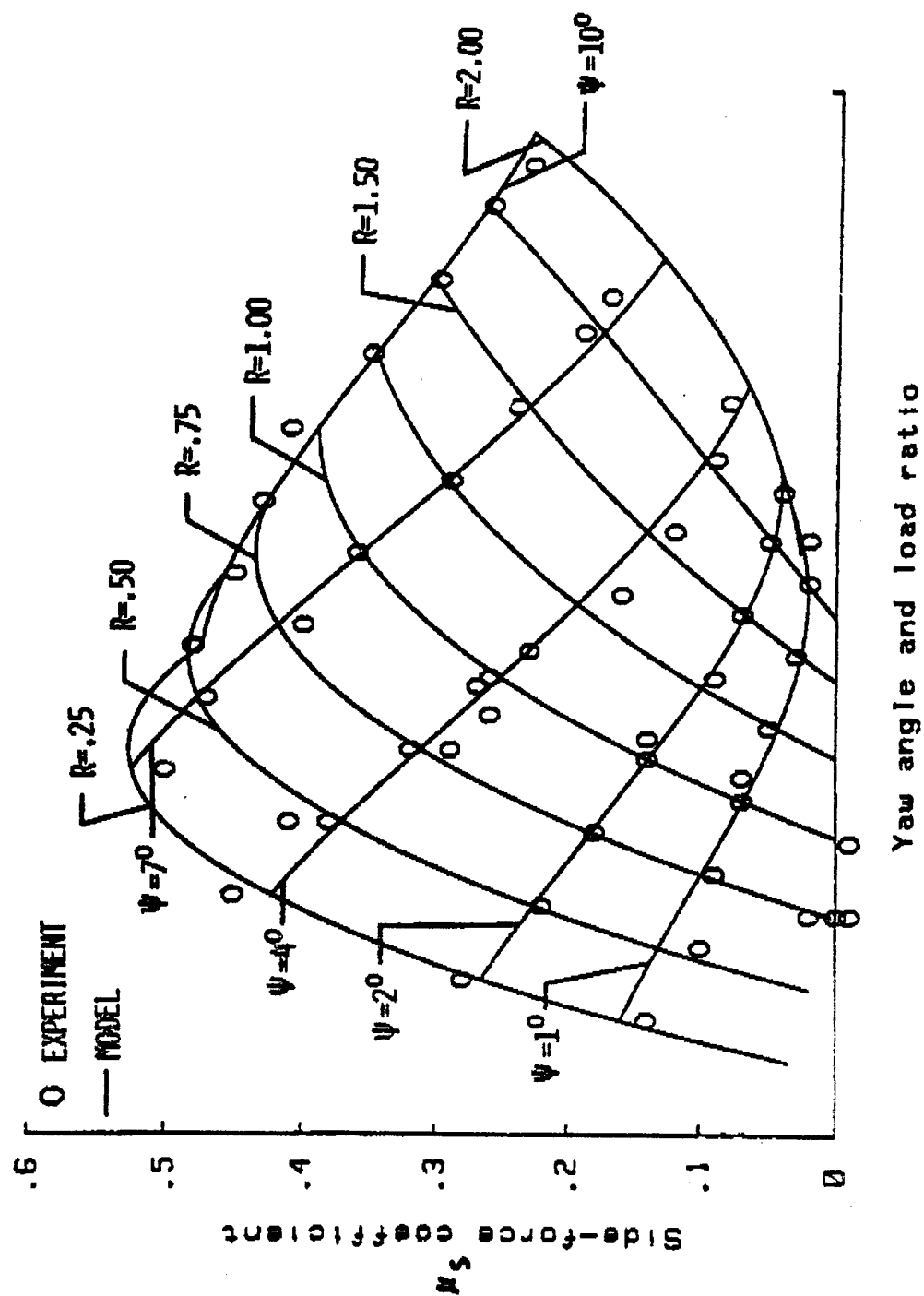
Fig. 7.2 - Variation of Orbiter main gear tire side-force friction coefficient with yaw angle and load ratio (from ref. 26).
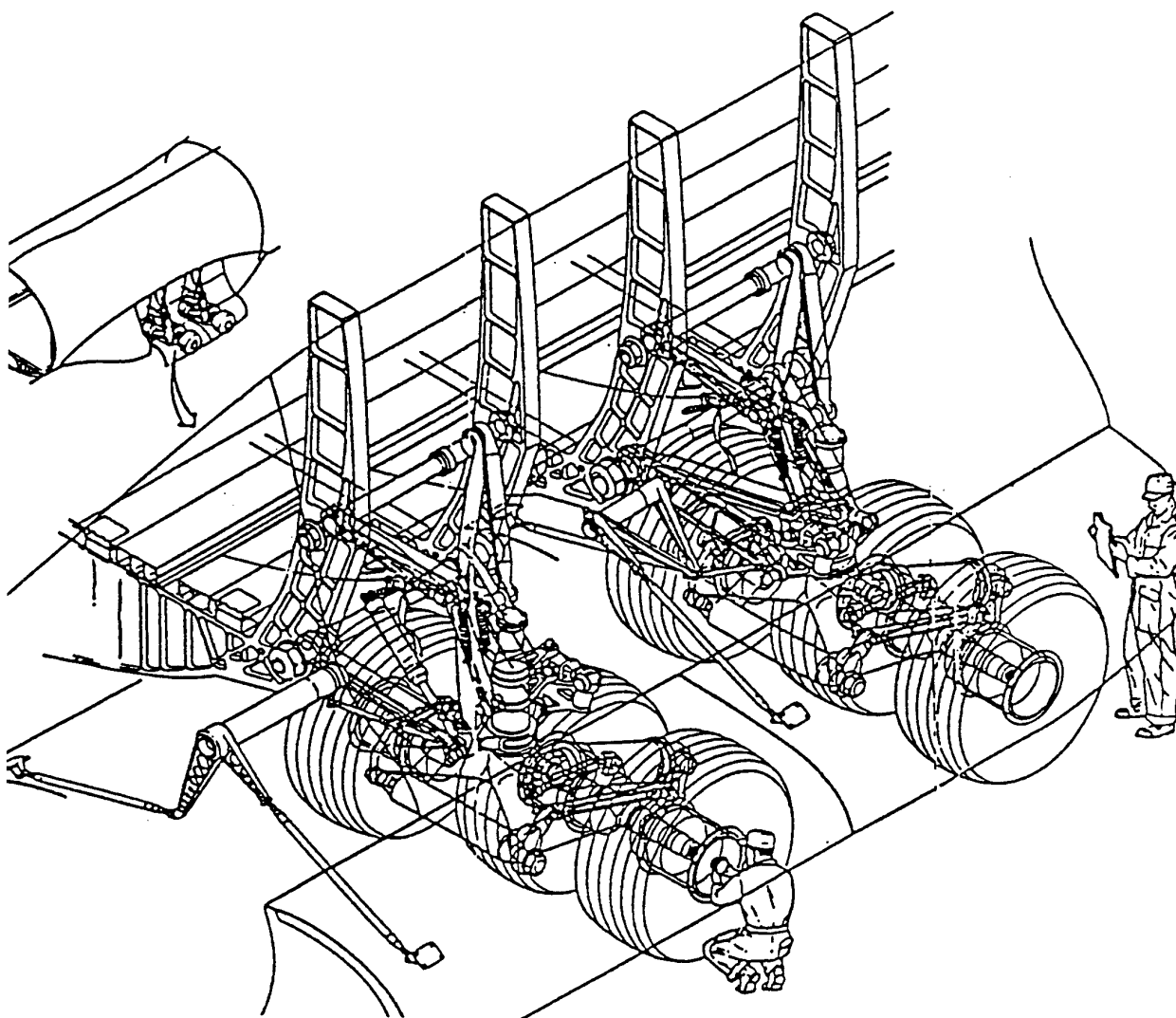
Figure 7.3 C-17 main gear layout (starboard)
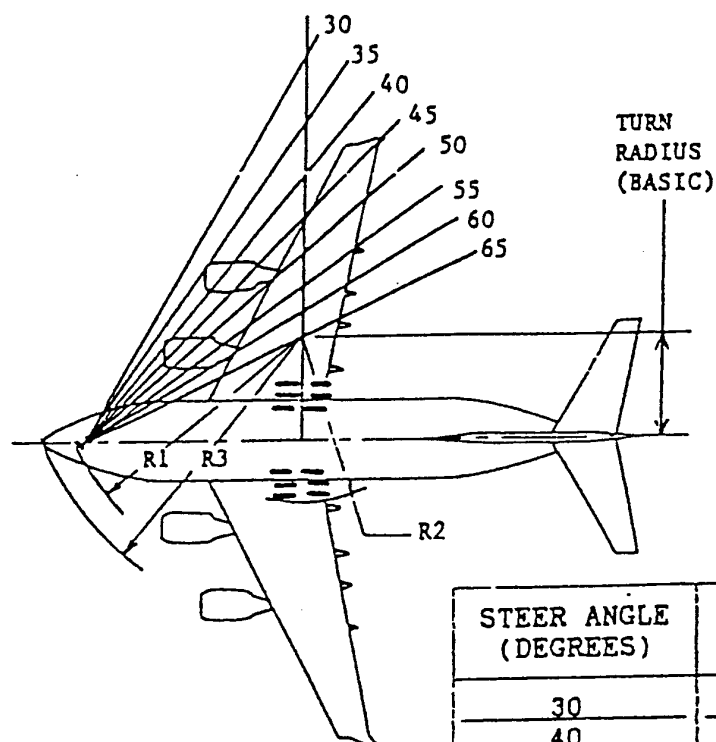
TURN
RADIUS
(BASIC)

$\mu_{SKID} = 0.8$

DIMENSIONS IN FEET

FORWARD VELOCITY
IS 'ZERO' MPH

570,000* MRW,
42.4 %MAC

NO DIFF. BRAKES
NO DIFF. THRUST

R1 R3

R2

STEER ANGLE (DEGREES)	EFFECTIVE STEER ANGLE (DEGREES)	TURN RADIUS
30	27.9	117.1
40	36.4	84.3
45	40.0	74.0
50	42.7 *	67.4
55	41.2 *	71.0
60	37.2 *	81.8
65	32.5 *	97.5

* Nose tires skidding.

Figure 7.4   C-17 turn radii at very low speed
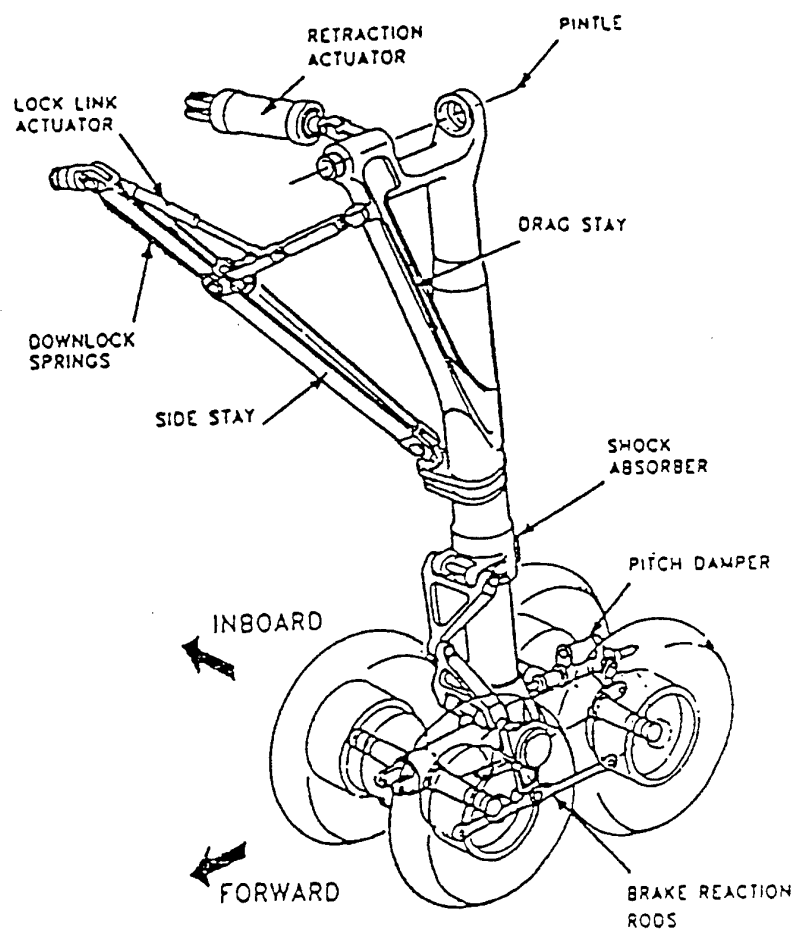
Figure 7.5 Typical main landing gear (reference 32)

Figure 7.6 Tire model (reference 33)

44
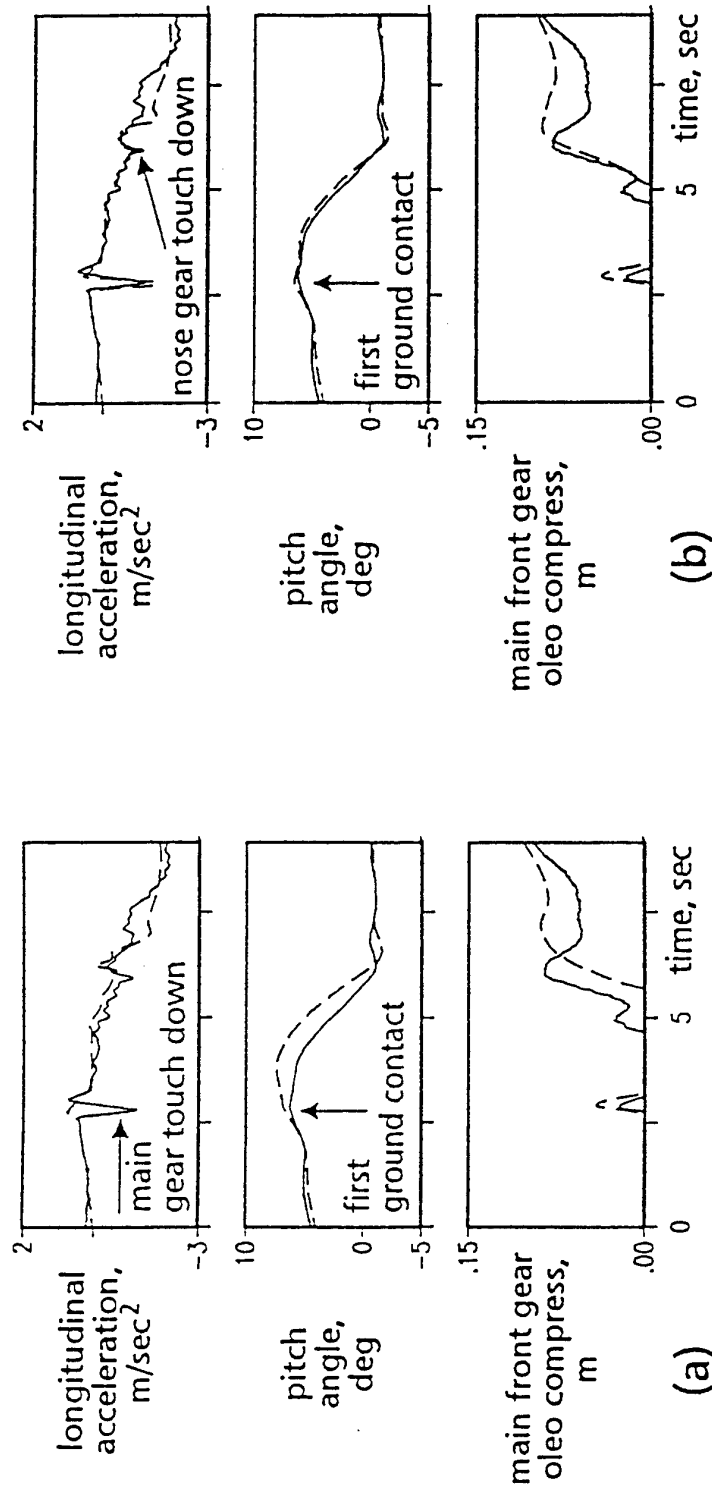
Figure 7.7 Influence of wheel spin-up (a) no impulse, (b) with impulse

Appendix A1

A Linearized Model of Ground Vertical Forces.

A.1.1   Strut Dynamics

A simple schematic of one landing gear element is seen on figure A1.1. The moving parts, the 'unsprung' mass, comprise the tire, wheel, axle, and piston assembly of the oleo. The pneumatic tire may be considered for the purpose of this model as a stiff spring with low damping. The non-moving parts, the 'sprung mass', comprise the body of the oleo, the strut leg, retraction mechanism, and the rest of the aircraft. The oleo and the tire are subjected to similar loads; the oleo has lower stiffness and higher damping than the tire, to allow the energy levels associated with touch-down to be absorbed in a progressive manner, without undue accelerations on the airframe.

Figure A.1.1

Typical values (fighter main leg)

	Sprung Mass	Unsprung Mass
Mass (kg)	5,000	150
Damping (kN/m/s)	50	2
Stiffness (kN/m)	250	2500

Figure A.1.2

Figure A1.2 shows a mathematical representation of the leg as a double spring. The sprung mass is m_s, and the unsprung mass is m_u. Damping and stiffness coefficients are d_s, d_u, k_s, k_u, and displacements relative to a fixed ground datum are x_s and x_u respectively. A general treatment of spring/mass systems is given in reference 6.

Kinematic equations of the double spring

$$m_s \ddot{x}_s = +m_s g + d_s (\dot{x}_s - \dot{x}_u) + k_s (x_s - x_u)$$

$$m_u \ddot{x}_u = +m_u g + d_s (\dot{x}_s - \dot{x}_u) + k_s (x_s - x_u) - d_u \dot{x}_u - k_u (x_u - x_g)$$

Steady state, on ground,

$$m_s g = -k_s (x_s - x_u)$$

$$m_u g = -k_s (x_s - x_u) - k_u x_u$$

Hence,   sprung compression (strut), $(x_s - x_u) = - m_s g/k_s$

unsprung compression (tire), $x_u = - (m_s + m_u)g/k_u$

For the typical aircraft values given above,

strut compression $= 20$ cm.   tire compression $= 2$ cm

<u>Dynamic response</u>   The state vector matrix is derived from

$$m_s \ddot{x}_s + d_s \dot{x}_s + k_s x_s \qquad - d_s \dot{x}_u - k_s x_u = 0$$

$$- d_s \dot{x}_s - k_s x_s + m_u \ddot{x}_u + (d_s + d_u) \dot{x}_u + (k_s + k_u) x_u = 0$$

$$
\begin{array}{cc}
x_s & x_u \\
\end{array}
$$

$$
\left|
\begin{array}{cc}
s^2 + d_s/m_s\, s + k_s/m_s & - d_s/m_s\, s - k_s/m_s \\
- d_s/m_u\, s - k_s/m_u & s^2 + (d_s + d_u)/m_u\, s + (k_s + k_u)/m_u
\end{array}
\right| = 0
$$

The characteristic equation is

$$s^4 + |\, m_s(d_s + d_u) + m_u d_s\,|\, /m_s m_u\, s^3 + |\, d_s d_u/m_s m_u + k_s/m_s + (k_s + k_u)/m_u|\, s^2$$

$$+ (d_s k_u + d_u k_s)/m_s m_u\, s + k_s (k_s + k_u)/m_s m_u = 0$$

All the coefficients are positive, and the equation can be factorized into two damped oscillatory modes, one oscillatory mode and two real roots or four real roots.

For a double spring representation of an aircraft leg, in which the tire stiffness k_u is an order greater than the strut stiffness k_s, the follow factors are a close approximation.

They identify two modes of oscillation.

$$|\, s^2 + d_s/m_s\, s + k_s/m_s\,|\, |\, s^2 + (d_s + d_u)/m_u\, s + (k_s + k_u)/m_u\,| = 0$$

The first mode represents the strut stiffness and damping, and the second mode represents the reaction of the unsprung mass against the total stiffness and damping of the landing gear. Both modes are well damped; their frequency separation makes them virtually uncoupled.

For the values given above,

	sprung mass	unsprung mass
natural frequency, (rad/sec)	7.1 (1.1 hz)	135 (22 hz)
relative damping ratio	0.70	1.67 (overcritical damping)
		$(s + 280)(s + 66)$

In contrast, consider the wheel and tire alone, as a single spring. Assuming a combined mass of 50 kg (1/3 the unsprung load), with the same stiffness and damping (since they are produced by the pneumatic tire), the natural frequency is approximately 50 hz, and the relative damping ratio is 0.12. Subjective confirmation of the low damping can be seen in the dynamic behavior of a single wheel, after hitting a bump when rolling down the road.

The above analysis illustrates how effective a double spring arrangement is in absorbing energy over a wide range of frequencies. There is a wide frequency separation between modes. It is greater for aircraft than for cars (typically for cars, the ratio of unsprung mass to sprung mass is 1:10, unsprung natural frequency to sprung natural frequency is 10 : 1 ; and the sprung frequency is around 1 hz). For aircraft, the wide separation and high damping justifies the omission of the tire mode in the equivalent model of the gear, for use in real-time simulation.

In constructing an equivalent model, manufacturers' data on the strut is needed, together with advice on mathematical representation. Strut force v deflection is non-linear, becoming stiffer at high deflections, to soften the ride at normal loadings, and avoid travel limits at high loads. The damping is also non-linear. In particular, the damping coefficient varies with direction of piston movement. The essential behavior associated with these non-linearities can be incorporated into a quasi-linear model without difficulty, and without transgressing the principles of model simplification described above. It is also worthwhile to adjust the static deflection of the equivalent strut, to match the actual height of the aircraft c.g.

Not all aircraft have a landing gear design of the type used earlier as a numerical example. Many old aircraft had large wheels with low pressure tires, and springy struts with less effective damping. Combined with a tail-sitter configuration and rough field operation, their dynamic behavior could lead to eventful landings. There has been little formal study of these interesting cases.

For most real-time applications, the strut/tire can be modeled by second order differential equation with steady, non-linear damping and stiffness coefficients. Each strut of the gear requires an individual model, the inputs of which are the displacement and rate of displacement of the strut, and gives the vertical force applied to the aircraft and to the ground.

For example, the nosewheel force, F_{zn}, is given by $F_{zn} = D_n z_n + K_n z_n$, where D_n and K_n are the non-linear damping and stiffness coefficients of the equivalent nose gear, and z_n is the vertical displacement of the equivalent strut. Nosewheel displacement in a full model is a function of many variables, including the geometry of the aircraft, its orientation and position in space, and the height of the ground below the nosewheel. Simpler subsets can be defined by constraining the degrees of freedom of the aircraft, to

help in model validation. Assuming small perturbations, these models can be linearized, to allow the dynamic behavior to be checked.

A.1.2   Aircraft Dynamic Response -Pitch/Heave

As an example of this procedure, the bounce/pitch modes of an aircraft during ground roll (Figure A.1.3) may be derived from the vertical displacement and pitch degrees of freedom.

Figure A.1.3   Bounce/pitch modes

The equations of motion, neglecting aerodynamic forces, and assuming small perturbations, are .

$$z_n = z + z_{ng} + a.\theta$$

$$z_m = z + z_{mg} - b.\theta$$

$$\dot{z}_n = \dot{z} + \dot{z}_{ng} + a.\dot{\theta}$$

$$\dot{z}_m = \dot{z} + \dot{z}_{mg} - b.\dot{\theta}$$

$$F_{zn} = d_n.\dot{z}_n + k_n.z_n$$

$$F_{zm} = d_m.\dot{z}_m + k_m.z_m$$

Vertical equation

$$m.\ddot{z} = m.g + F'_{zn} + F'_{zm}$$

Pitch equation

$$B\ddot{\theta} = F'_{zn}.a + F'_{zm}.b$$

where $F'_{zn}, F'_{zm} = F_{zn}, F_{zm}$ for $F_{zn}, F_{zm} < 0$

$\qquad\qquad\qquad\; = 0$ for $F_{zn}, F_{zm} > 0$

Assume that $F_n, F_m < 0$, and $z_{ng} = z_{mg} = 0$, then

$$m.\ddot{z} + d_n.\dot{z}_n + d_m.\dot{z}_m + k_n.z_n + k_m.z_m = m.g$$

$$B\ddot{\theta} + a.d_n.\dot{z}_n + b.d_m.\dot{z}_m + a.k_n.z_n + b.k_m.z_m = 0$$

$$m.\ddot{z} + (d_n + d_m).\dot{z} + (k_n + k_m).z + (a.d_n + b.d_m)\dot{\theta} + (a.k_n + b.k_m)\theta = m.g$$

$$(a.d_n + b.d_m)\dot{z} + (a.k_n + b.k_m)z + B\ddot{\theta} + (a^2.d_n + b^2.d_m).\dot{\theta} + (a^2.k_n + b^2.k_m).\theta = 0$$

These equations not only define the two modes of vibration, they also define the oscillation centers in pitch and bounce, which indicate the likely ride comfort. They are equally applicable to ground vehicles, for which ride comfort is a key consideration. (Reference 7). Spring stiffness, damping, and c.g location are all chosen with ride quality in mind. For aircraft on the ground, it is not so important, and the c.g. position is dictated by the need to rotate and de-rotate the aircraft during transition from ground-borne to airborne flight.

If $a.k_n = -bk_m$, the pitch center is located at the c.g., which is approximately true for most aircraft. Additionally, if $a.d_n = -b.d_m$, which implies similar damping ratios in each strut, the pitch and bounce modes are uncoupled, and the characteristic equation may be written

$$[s^2 + (d_n + d_m)/m\ s + (k_n + k_m)/m].[s^2 + (a^2.d_n + b^2.d_m)/B\ s + (a^2.k_n + b^2.k_m)/B] = 0$$

for a typical fighter, $m = 11{,}000$ kg. $B = 50{,}000$ kg.m^2
                             $a = 4.0$ m $b = 0.4$ m
                             $d_n = 10$ kN./m/s $d_m = 100$ kN./m/s
                             $k_n = 50$ kN/m $k_m = 500$ kN/m

which gives

$$(s^2 + 11.0\ s + 50)(s + 3.5\ s + 17.6) = 0 \quad \text{for the bounce and pitch modes.}$$

The bounce mode has an undamped natural frequency of 7.1 rad/sec., and a relative damping ratio of 0.70.

The pitch mode has an undamped natural frequency of 4.2 rad/sec., and a relative damping ratio of 0.41. This mode appears to the pilot as the nodding of the nose in response to brake application, and as attitude changes from other sources of pitch excitation during ground roll.

In this appendix, it has only been possible to present the simplest form of analysis to support the validation of the complete model of the aircraft on the ground. In practice, a library of cases needs to be available, introducing more degrees of freedom, and non-linearities.

Appendix 2

<u>A Model of Tire/Runway Friction</u>

A.2.1 Introduction.

The friction generated by contact between an aircraft tire and a runway surface varies with contact conditions, including contamination, tire pressure, speed, and wheel braking. In this Appendix, published data of lateral friction coefficients is identified, and analytical functions are defined, of sufficient accuracy and simplicity to use in the real-time simulation of an aircraft during the ground-roll phase of flight. The functions provide an alternative method to the look-up tables often used in current simulators.

A.2.2 Discussion

The deceleration of an aircraft when braking depends on many factors. They include the type of runway surface and its irregularities, contamination of the surface by water, ice, or snow, the type of tire and its inflation pressure, the speed of the aircraft, the loading on the wheels, and the efficiency of the brakes.

Tests over the last forty years provide information to quantify the effects of these parameters. They cover different types of runway surfaces and tires over a wide speed range. Most of the published data relate to dry or wet surface conditions; data relating to other levels of contamination are less complete, and exhibit more scatter. The models to be described are derived from these data, converted to a form which facilitates implementation on a digital computer for use in real-time simulation of aircraft performance under piloted control.

The retarding force produced by the tire on a braked wheel, F_X, is the product of the vertical load on the tire F_Z, and a coefficient of friction μ, which varies with runway surface type, surface contamination, aircraft speed, and tire pressure. Two friction coefficients influence braking performance. They are the maximum braking coefficient μ_{bmax}, which is available just before slipping of the rolling wheel occurs, and the tire skid coefficient, μ_{skid}, the friction coefficient of the locked wheel (fully developed skid). In a fully developed skid, the available retarding force is greatly reduced, and brakes should be operated to avoid this condition. Manual operation in critical conditions requires skill; consequently, most aircraft are fitted with an ABS (automatic braking system), to prevent skidding. An ABS reduces the maximum available deceleration by about 10% on dry and wet runways, and by about 20% on flooded, icy, and snow-covered runways. A third braking coefficient, the braking effectiveness coefficient, μ_{eff}, is used to take account of ABS efficiency. These braking coefficients are used to calculate the forces tangentially on the tyre, in the plane of wheel rotation.

Side-force is generated when the plane of a rolling wheel is yawed relative to its direction of motion by an angle ψ. To calculate the side-force, two additional friction coefficients are needed - the maximum lateral friction coefficient, $\mu_{\psi max}$, and the limiting lateral friction coefficient, $\mu_{\psi lim}$. $\mu_{\psi max}$ is the maximum attainable lateral friction coefficient in unbraked yawed rolling, and $\mu_{\psi lim}$ is the maximum attainable lateral friction coefficient during braked yawed rolling. The model must include the effect of braking, because it can reduce considerably the maximum side-force generated by a yawed wheel.

The data presented relate to a Type C runway surface (wire-brushed concrete). Similar algorithms could be constructed for other surfaces, using the reference material. UK ESDU Data Sheets are used for the cases of a dry surface and a wet surface, since they present a cohesive picture. Data on other types of surface contamination are less complete, and extrapolation has to be applied to specific test results. Many of these tests were made in the US, as part of the research activities at NASA Langley.

A.2.3 Identities for Dry and Wet Runways

The identities are based on the tables and graphs in UK ESDU Sheets, References 8 and 9. These references use many sources. Reference 8 gives the relationships of $\mu_{b max}$ v speed and tire pressure, $\mu_{skid} / \mu_{b max}$ v speed, and μ_{eff} v $\mu_{b max}$ for an adaptive braking system. Reference 9 gives the relationships between $\mu_{b max}$ and $\mu_{\psi max}$ for dry and wet runways, and between $\mu_{\psi max}$ and $\mu_{\psi lim}$. (this formula produces the traction envelope required by physical considerations - the total friction is shared between side-force generation and longitudinal deceleration).

Dry Runway Surface

$$\mu_{b\,max} = 0.912(1 - 0.0011p) - 0.00079\,V_{kts}$$

where p is the tire pressure in psi

$$\mu_{effective} = -0.03 + 0.94\,\mu_{b\,max}$$

$$\mu_{skid} = \frac{48.1}{\left(50.2 + V_{kts}\right)}\mu_{b\,max} \qquad \text{for } V < 106 \text{ knots}$$

$$= 0.31\,\mu_{b\,max} \qquad \text{for } V > 106 \text{ knots}$$

$$\mu_{\psi_{max}} = \mu_{b\,max}$$

$$\mu_{\psi\,lim} = \mu_{b\,max}\sqrt{1-\left(k_b \cdot \frac{\mu_{eff}}{\mu_{b\,max}}\right)^2}$$

where k_b is the proportion of braking being applied.

Figure A.2.1   Effect of tire pressure on max braking coefficient

Figure A.2.2 $\mu_{b\,max}$, μ_{eff}, and μ_{skid} - dry runway

Wet Runway Surface

$$\mu_{b\,max} = (0.91 - 0.001p)(1 - 0.0052V_{kts}) \qquad \text{for } V < 140 \text{ knots}$$

$$= 0.265(0.91 - 0.001p) \qquad \text{for } V > 140 \text{ knots}$$

where p = tire pressure in psi.

$$\mu_{effective} = -0.03 + 0.94\mu_{b\,max}$$

$$\mu_{skid} = \frac{(23.2 - 0.031p)}{(26.5 + V_{kts})} \qquad \text{where } p = \text{tire pressure in psi.}$$

$$\mu_{\psi_{max}} = 0.64\mu_{b\,max} + 0.15(\mu_{b\,max})^2$$

$$\mu_{\psi\,lim} = \mu_{b\,max}\sqrt{1-\left(k_b \cdot \frac{\mu_{eff}}{\mu_{b\,max}}\right)^2}$$

where k_b is the proportion of braking being applied.

Figure A.2.3 $\mu_{b\,max}$, μ_{eff}, and μ_{skid} - wet runway

A.2.4   Identities for Flooded, Icy, and Snow-covered Runways

References 10 to 15 have been used to construct the identities given below. The primary data source of the documents is the full scale testing carried out over many years at NASA Langley. Much of the testing has been directed to measure aircraft deceleration, from which μ_{eff} may be derived.   The nature of the testing is prone to scatter (for example, runway contamination can vary along the runway as a test is underway), and inconsistencies are seen between reference material. Consequently, interpretation and extrapolation has been necessary in this report. A level of ABS efficiency, based on ESDU recommendations, has been assumed, to deduce expressions for μ_{bmax} from the μ_{eff} data. Also, the chosen identities ensure that μ_{skid} is at all times less than μ_{eff} (a physical necessity).

The magnitudes of all the friction coefficients relating to severe contamination are much lower than those relating to dry or wet runways, so that scatter in the data has less significance. When the runway is severely contaminated, the influences of the type of runway surface and tire pressure are small, and can be neglected for this type of model.

Flooded Runway Surface

$$\mu_{b\,max} = 0.2125 - 0.0021V_{kts} \qquad\qquad \text{for } V < 80 \text{ knots}$$

$$= 0.0425 \qquad\qquad \text{for } V > 80 \text{ knots}$$

$$\mu_{effective} = 0.8\,\mu_{b\,max}$$

$$\mu_{skid} = \mu_{b\,max}\,(0.8 - 0.004V_{kts}) \qquad\qquad \text{for } V < 50 \text{ knots}$$

$$= 0.6\,\mu_{b\,max} \qquad\qquad \text{for } V > 50 \text{ knots}$$

$$\mu_{\psi\,max} = 0.64\,\mu_{b\,max} + 0.15\left(\mu_{b\,max}\right)^2$$

$$\mu_{\psi\,lim} = \mu_{\psi\,max}\sqrt{1 - \left(k_b \cdot \frac{\mu_{eff}}{\mu_{b\,max}}\right)^2}$$

where k_b is the proportion of braking being applied.

Figure A.2.4 $\mu_{b\,max}$, μ_{eff}, and μ_{skid} - flooded runway

Icy Runway Surface

$$\mu_{b\,max} = 0.049 - 0.00029 V_{kts} \qquad \text{for } V < 100 \text{ knots}$$

$$= 0.02 \qquad \text{for } V > 100 \text{ knots}$$

$$\mu_{effective} = 0.8\,\mu_{b\,max}$$

$$\mu_{skid} = \mu_{b\,max}\,(0.8 - 0.004 V_{kts}) \qquad \text{for } V < 50 \text{ knots}$$

$$= 0.6\,\mu_{b\,max} \qquad \text{for } V > 50 \text{ knots}$$

$$\mu_{\psi\,max} = 0.64\,\mu_{b\,max} + 0.15\left(\mu_{b\,max}\right)^2$$

$$\mu_{\psi\,lim} = \mu_{\psi\,max}\sqrt{1 - \left(k_b \cdot \frac{\mu_{eff}}{\mu_{b\,max}}\right)^2}$$

where k_b is the proportion of braking being applied.

Figure A.2.5 $\mu_{b\,max}$, μ_{eff}, and μ_{skid} - icy runway

Snow Covered Runway Surface

$$\mu_{b\,max} = 0.185$$

$(+ 0.001\,V_{kts}$, independent of brakes, to represent 6 ins of snow)

$$\mu_{effective} = 0.8\,\mu_{b\,max}$$

$$\mu_{skid} = \mu_{b\,max}(0.8 - 0.004\,V_{kts}) \qquad \text{for} \quad V < 50 \quad \text{knots}$$

$$= 0.6\,\mu_{b\,max} \qquad\qquad \text{for} \quad V > 50 \quad \text{knots}$$

$$\mu_{\psi_{max}} = 0.64\,\mu_{b\,max} + 0.15\left(\mu_{b\,max}\right)^2$$

$$\mu_{\psi\,lim} = \mu_{\psi_{max}}\sqrt{1 - \left(k_b \cdot \frac{\mu_{eff}}{\mu_{b\,max}}\right)^2}$$

where k_b is the proportion of braking being applied.

Figure A.2.6 $\mu_{b\,max}$, μ_{eff}, and μ_{skid} - snow-covered runway

A.2.5   Conclusion

Mathematical expressions have been derived from published sources to define the coefficients of friction between the runway surface and an aircraft wheel. They are intended for use in flight simulation, as an alternative to look-up tables. It must be remembered that for the severe surface-contamination cases, measured friction coefficients are scarce, and gross extrapolation of data has been necessary. No account has been taken of the scatter associated with the measurements, but the magnitude of friction coefficients for flooded, icy, and snow packed runways is small, and so scatter is not of great significance.

The expressions apply to a Type C runway (brushed concrete). Similar expressions are needed to represent other surfaces, and could be easily derived from the referenced material. A definition of friction coefficients for all operating conditions is needed not only for braking perfomance prediction, but also to assess directional stability and control on the ground.
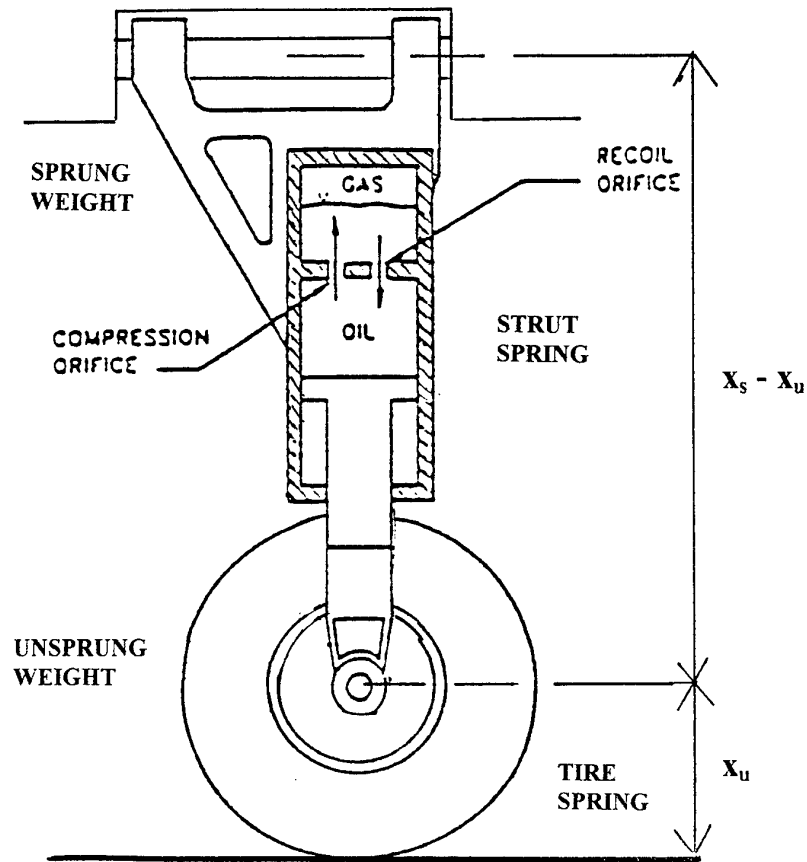
Figure A.1.1   Strut/wheel schematic
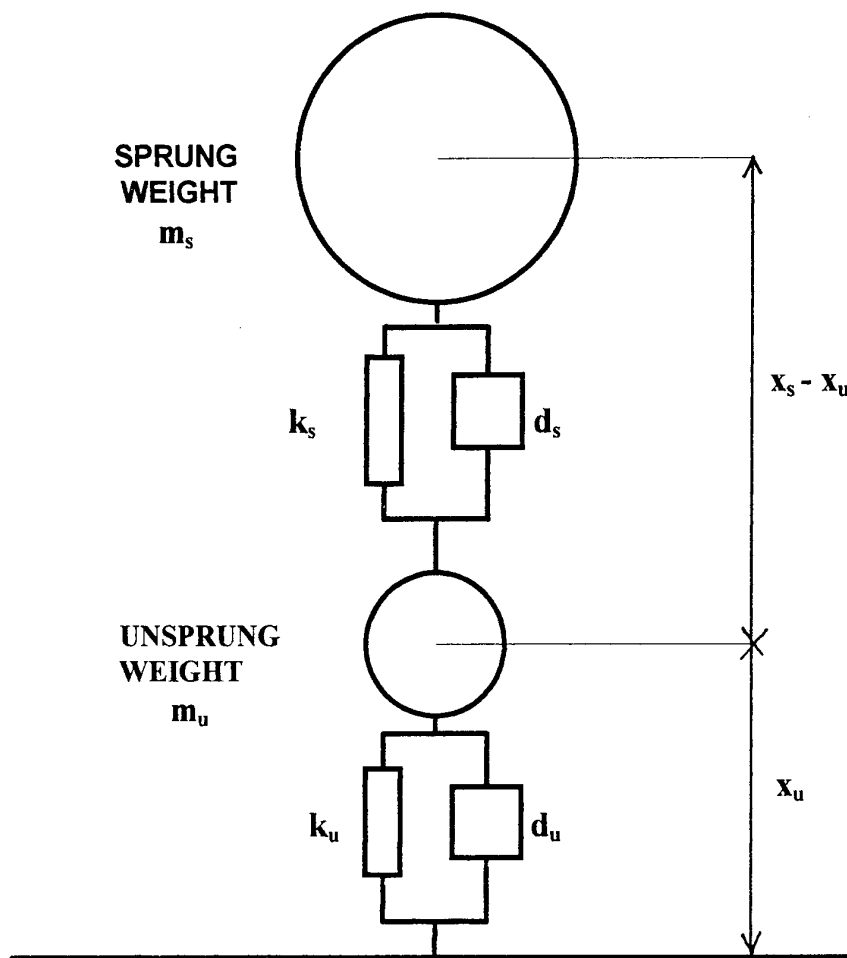
Figure A.1.2   Strut/wheel Equivalent Model
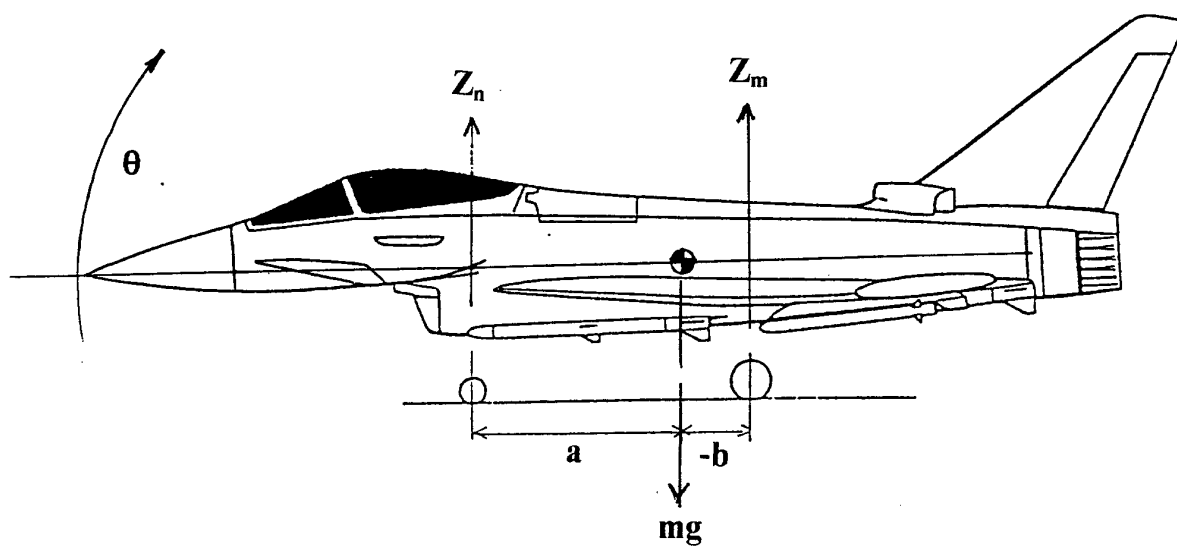
Figure A.1.3   Bounce/pitch modes
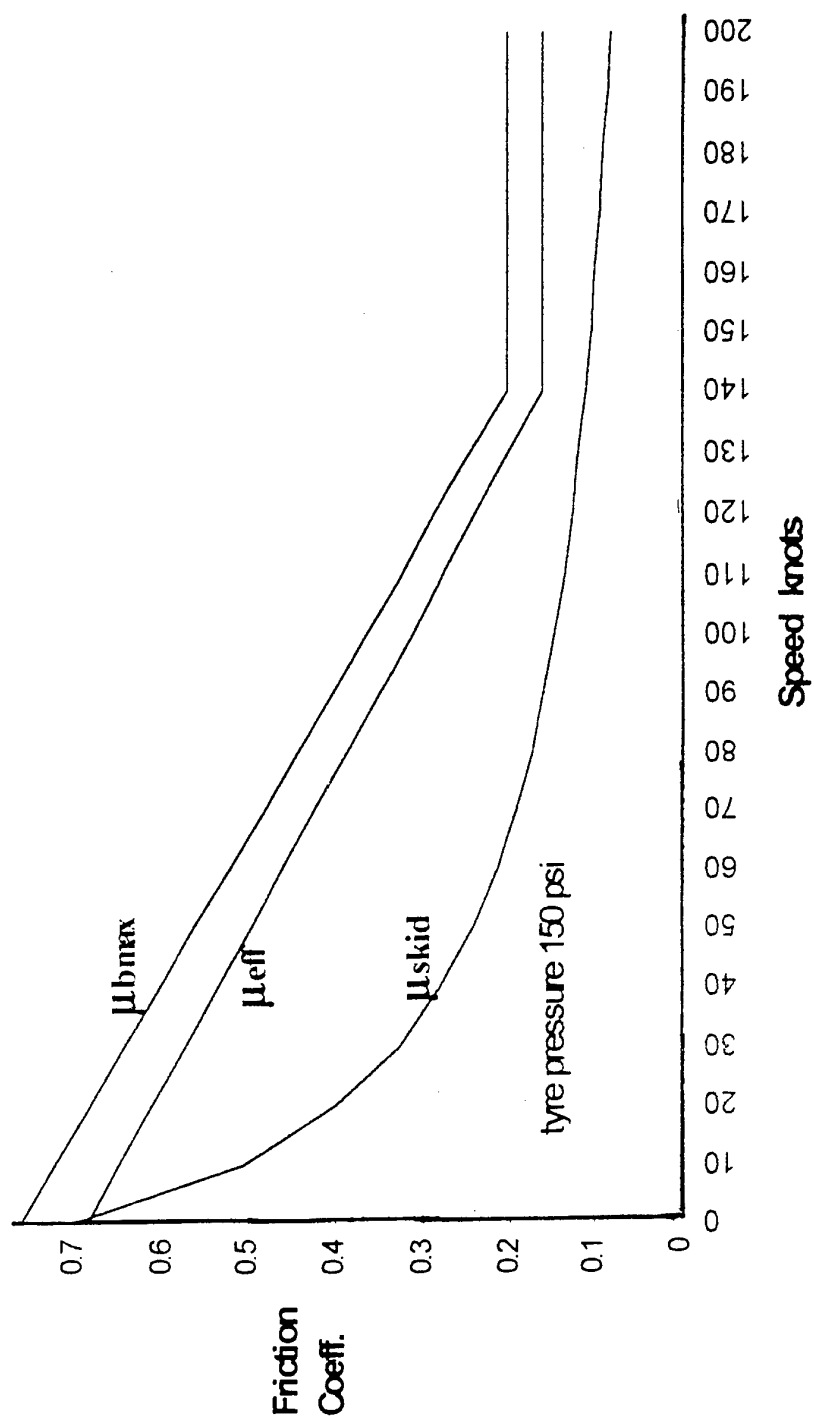
58

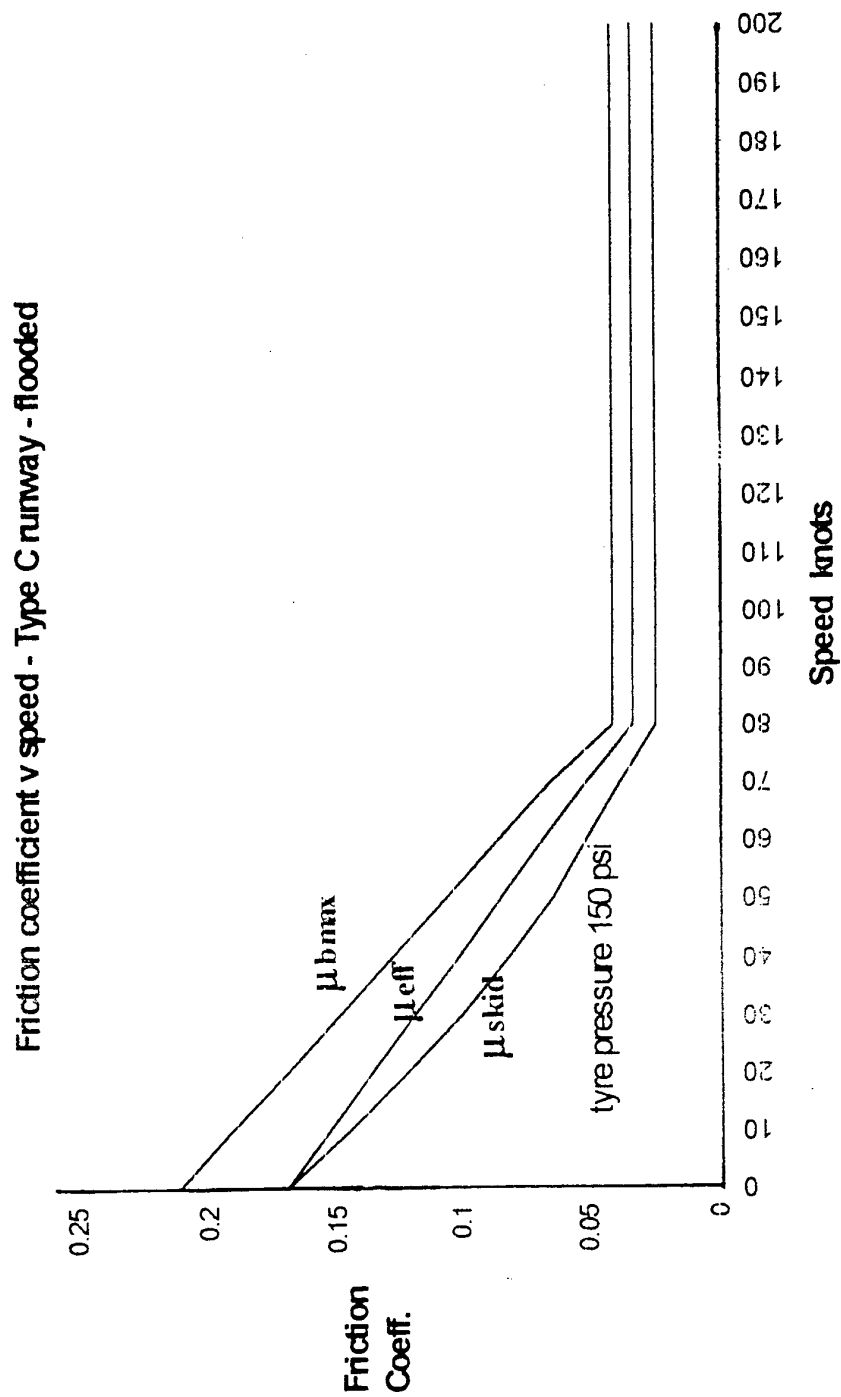**Figure A.2.3** μ_{bmax}, μ_{eff}, and μ_{skid} - wet runway

Friction coefficient v speed - Type C runway - flooded

μbmax

μeff

μskid

tyre pressure 150 psi

Friction Coeff.

Speed knots

Figure A.2.4 μ_{bmax}, μ_{eff}, and μ_{skid} - flooded runway

Friction coefficient v speed - Type C runway - icy
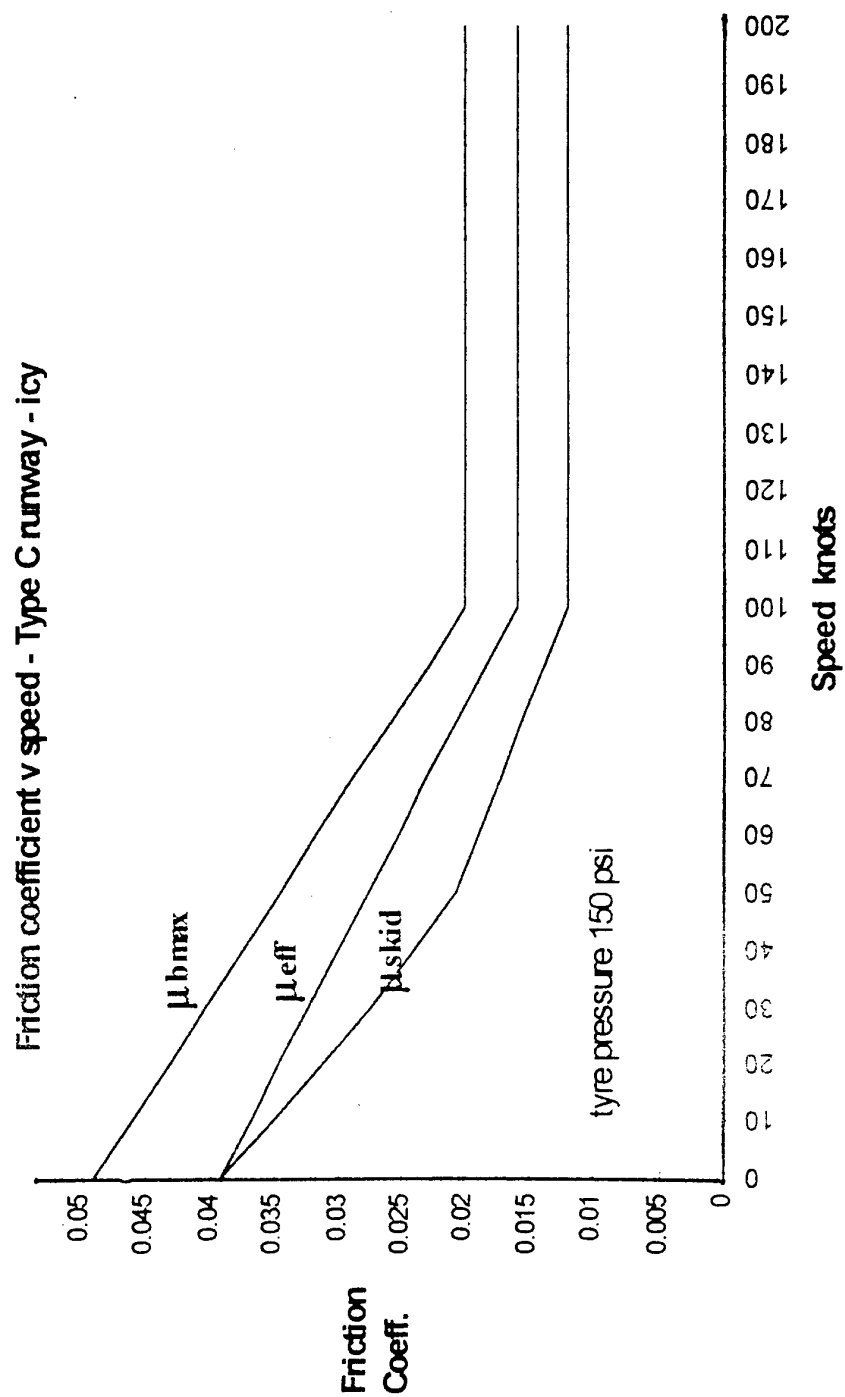
Figure A.2.5 $\mu_{b\,max}$, μ_{eff}, and μ_{skid} - icy runway
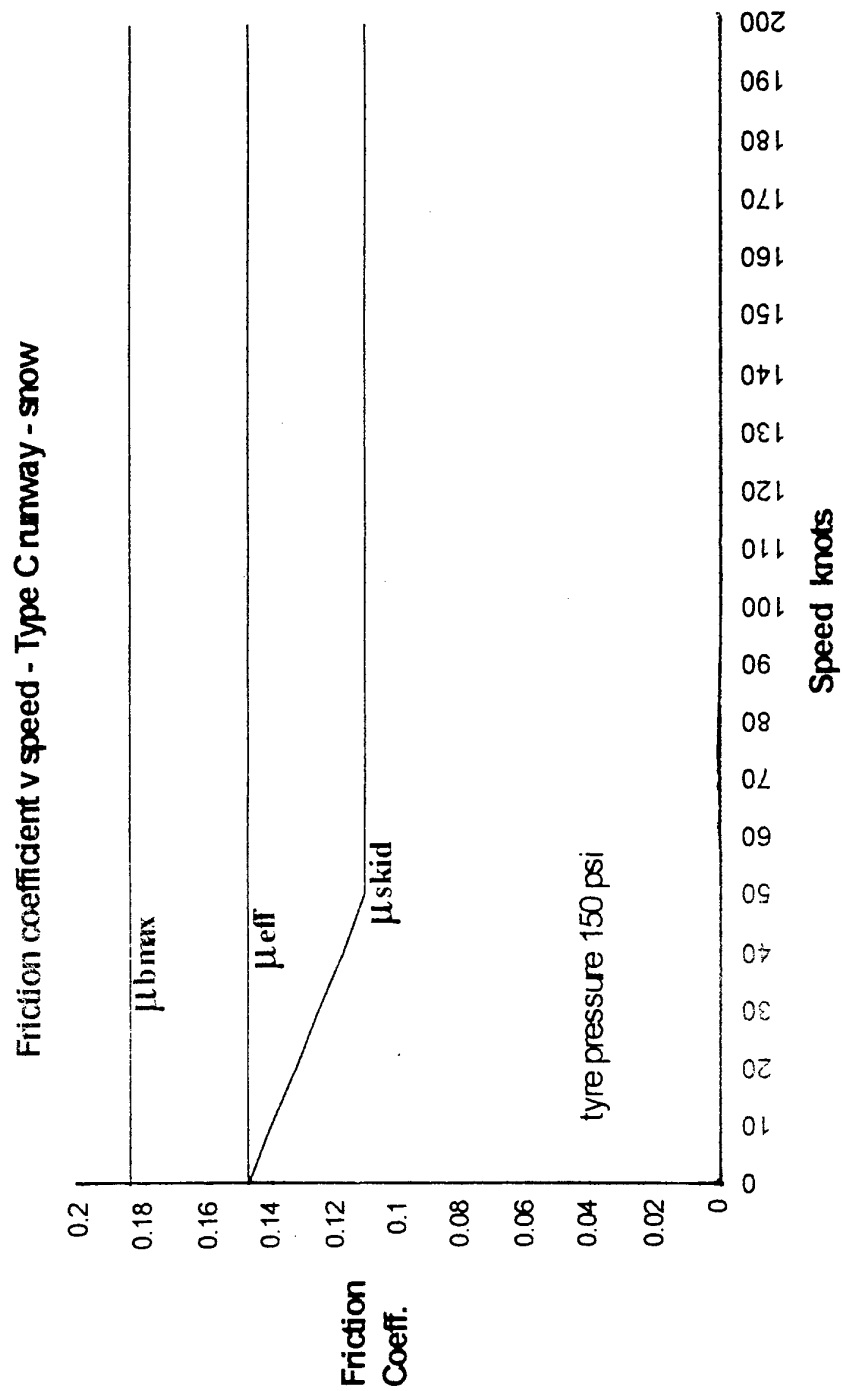
Figure A.2.6 $\mu_{b\,max}$, μ_{eff}, and μ_{skid} - snow-covered runway

Appendix 3

A Model of Lateral Tire Forces

A.3.1. Introduction

The model is designed for use in dynamic analysis and real-time simulation. It represents the contact conditions between tire and ground, as speed, yaw angle of the tire, and load on the tire vary. It takes account of variation in ground surface conditions (contamination), and is valid over a large range of speeds and tire yaw angles. An adaptive braking system (ABS) is assumed (to avoid the complications of modeling wheel slip when braking). Tire pressure may also be varied.

The model uses mathematical expressions for on-line computation, and is an alternative to earlier methods, which require the storage of large amounts of data in look-up tables containing discrete values, which are then retrieved and interpolated.

A.3.2 Rated load and Cornering Power

Associated with the tire is the recommended maximum, or rated pressure, p_r (psi), and the
rated tire load, F_R (lbs). F_R may be calculated from the rated pressure, diameter, and width, as follows

$$F_R = 0.57 p_r w \sqrt{wd} \qquad \text{(Reference 17)}$$

Except for transients, the vertical force on the tire due to the ground, F_z, is less than F_R.

The Cornering Power of the tire, N, is defined as

$$N = F_z \frac{\delta \mu_\psi}{\delta \psi} \qquad \text{for small values of } \psi \text{, the tire yaw angle.}$$

A.3.3 Cornering Power as a function of tire pressure and vertical force on the tire.

(all formulae from Reference 17, and valid at or near the tire operating conditions)

Tire footprint area $A_g = 2.3\, \delta \sqrt{wd}$ (static) (g for gross)

Vertical force from the ground, $F_z = p_g A_g$ (no carcass stiffness)   (p_g = footprint pressure)

$$p_g \approx p, \quad \text{tire inflation pressure}$$

$$F_z = 2.3 \ \delta p \sqrt{wd}$$

At the rated conditions of the tire, $F_z = 0.57 pw \sqrt{wd}$

A.3.4 Cornering Power N, as a function of vertical load, tire dimensions, and tire pressure

For most purposes (i.e. loads and tire pressures below the ratings of the tire),

$$N = 31.3 w^2 (p + 0.44 p_r)(1 - 3.17x)x \qquad \text{where} \quad x = \frac{F_z}{pd\sqrt{(wd)}}$$

At the rated pressure,

$$N = 45.1 w^2 p_r (1 - 3.17x)x$$

For loads well below the rated load,

$$N = 45.1 w^2 p_r x \qquad = \qquad 45.1 \left(\frac{w}{d}\right)^{\frac{3}{2}} F_z$$

This relationship may be used to calculate

$$\frac{N}{F_z} = \left(\frac{\partial \mu_\psi}{\partial \psi}\right)_{\psi = 0} \qquad \text{per radian)}$$

- a parameter required for quasi-linear analysis of ground roll stability, and which is used to calculate the lateral friction coefficient at large yaw angles.

At the rated load of the tire, x = 0.20, approximately, and

$$N = 33 \left(\frac{w}{d}\right)^2 F_R$$

A.3.5 Cornering Force, as a function of cornering power, vertical load, and tire yaw angle.

The cornering force, F_y, is the lateral force perpendicular to the plane of the wheel, generated by a rolling wheel yawed by an angle ψ relative to the direction of motion.

$$F_y = F_z \mu_\psi,$$ where μ_ψ is the lateral friction coefficient, and is a function of ψ.

The cornering force is affected by many factors. To avoid an over-complex model, the effects of a non-vertical wheel, of self-aligning torque, and of pneumatic castor, are neglected in the following cornering force model. In general, these effects have little influence on the performance and dynamic stability of modern aircraft during ground roll, although their omission means that a high bandwidth problem such as nose-wheel shimmy cannot be represented by this model.

From reference 15,
$$\frac{F_y}{\mu_{\psi\,max} F_z} = \phi - \frac{4}{27}\phi^3 \qquad \text{for } |\phi| < 1.5$$

$$= \phi / |\phi| \qquad \text{for } |\phi| > 1.5$$

where $\mu_{\psi\,max}$ is a constant, defined below, and $\phi = \dfrac{N\psi}{\mu_{\psi\,max} F_z}$

(the modulus in the condition on ϕ is needed to allow ψ to be +ve or -ve)

This empirical relationship is valid for vertical deflections of the tire up to its rated value, and for angle of yaw sufficient to generate its maximum cornering force. (say, less than 20 degrees).

The relationship between $\mu_{\psi\,max}$ and the maximum braking coefficient of the wheel, $\mu_{b\,max}$, is given in reference 7. Approximately,

$$\mu_{\psi\,max} = \mu_{b\,max} \qquad \text{for dry runways,}$$

and
$$= 0.64\,\mu_{b\,max} + 0.15\left(\mu_{b\,max}\right)^2 \qquad \text{for wet runways.}$$

In the absence of other data, the expression for wet runways is an intuitive choice for the relationship between $\mu_{\psi_{max}}$ and $\mu_{b_{max}}$ for flooded, icy, and snow covered runways. Measured values of $\mu_{b_{max}}$ in these conditions are very low, and show large scatter, so that the consequences of this extrapolation are not serious.

A.3.6 Lateral Friction Coefficient as a function of cornering power, vertical load, maximum lateral friction coefficient, and tire yaw angle.

$$\mu_\psi = \mu_{\psi \, max} \cdot \left| \phi - \frac{4}{27}\phi^3 \right| \qquad \text{for} \quad |\phi| < 1.5$$

$$= \mu_{\psi \, max} \qquad \text{for} \quad |\phi| > 1.5$$

The lateral friction coefficient v tire yaw angle for a typical transport aircraft tire is seen on figure A.3.1

A.3.7 Effect of Braking.

The braking performance of an aircraft equipped with ABS is calculated by introducing the concept of a braking coefficient which allows for the efficiency of the ABS, the effective braking coefficient, μ_{eff}. As brakes are applied to a wheel, the maximum lateral friction coefficient of the wheel is reduced. The effect is included in the model by replacing $\mu_{\psi_{max}}$ in the above analysis by $\mu_{\psi \, lim}$, the limiting friction coefficient during braked yawed rolling (see reference 8). Expressions for $\mu_{\psi \, lim}$ as a function of $\mu_{\psi_{max}}$, μ_{eff}, and proportion of braking are given in Appendix 2.

A.3.8 Lateral Friction Coefficient at small yaw angles (sya)

is given by
$$\mu_{sya} = \mu_{\psi \, lim} \cdot \left| \phi - 0.148\phi^3 \right| \qquad \text{for} \quad |\phi| < 1.5$$

$$= \mu_{\psi \, lim} \qquad \text{for} \quad |\phi| > 1.5$$

Both of the above expressions, for Cornering Force and Lateral Friction Coefficient, are valid for small to moderate angles of yaw (say, less than 20°). At large angles of yaw, they give a constant value of $\mu_{\psi max}$. It is necessary to modify $\mu_{\psi max}$ at large yaw angles. The following analysis is based on the empirical method described in reference 9. The method can be modified to include the effect of braking, by replacing $\mu_{\psi max}$ by $\mu_{\psi lim}$.

The tire yaw angle beyond which the lateral friction coefficient decreases, $\left(\psi_{tyre}\right)_{\mu_{\psi lim}}$ is required. A good approximation is given by

$$\left(\psi_{tyre}\right)_{\mu_{\psi lim}} = \frac{2.0 \,\mu_{\psi lim}}{\left(\dfrac{\partial \mu_{\psi}}{\partial \psi}\right)\psi = 0}$$

It is the value of ψ at the intersection of the μ_{ψ} v ψ curve with a line from the origin at half the initial slope of the curve (see figure A.3.2).

Figure A.3.2   Approximation for $\mu_{\psi lim}$ v ψ

Define $\quad h = \left(\psi_{tyre}\right)_{\mu_{\psi lim}} = 2\mu_{\psi lim} \cdot \dfrac{F_Z}{N}$

μ_{ψ} - μ_{skid} = f(h).($\mu_{\psi max}$ - μ_{skid})   (Reference 8)

Figure A.3.3 (from Reference 9) shows the relationship which defines f(h)

Figure A.3.3   Relationship to define f(h)

Next define $\quad i = \dfrac{\left(\psi_{tyre}\right) - \left(\psi_{tyre}\right)_{\mu_{\psi lim}}}{90^{o} - \left(\psi_{tyre}\right)_{\mu_{\psi lim}}}$

Converting from degrees to radians, and allowing for positive and negative values of ψ, with the following conditions, to allow values of ψ up to 180°. (a condition on the sign of F_y will also be needed, for yaw angles greater than 90°)

$$i = 0 \qquad \text{for} \quad 0 < |\psi| < h$$

$$i = \frac{|\psi| - h}{1.57 - h} \qquad \text{for} \quad h < |\psi| < 1.57$$

$$i = 2 + \frac{h - |\psi|}{1.57 - h} \qquad \text{for} \quad 1.57 < |\psi| < 3.14 - h$$

$$i = 0 \qquad \text{for} \quad 3.14 - h \leq |\psi|$$

Figure A.3.4   Subsidiary function i v ψ

Define j, an approximation for $\qquad \dfrac{\mu_\psi - \mu_{skid}}{\left(\mu_\psi\right)_{lim} - \mu_{skid}}$

j is used to define the lateral friction coefficient at large yaw angles (lya),

$$j = 1 - 1.93\, i \qquad \text{for} \quad i < 0.3$$

$$= 0.58 - 0.575\, i \qquad \text{for} \quad i > 0.3$$

Figure A.3.5   Subsidiary function j v i

A.3.9   Lateral Friction Coefficient at large yaw angles

$$\mu_{lya} = \mu_{skid} + j\,(\mu_{\psi\,lim} - \mu_{skid}) \qquad \text{for} \quad \mu_{\psi\,lim} > \mu_{skid}$$

$$= \mu_{\psi\,lim} \qquad \text{for} \quad \mu_{\psi\,lim} < \mu_{skid}$$

Finally, the lateral friction coefficient, μ_ψ, is given by

$$\mu_\psi = \mu_{sya} \quad \text{for} \quad |\psi| < h$$

$$= \mu_{lya} \quad \text{for} \quad |\psi| > h$$

The lateral force on the tire, F_y, is then calculated from the simple relationship

$$F_y = F_z \cdot \mu_\psi \quad \text{for} \quad \psi > 0$$

$$F_y = -F_z \cdot \mu_\psi \quad \text{for} \quad \psi < 0$$

The expressions above allow F_ψ and μ_ψ to be calculated for all realistic values of tire dimensions, tire pressure, aircraft speed, wheel load, and level of braking, and for different levels of runway surface contamination. Figure A.3.6 shows the effect of speed, surface condition, and wheel braking on μ_ψ v ψ for a Boeing 747-200 main wheel tire.

Figure A.3.6   Lateral friction coefficient v tire yaw angle

A.3.10 Conclusion

The mechanism by which forces are generated on a tire is a complex one. This report has identified the major factors which influence the side-forces on an aircraft tire, in contact with a runway. From the published data, mathematical expressions have been derived which can be implemented on a computer, to allow the side-force to be computed continuously, as a function of these factors. They include the type of runway, the contamination on the runway, the type and size of tire, its inflation pressure, the speed of the aircraft, and the load on the wheel.
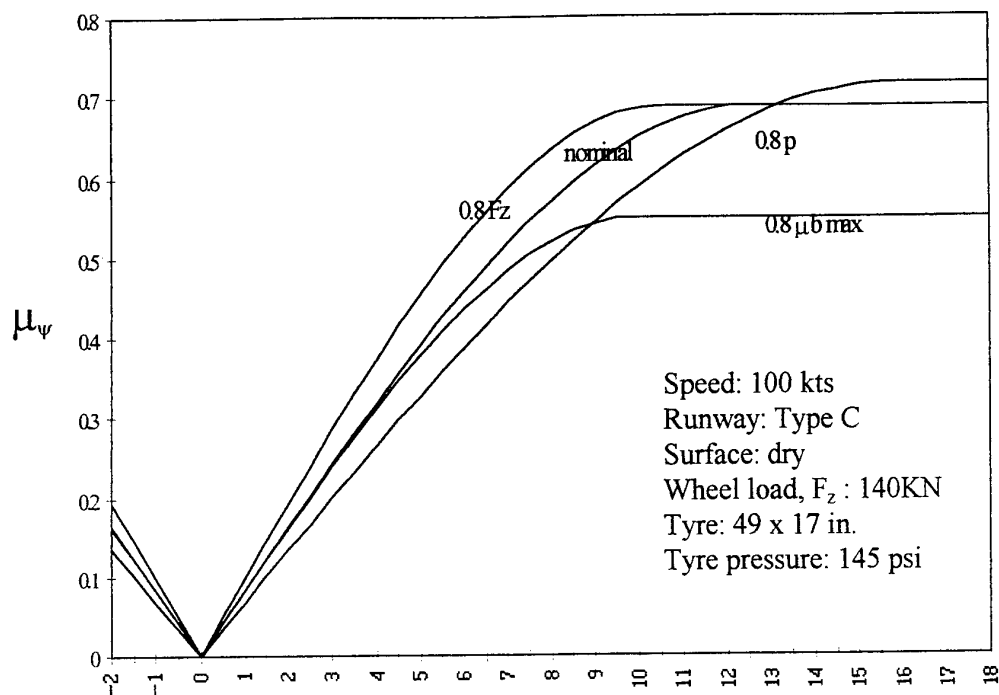
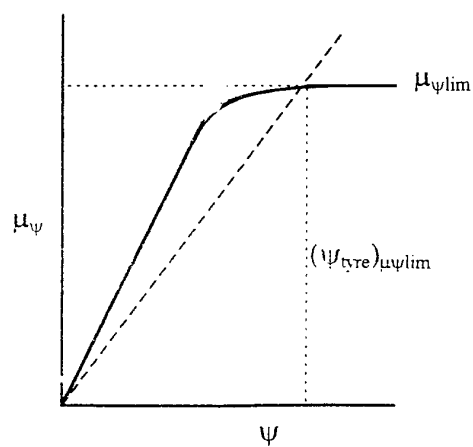**Figure A.3.1 Lateral friction coefficient v tire yaw angle**

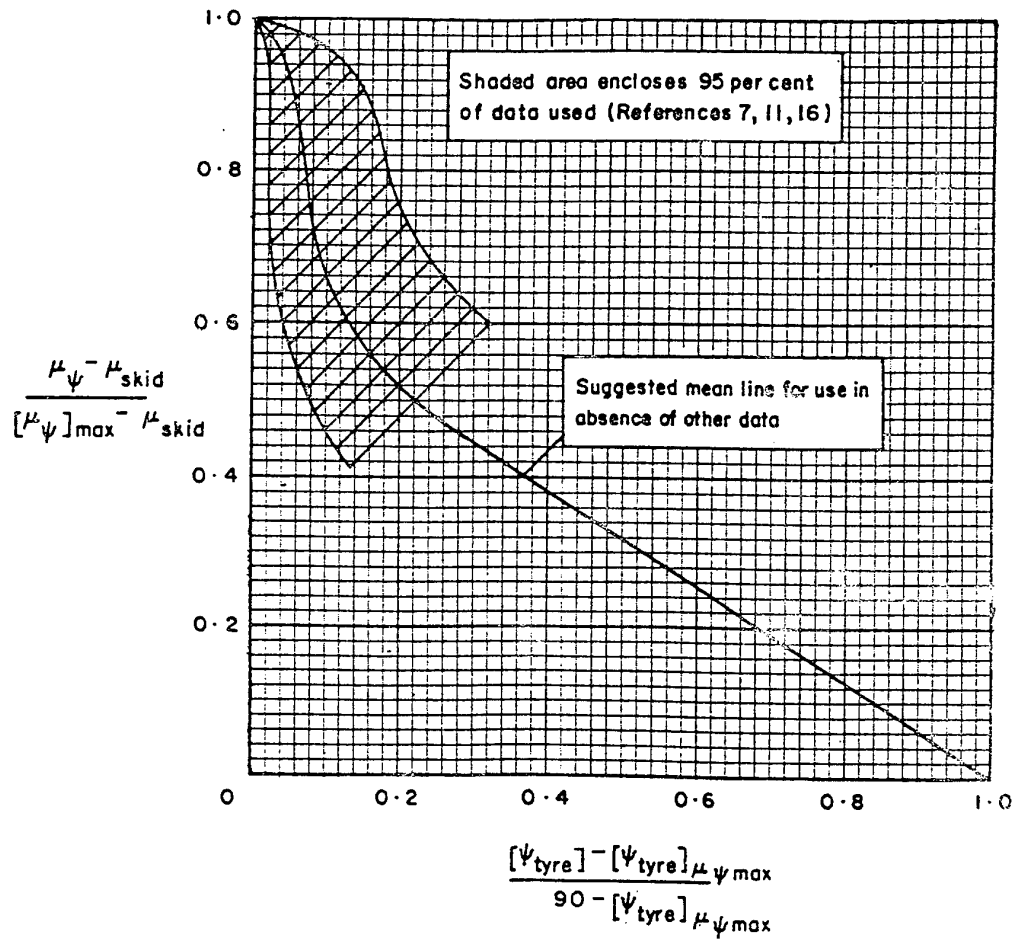**Figure A.3.2 Approximation for $\mu_{\psi\,lim}$ v ψ**
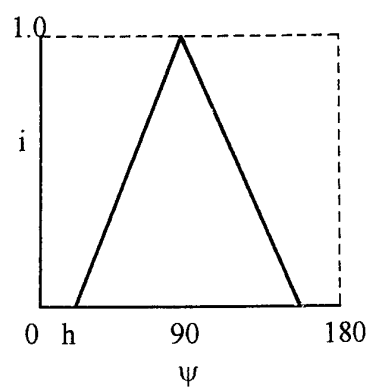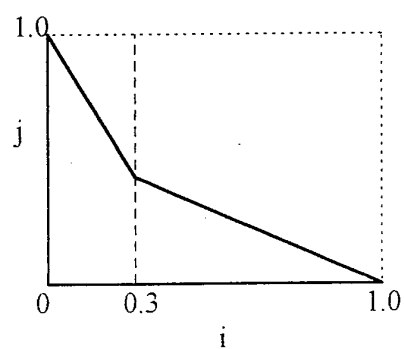
Figure A.3.3 Relationship to define f(h)

Figure A.3.4   Subsidiary function i v ψ

Figure A.3.5   Subsidiary function j v i

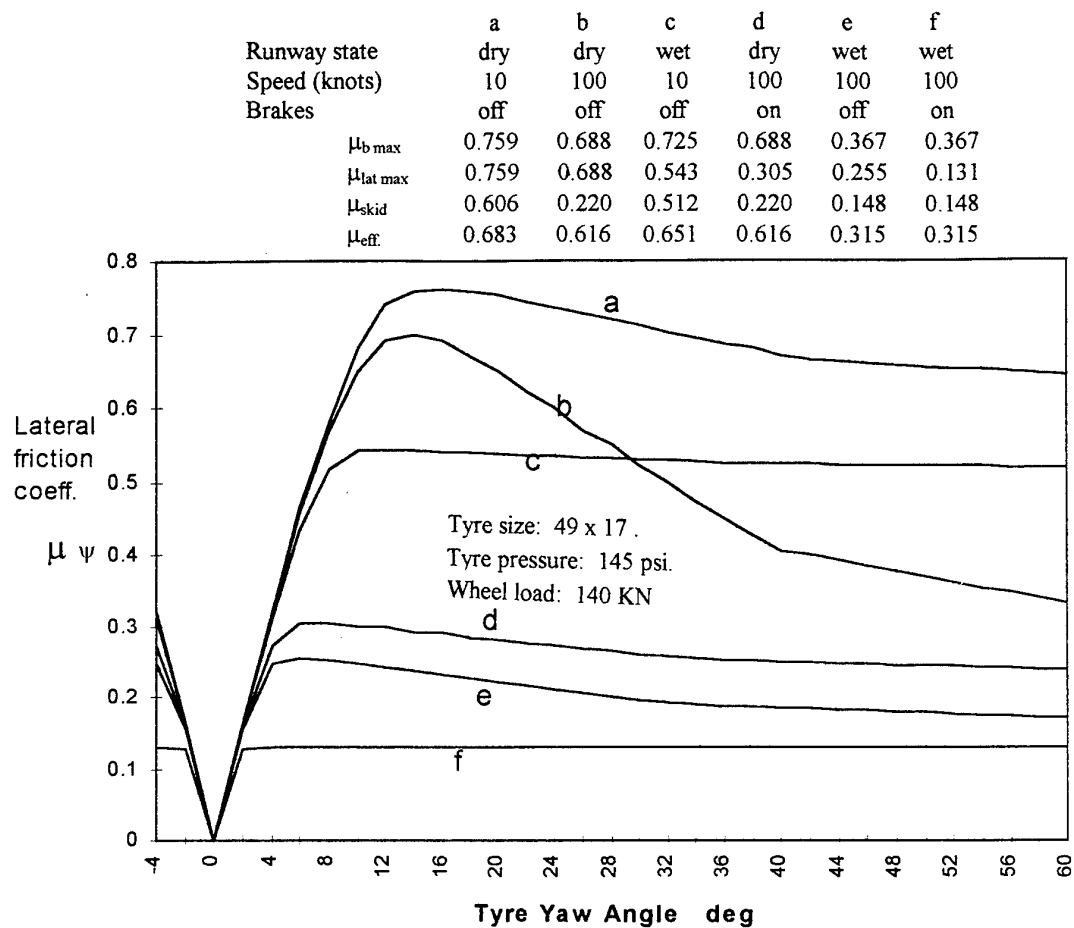|	a	b	c	d	e	f
Runway state	dry	dry	wet	dry	wet	wet
Speed (knots)	10	100	10	100	100	100
Brakes	off	off	off	on	off	on
$\mu_{b\,max}$	0.759	0.688	0.725	0.688	0.367	0.367
$\mu_{lat\,max}$	0.759	0.688	0.543	0.305	0.255	0.131
μ_{skid}	0.606	0.220	0.512	0.220	0.148	0.148
μ_{eff}	0.683	0.616	0.651	0.616	0.315	0.315

Figure A.3.6 Lateral friction coefficient v tire yaw angle

Appendix 4

A Linearized Model of Ground Lateral Forces.

A.4.1 Introduction

The stability, dynamic response, and trajectory of an aircraft rolling on the ground at low speed is determined by the lateral forces generated by contact between the tires and the ground. Section 5 describes the complex relationships which govern these forces. They are functions of many variables. Figure A.3.1 is typical of the variation of lateral friction coefficient μ, with tire slip angle λ. In normal operating conditions, the angular excursions are small, and the friction coefficient varies linearly with slip angle. In dry conditions, the tires can generate high lateral forces, and the possibility exists of the aircraft overturning in roll during ground maneuvers, particularly if the speed is high, the wheel track is narrow, and aerodynamic forces are being generated. It is normally sufficient to use a static balance calculation to calculate the maximum permissible wheel steering angle

For the following analysis, it is convenient to neglect aerodynamic forces (at low speed they are insignificant), and to assume constant speed, and small perturbations. Although the case with three degrees of freedom (sideways displacement, yaw, and roll) is tractable, gear designs for most aircraft ensure that roll angles on the ground are small, so that a two degree of freedom analysis is adequate. It provides an insight into how the stability and control of the aircraft during ground roll varies with speed, gear layout and ground contact conditions. The modal parameters associated with the dynamic response, and the steady state relationships due to control, can be used to validate the model, and to predict handling qualities on the ground.

Consider the case of an aircraft with a tricycle gear, with two fixed mainwheels, and a third wheel which can either be steered, or can castor. For the purpose of this analysis, a castoring wheel cannot generate side forces. The two degree of freedom case may be considered as a bicycle layout, in which the loads on the port and starboard main wheels are combined into single main wheel loads. The configuration is seen on figure A.4.1 (note that by choosing the values of a and b, either a nosewheel or tailwheel configuration can be represented).

The lateral friction derivative, $d\mu_\lambda/d\lambda$, is the local slope of the μ_λ v λ curve at a given value of tire slip angle λ.

For small perturbations, $\quad \mu_\lambda = d\mu_\lambda/d\lambda \cdot \lambda$

If the load on the wheel is F_z, the cornering power of the tire, $N = F_z.(d\mu_\lambda/d\lambda)$, and the lateral force, or cornering force, generated by the tire is

$$F_z.\mu_\lambda = F_z.d\mu_\lambda/d\lambda.\lambda$$

Figure A.4.1   Lateral forces due to ground contact

Static balance of vertical loads gives

$$Z_n = -mg.\,b/(a-b) \qquad Z_m = mg.\,a\,/(a-b)$$

Define

$$k_n = Z_n.(d\mu_{\lambda n}/d\lambda_n) = -[b/(a-b)].mg\,(d\mu_{\lambda n}/d\lambda_n)$$

and

$$k_m = Z_m.(d\mu_{\lambda m}/d\lambda_m) = [a/(a-b)].mg\,(d\mu_{\lambda m}/d\lambda_m)$$

The lateral forces on the wheels, Y_n and Y_m , are given by

$$Y_n = -(d\mu_{\lambda n}/d\lambda_n)\,Z_n\,\lambda_n = -k_n\,\lambda_n$$

$$Y_m = -(d\mu_{\lambda m}/d\lambda_m)\,Z_m\,\lambda_m = -k_m\,\lambda_m$$

A.4.2   Dynamic Stability

Lateral velocities at nosewheel and mainwheels.

$$v_n{}' = v + a.r \qquad v_m = v + b.r$$

$$v_n = v_n{}'\cos\delta - V\sin\delta$$

$$V_n = v_n{}'\sin\delta + V\cos\delta$$

$$\lambda_m = v_m/V = (v + b.r)/V$$

$$\lambda_n = v_n/V = \{(v + a.r)\cos\delta - V\sin\delta\}/\{(v + a.r)\sin\delta + V\cos\delta\}$$

for small δ, and $v_n \ll V$

$$\lambda_n = (v + a.r - V.\delta)/V$$

Hence

$$Y_n = -k_n.(v + a.r)/V + k_n.\delta$$

$$Y_m = -k_m.(v + b.r)/V$$

Sideforce Equation

$$m.\dot{v} = -m.V.r + Y_n + Y_m$$

Yaw Equation

$$C.\dot{r} = Y_n.a + Y_m.b$$

$$m.\dot{v} = -m.V.r - k_n(v + a.r)/V - k_m.(v + b.r)/V + k_n.\delta$$

$$C.\dot{r} = -k_n.(v + a.r).a/V - k_m.(v + b.r).b/V + k_n.a.\delta$$

$$\dot{v} + [(k_n + k_m)/m.V].v + [V + (k_n.a + k_m.b)/m.V].r = k_n.\delta/m$$

$$\dot{r} + [(k_n.a + k_m.b)/CV].v + [(k_n.a^2 + k_m.b^2)/CV].r = a.k_n.\delta/C$$

The characteristic equation is

$$s^2 + [(k_n + k_m)/m.V + (a^2k_n + b^2k_m)/C.V].s$$
$$+ [(a - b)^2.k_n.k_m/m.C.V^2 - (a.k_n + b.k_m)/C] = 0$$

It is a quadratic which yields the modal parameters (either two real roots, or real and imaginary parts) which describe the stability of the aircraft in the ground roll. The effects of speed, gear geometry, weight distribution, wheel size, and tire type may all be studied. The s coefficient is always positive, but the associated damping decreases with speed. The signs of a and b depend on configuration (e.g. nosewheel or tailwheel), but are opposite (the c.g. must always lie between the front and rear wheels). Most configurations have two stable real roots when the wheels do not castor, but in some circumstances, such as braking at high speed, with a nosewheel tyre chosen for good steering (high $d\mu_\lambda/d\lambda$), either an oscillatory mode or an instability can occur.

A.4.3 Similar Tires

When the tires are operating at their rated pressures, and below their rated loads, the value of the lateral friction partial derivative $d\mu_\lambda/d\lambda$ (to be written forthwith as $\mu_{\lambda\lambda}$ for convenience) is the same for all wheels, for most aircraft. Under static loading conditions, and with no aerodynamic forces,

$$k_n + k_m = mg.(d\mu_\lambda/d\lambda)$$

and the characteristic equation can be re-formulated as

$$s^2 + \mu_{\lambda\lambda}.(1 - a.b.m/C).g/V - \mu_{\lambda\lambda}^2.a.b.m.g^2/C.V^2 = 0$$

which has factors $(s + \mu_{\lambda\lambda}.g/V)$ and $(s - \mu_{\lambda\lambda}.a.b.m.g/CV)$

Both roots are positive for all configurations and speeds (either a or b is negative). The first root depends on speed and tire behavior, but is independent of aircraft size and configuration. The second root depends on speed, tire behavior, and configuration, but is not strongly influenced by aircraft size. The roots define times to double amplitude in response to a step disturbance.

	m (kg.10^{-3})	C (kg.m^2.10^{-3})	a (m)	$-b$ (m)
large transport aircraft	300	70,000	24	3
small fighter aircraft	11	50	3	0.4
saloon car	1.3	1.8	1	1.6

The stability of these vehicles, with non-castoring wheels, and assuming $\mu_{\lambda\lambda} = 7.0$ in each case, is plotted on Figure A.4.2. As might be expected, the aircraft take much longer than the car to reach a steady state after a disturbance, due both to size and the disposition of the c.g. relative to the wheels.

Figure A.4.2 Ground roll stability v speed - fixed nosewheel

Transfer functions

Side velocity to steer angle

$$\frac{v}{\delta} = \frac{-\dfrac{bg\mu_{\lambda\lambda}}{(a-b)}\left(s + \dfrac{abmg}{CV}\mu_{\lambda\lambda} + \dfrac{abmgV}{(a-b)C}\mu_{\lambda\lambda}\right)}{\left(s + \dfrac{g}{V}\mu_{\lambda\lambda}\right)\left(s + \dfrac{abmg}{CV}\mu_{\lambda\lambda}\right)}$$

Yaw rate to steer angle

$$\frac{r}{\delta} = \frac{\dfrac{abmg}{(a-b)C}\mu_{\lambda\lambda}}{(s + \dfrac{abmg}{CV}\mu_{\lambda\lambda})}$$

The denominator is the yaw rate root plotted above. At speeds above 50 knots, the time to reach a steady rate of yaw is long ($t_{1/2} > 1.0$ seconds), compared to motor vehicles. Aircraft are not required to maneuver at these speeds.

Initial lateral acceleration at the nose-wheel due to step δ

$$a_y = -\frac{b}{(a-b)}g\mu_{\lambda\lambda} + a.\dot{r} \quad _{initial}$$

$$= -\frac{b}{(a-b)}g.\mu_{\lambda\lambda}(1 + \frac{a^2 m}{C})$$

For most aircraft, $m.a^2 > C$. Hence, the initial lateral acceleration at the nosewheel is at least double that at the c.g.. The pilot position is often in the region of the nosewheel, and the accelerations he senses are also increased relative to those at the c.g., and will most likely influence his impressions of the steering task.

Steady state response to step δ

Steady turn rate $\quad r_{ss}/\delta = V/(a\text{-}b)$

Radius of turn $\quad R = (a\text{-}b)/\delta$

(this is the well-known expression relating turn radius to wheel-base and steer angle)

Tire slip angle at c.g.,

$$\lambda_{c.g.ss} = -\frac{b}{(a\text{-}b)}\left(1 + \frac{V^2}{bg\mu_{\lambda\lambda}}\right).\delta$$

Tire slip angle at nosewheel and mainwheel,

$$\lambda_{ss} = -\frac{V^2.\delta}{(a-b)g\mu_{\lambda\lambda}}$$

A.4.4 Castoring Wheel (nose-wheel or tailwheel)

A castored wheel ideally cannot generate a cornering force. In practice, ideal castoring is undesirable, since a slope, or runway camber would induce a down-slope turn (breakout friction avoids such inconveniences). For this analysis, ideal castoring is assumed, so that $k_n = 0$, and the characteristic equation becomes

$$s^2 + [(1/m + b^2/C).k_m/V] s - b.k_m/C = 0$$

which may be written as

$$s^2 + \left(\frac{a}{(a-b)} \left[1 + \frac{mb^2}{C} \right] \frac{g}{V} \mu_{\lambda\lambda} \right) s - \frac{a}{(a-b)} \cdot \frac{m}{C} g\mu_{\lambda\lambda} = 0$$

The stiffness term is independent of speed, and the damping term reduces with speed. A nosewheel configuration is stable (b is negative), and a tailwheel configuration is unstable (b is positive).

The natural frequency and relative damping ratio of the characteristic equation for the vehicles on figure A.4.2, assuming a castoring nosewheel/front wheel are seen on figure A.4.3. Vehicle size, mass distribution, and c.g. location all influence the natural frequency. At 50 knots, the times to half amplitude for the large transport aircraft, the small fighter, and the car are respectively 10, 4, and 0.8 seconds.

Figure A.4.3 Ground roll stability v speed - castoring nosewheel

Steering of an aircraft on the ground is influenced by the above parameters. The reduction in damping with speed adversely affects the steering task. However, with increasing speed, aerodynamic terms play an increasing part, enhancing stability and providing yaw control through the rudder.
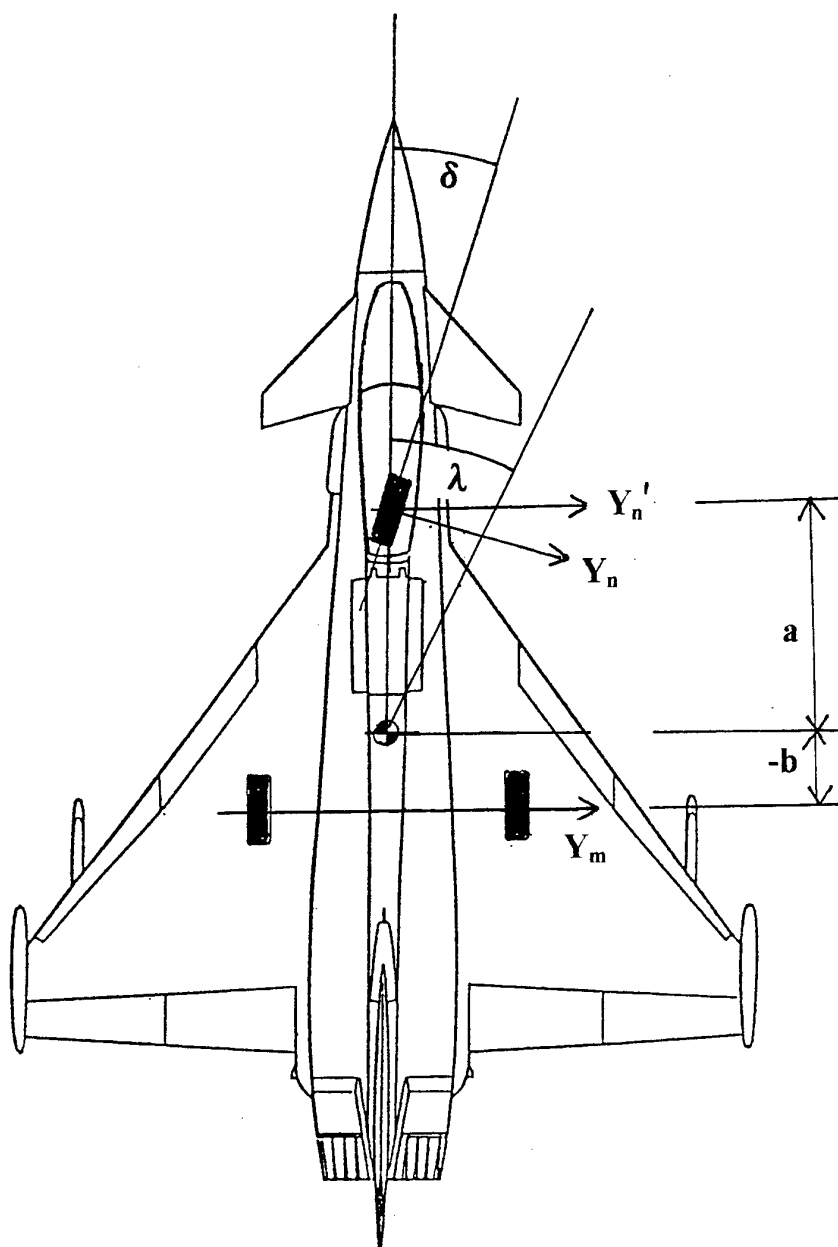
Figure A.4.1   Lateral forces due to ground contact

a) lateral velocity root

time to
half amplitude

(seconds)

all vehicles

Speed knots

b) yaw rate root

time to
half amplitude

(seconds)
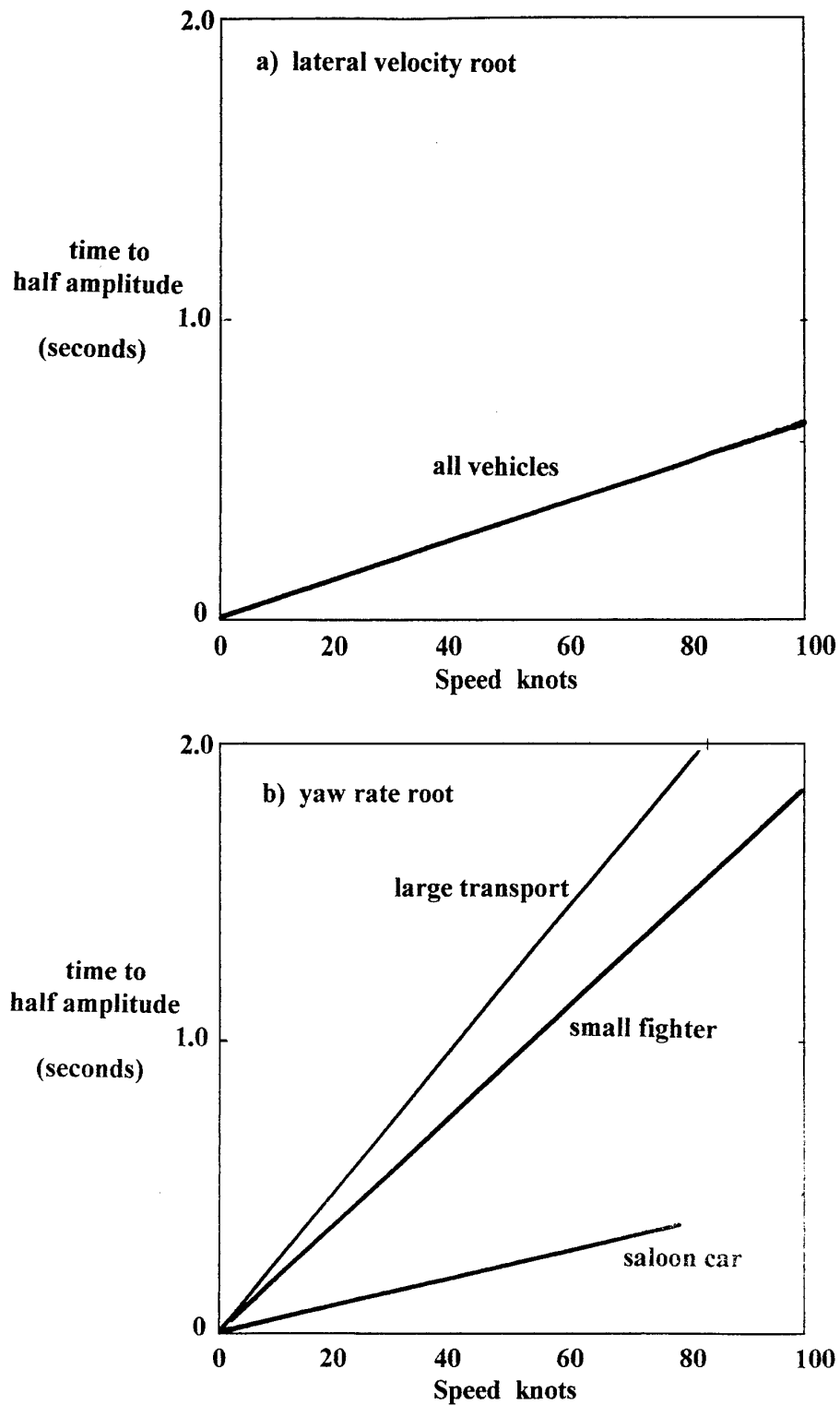
large transport

small fighter

saloon car

Speed knots

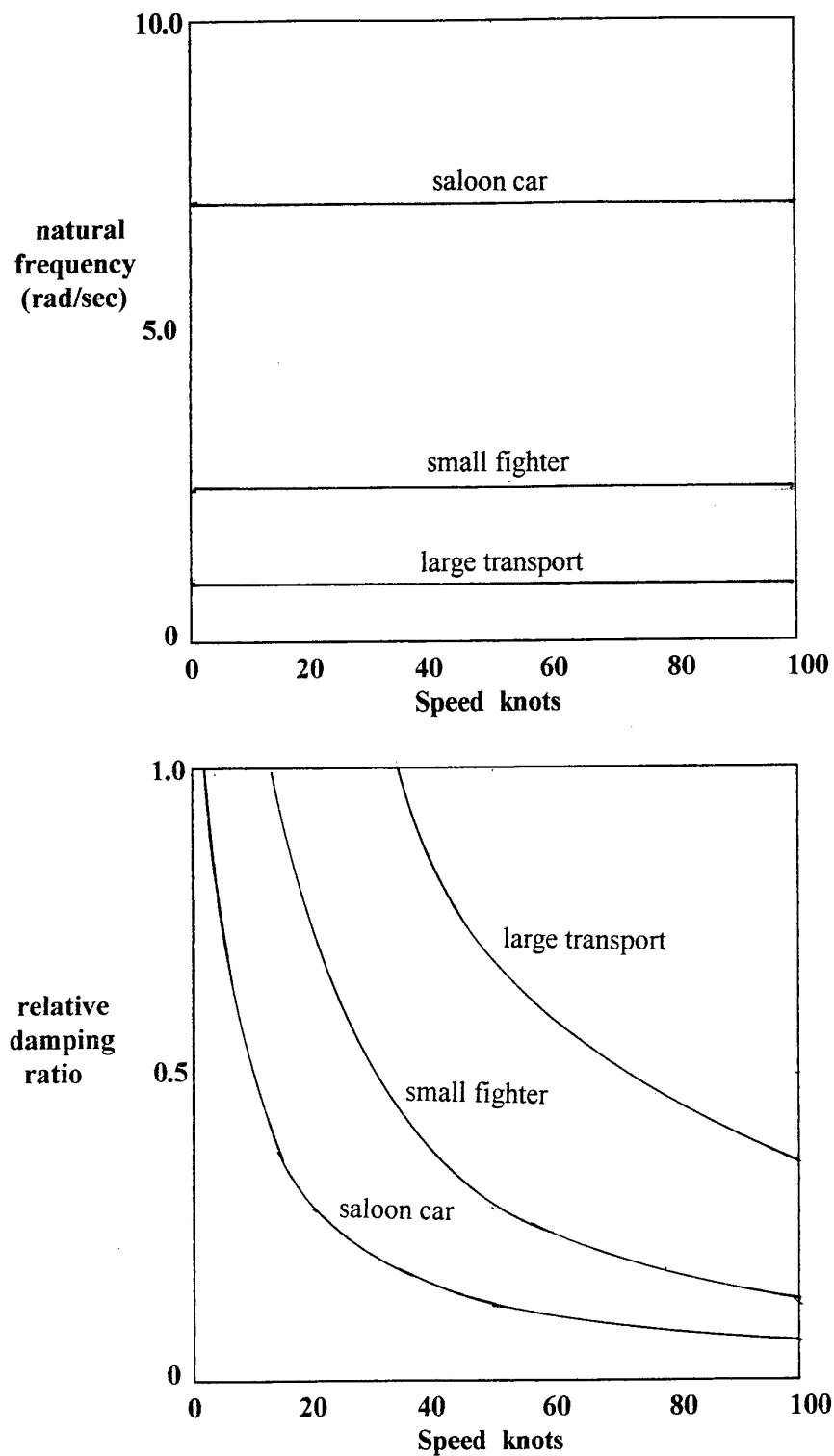Figure A.4.2 Ground roll stability v speed - fixed nosewheel

Figure A.4.3 Ground roll stability v speed - castoring nosewheel

REPORT DOCUMENTATION PAGE

1. Recipient's Reference	2. Originator's Reference	3. Further Reference	4. Security Classification of Document
	AGARD-AG-333	ISBN 92-836-1066-0	UNCLASSIFIED/ UNLIMITED

5. Originator Advisory Group for Aerospace Research and Development
North Atlantic Treaty Organization
7 rue Ancelle, 92200 Neuilly-sur-Seine, France

6. Title
Enhancement of Aircraft Ground Handling Simulation Capability

7. Presented at/sponsored by
The Flight Vehicle Integration Panel.

8. Author(s)/Editor(s)	9. Date
Multiple	August 1998

10. Author's/Editor's Address	11. Pages
Multiple	88

12. Distribution Statement There are no restrictions on the distribution of this document.
Information about the availability of this and other AGARD
unclassified publications is given on the back cover.

13. Keywords/Descriptors

Aircraft	Struts
Ground handling equipment	Pilots (personnel)
Computerized simulation	Tires
Performance	Runways
Mathematical models	Friction
Force	Flight simulators
Surface properties	Stability
Flight simulation	Research projects
Dynamic response	

14. Abstract

This report is a guide to methods of representing in a flight simulator, the stability and control of an aircraft on the ground. It updates an earlier publication, AGARDograph 285, in the light of simulation technology improvements over a ten year period. Emphasis is placed on the modeling of the vehicle dynamics, and on the modeling of the tire forces generated by the runway surface. Areas are identified where some current simulators are deficient. The different needs of pilot-in-the-loop and non-real-time simulations are discussed, and topics for further research are identified.

AGARD

NATO ⊕ OTAN

7 RUE ANCELLE • 92200 NEUILLY-SUR-SEINE

FRANCE

Télécopie 0(1)55.61.22.99 • Télex 610 176

DIFFUSION DES PUBLICATIONS

AGARD NON CLASSIFIEES

L'AGARD détient un stock limité de certaines de ses publications récentes. Celles-ci pourront éventuellement être obtenus sous forme de copie papier. Pour de plus amples renseignements concernant l'achat de ces ouvrages, adressez-vous à l'AGARD par lettre ou par télécopie à l'adresse indiquée ci-dessus. *Veuillez ne pas téléphoner.*

Des exemplaires supplémentaires peuvent parfois être obtenus auprès des centres de diffusion nationaux indiqués ci-dessous. Si vous souhaitez recevoir toutes les publications de l'AGARD, ou simplement celles qui concernent certains Panels, vous pouvez demander d'être inclus sur la liste d'envoi de l'un de ces centres.

Les publications de l'AGARD sont en vente auprès des agences de vente indiquées ci-dessous, sous forme de photocopie ou de microfiche. Certains originaux peuvent également être obtenus auprès de CASI.

CENTRES DE DIFFUSION NATIONAUX

ALLEMAGNE
Fachinformationszentrum Karlsruhe
D-76344 Eggenstein-Leopoldshafen 2

BELGIQUE
Coordonnateur AGARD - VSL
Etat-major de la Force aérienne
Quartier Reine Elisabeth
Rue d'Evere, B-1140 Bruxelles

CANADA
Directeur - Gestion de l'information
  (Recherche et développement) - DRDGI 3
Ministère de la Défense nationale
Ottawa, Ontario K1A 0K2

DANEMARK
Danish Defence Research Establishment
Ryvangs Allé 1
P.O. Box 2715
DK-2100 Copenhagen Ø

ESPAGNE
INTA (AGARD Publications)
Carretera de Torrejón a Ajalvir, Pk.4
28850 Torrejón de Ardoz - Madrid

ETATS-UNIS
NASA Center for AeroSpace Information (CASI)
Parkway Center, 7121 Standard Drive
Hanover, MD 21076

FRANCE
O.N.E.R.A. (Direction)
29, Avenue de la Division Leclerc
92322 Châtillon Cedex

GRECE
Hellenic Air Force
Air War College
Scientific and Technical Library
Dekelia Air Force Base
Dekelia, Athens TGA 1010

ISLANDE
Director of Aviation
c/o Flugrad
Reykjavik

ITALIE
Aeronautica Militare
Ufficio Stralcio AGARD
Aeroporto Pratica di Mare
00040 Pomezia (Roma)

LUXEMBOURG
Voir Belgique

NORVEGE
Norwegian Defence Research Establishment
Attn: Biblioteket
P.O. Box 25
N-2007 Kjeller

PAYS-BAS
Netherlands Delegation to AGARD
National Aerospace Laboratory NLR
P.O. Box 90502
1006 BM Amsterdam

PORTUGAL
Estado Maior da Força Aérea
SDFA - Centro de Documentação
Alfragide
P-2720 Amadora

ROYAUME-UNI
Defence Research Information Centre
Kentigern House
65 Brown Street
Glasgow G2 8EX

TURQUIE
Millî Savunma Başkanliği (MSB)
ARGE Dairesi Başkanliği (MSB)
06650 Bakanliklar - Ankara

AGENCES DE VENTE

NASA Center for AeroSpace Information (CASI)
Parkway Center, 7121 Standard Drive
Hanover, MD 21076
Etats-Unis

The British Library Document Supply Division
Boston Spa, Wetherby
West Yorkshire LS23 7BQ
Royaume-Uni

Les demandes de microfiches ou de photocopies de documents AGARD (y compris les demandes faites auprès du CASI) doivent comporter la dénomination AGARD, ainsi que le numéro de série d'AGARD (par exemple AGARD-AG-315). Des informations analogues, telles que le titre et la date de publication sont souhaitables. Veuiller noter qu'il y a lieu de spécifier AGARD-R-nnn et AGARD-AR-nnn lors de la commande des rapports AGARD et des rapports consultatifs AGARD respectivement. Des références bibliographiques complètes ainsi que des résumés des publications AGARD figurent dans les journaux suivants:

Scientific and Technical Aerospace Reports (STAR)
STAR peut être consulté en ligne au localisateur de
ressources uniformes (URL) suivant:
    http://www.sti.nasa.gov/Pubs/star/Star.html
STAR est édité par CASI dans le cadre du programme
NASA d'information scientifique et technique (STI)
STI Program Office, MS 157A
NASA Langley Research Center
Hampton, Virginia 23681-0001
Etats-Unis

Government Reports Announcements & Index (GRA&I)
publié par le National Technical Information Service
Springfield
Virginia 2216
Etats-Unis
(accessible également en mode interactif dans la base de
données bibliographiques en ligne du NTIS, et sur CD-ROM)

AGARD

NATO ✦ OTAN

7 RUE ANCELLE • 92200 NEUILLY-SUR-SEINE

FRANCE

Telefax 0(1)55.61.22.99 • Telex 610 176

DISTRIBUTION OF UNCLASSIFIED

AGARD PUBLICATIONS

AGARD holds limited quantities of some of its recent publications, and these may be available for purchase in hard copy form. For more information, write or send a telefax to the address given above. *Please do not telephone.*

Further copies are sometimes available from the National Distribution Centres listed below. If you wish to receive all AGARD publications, or just those relating to one or more specific AGARD Panels, they may be willing to include you (or your organisation) in their distribution.

AGARD publications may be purchased from the Sales Agencies listed below, in photocopy or microfiche form. Original copies of some publications may be available from CASI.

NATIONAL DISTRIBUTION CENTRES

BELGIUM
Coordonnateur AGARD - VSL
Etat-major de la Force aérienne
Quartier Reine Elisabeth
Rue d'Evere, B-1140 Bruxelles

CANADA
Director Research & Development
Information Management - DRDIM 3
Dept of National Defence
Ottawa, Ontario K1A 0K2

DENMARK
Danish Defence Research Establishment
Ryvangs Allé 1
P.O. Box 2715
DK-2100 Copenhagen Ø

FRANCE
O.N.E.R.A. (Direction)
29 Avenue de la Division Leclerc
92322 Châtillon Cedex

GERMANY
Fachinformationszentrum Karlsruhe
D-76344 Eggenstein-Leopoldshafen 2

GREECE
Hellenic Air Force
Air War College
Scientific and Technical Library
Dekelia Air Force Base
Dekelia, Athens TGA 1010

ICELAND
Director of Aviation
c/o Flugrad
Reykjavik

ITALY
Aeronautica Militare
Ufficio Stralcio AGARD
Aeroporto Pratica di Mare
00040 Pomezia (Roma)

LUXEMBOURG
See Belgium

NETHERLANDS
Netherlands Delegation to AGARD
National Aerospace Laboratory, NLR
P.O. Box 90502
1006 BM Amsterdam

NORWAY
Norwegian Defence Research Establishment
Attn: Biblioteket
P.O. Box 25
N-2007 Kjeller

PORTUGAL
Estado Maior da Força Aérea
SDFA - Centro de Documentação
Alfragide
P-2720 Amadora

SPAIN
INTA (AGARD Publications)
Carretera de Torrejón a Ajalvir, Pk.4
28850 Torrejón de Ardoz - Madrid

TURKEY
Millî Savunma Başkanliği (MSB)
ARGE Dairesi Başkanliği (MSB)
06650 Bakanliklar - Ankara

UNITED KINGDOM
Defence Research Information Centre
Kentigern House
65 Brown Street
Glasgow G2 8EX

UNITED STATES
NASA Center for AeroSpace Information (CASI)
Parkway Center, 7121 Standard Drive
Hanover, MD 21076

SALES AGENCIES

NASA Center for AeroSpace Information (CASI)
Parkway Center, 7121 Standard Drive
Hanover, MD 21076
United States

The British Library Document Supply Centre
Boston Spa, Wetherby
West Yorkshire LS23 7BQ
United Kingdom

Requests for microfiches or photocopies of AGARD documents (including requests to CASI) should include the word 'AGARD' and the AGARD serial number (for example AGARD-AG-315). Collateral information such as title and publication date is desirable. Note that AGARD Reports and Advisory Reports should be specified as AGARD-R-nnn and AGARD-AR-nnn, respectively. Full bibliographical references and abstracts of AGARD publications are given in the following journals:

Scientific and Technical Aerospace Reports (STAR)
STAR is available on-line at the following uniform resource locator:
    http://www.sti.nasa.gov/Pubs/star/Star.html
STAR is published by CASI for the NASA Scientific and Technical Information (STI) Program
STI Program Office, MS 157A
NASA Langley Research Center
Hampton, Virginia 23681-0001
United States

Government Reports Announcements & Index (GRA&I)
published by the National Technical Information Service
Springfield
Virginia 22161
United States
(also available online in the NTIS Bibliographic Database or on CD-ROM)